ULTRASOUND BASED MEASURES OF MUSCLE FATIGUE AND RECOVERY AFTER ELECTRICAL MUSCLE STIMULATION

by

Joseph Amir Majdi
A Dissertation
Submitted to the
Graduate Faculty
of
George Mason University
in Partial Fulfillment of
The Requirements for the Degree
of
Doctor of Philosophy
Bioengineering

Committee:

_____ Dr. Siddhartha Sikdar, Dissertation Director

_____ Dr. Parag Chitnis, Committee Member

_____ Dr. Shani Ross, Committee Member

_____ Dr. Eugene Civillico, Committee Member

_____ Dr. Shani Ross, Department Chair

Date:_____ Summer Semester 2022
George Mason University
Fairfax, VA

Ultrasound Based Measures of Muscle Fatigue and Recovery after Electrical Muscle Stimulation

A Dissertation submitted in partial fulfillment of the requirements for the degree of Doctor of Philosophy at George Mason University

by

Joseph Amir Majdi
Master of Science
George Mason University, 2017
Master of Science
Tulane University, 2012
Bachelor of Science
Tulane University, 2012

Director: Siddhartha Sikdar, Professor
Department of Bioengineering

Summer Semester 2022
George Mason University
Fairfax, VA

DEDICATION

I would like to dedicate this dissertation to my family who always supported me and believed in me with no reservations. I would also like to dedicate this dissertation to my dog Rufus with whom I lost thousands of hours in order to complete this work. Nevertheless, he got me through my toughest times until his passing in December 2021.

ACKNOWLEDGEMENTS

I would like to thank all of the members of the lab, past and present, for providing me with such a great environment to come into every day. I would especially like to thank Shriniwas Patwardhan for providing me with his friendship or tough love, depending on what I needed at the time.

TABLE OF CONTENTS

LIST OF TABLES

LIST OF FIGURES

LIST OF EQUATIONS

LIST OF ABBREVIATIONS AND SYMBOLS

Adenosine Diphosphate ..... ADP
Adenosine Triphosphate ..... ATP
Acoustic Myography (also called Phonomyography) ..... AMG
Center Frequency of Ultrasound Transducer ..... f_c
Continuous Wave ..... CW
Continuous Passive Motion ..... CPM
Contractile Element 'i' ..... E_c^i
Electromyography (Implanted) ..... EMG
Electrical Muscle Stimulation ..... EMS
Excitation-Contraction Coupling ..... ECC
Fast Fatigable Motor Unit ..... FFMU
Fast Intermediate Motor Unit ..... FIMU
Fast Resistant Motor Unit ..... FRMU
Force of Element 'i' ..... F_i
Frequency Modulated Continuous Wave ..... FMCW
Maximum Voluntary Isometric Contraction ..... MVIC
Mechanomyography ..... MMG
Motor Unit ..... MU
Pennation Angle ..... φ
Phase Angle ..... θ
Phonomyography ..... PMG
Phosphate (Inorganic Phosphate) ..... P_i
Pulse Repetition Frequency ..... PRF
Repeated Measures Analysis of Variance ..... rmANOVA
Slow Motor Unit ..... SMU
Stiffness of Element 'i' ..... k_i
Stimulation Current Required to Generate 20% of the MVIC Torque ..... I_{20}
Surface Electromyography ..... sEMG
Tendon Viscosity ..... Λ
Tensiomyography ..... TMG
Tissue Doppler Imaging ..... TDI
Ultrasound ..... US
Velocity-Time Integral ..... VTI

ABSTRACT

ULTRASOUND BASED MEASURES OF MUSCLE FATIGUE AND RECOVERY AFTER ELECTRICAL MUSCLE STIMULATION

Joseph Amir Majdi, PhD

George Mason University, 2022

Dissertation Director: Dr. Siddhartha Sikdar

Electrical muscle stimulation (EMS) can restore or increase function in skeletal muscle by stimulating motor neurons through adhesive skin electrodes, which can greatly increase the quality of life for those suffering from paralysis. However, the unnatural muscle fiber recruitment pattern from EMS causes muscles to fatigue and lose force rapidly, which limits the utility. Although technologies such as external exoskeletons exist to supplement muscle function, there is an open need for muscle fatigue feedback to gauge muscle strength in freely moving humans for EMS applications, as the current gold standard for measuring muscle fatigue, surface electromyography (sEMG), is generally incompatible. I believe that Doppler ultrasound will provide a better solution with fast (millisecond) time resolution, depth resolved measurements, and compatibility with EMS. Further, Doppler ultrasound provides information that is both independent of and complementary to sEMG and has utility outside of EMS applications in the fields of biomechanics, sports science, rehabilitation, and beyond.

In this work, I explored signs of muscle fatigue and recovery induced by EMS using tissue Doppler imaging (TDI) with a bulky commercial ultrasound machine to establish the feasibility of this method. With this setup, I found that recovery in muscle twitch toque can be predicted from features of the average tissue velocity waveform, and that this model is subject specific. Next, for a portable solution, I performed experiments using a low power continuous wave (CW) ultrasound probe. The CW probe is portable, low power, and has much lower computational and memory requirements than the commercial TDI machine. For these experiments, I observed that the duration of audio signal at the onset of muscle contraction correlates with the peak join torque (a proxy for muscle force), and that audio signals are generated at both the onset and the release of muscle contraction in both EMS and voluntary movements. Finally, I conclude this study with multi-scale muscle modeling using a modified Hill-type model to help understand and explain our observations and predict muscle behavior.

CHAPTER ONE: BACKGROUND AND MOTIVATION

Project Narrative

There is a dearth of methods to study muscle function in detail, particularly when paired with electrical muscle stimulation (EMS). As we will see, this is a severely limiting problem for those who would benefit from EMS therapies like those suffering from spinal cord injury or stroke. In this introductory chapter, I will establish the need for new techniques to monitor muscle activation and fatigue and make the case for using medical ultrasound imaging for this task. The subsequent chapters will be devoted to establishing feasibility for using Doppler ultrasound (tissue Doppler imaging, TDI) as a technique for monitoring muscle fatigue, extending those lessons into a portable (continuous wave, CW) system, and to using muscle modeling to help explain and interpret our results. I then conclude with a summary of the main findings of this project and future directions to take advantage of these insights.

The Scope of the Problem and Target Population

Problem Scope and Target Population

Skeletal muscle function is critical for everyday life activities, functioning as actuators that not only control movement, but form critical infrastructure for other body systems including standing (skeletal), balance (vestibular), breathing (respiratory), and eye movements (vision) among others. Muscle function is also critical for healthy exercise, burning calories and improving cardiovascular health. All of which is

jeopardized by paralysis, which can severely reduce a person's quality of life and have negative health effects including muscle atrophy, cardiovascular disfunction, metabolic disfunction, and secondary health effects like diabetes caused by lack of regular muscle use [1].

Further, SCI is associated with high economic impact, not just from the loss of productivity, but also the high medical costs associated with treatment ranging from $370,000 to $1.13 million in the first year alone, and $40,000-190,000 per year thereafter [1]. It is estimated that the prevalence of long term spinal cord injuries in the US is over 2.6 million cases, and over 27 million worldwide as of 2016 [2]. Recovery of motor function, if any, is varies by patient and depends on the extent of the injury [3]. Obviously, the greater the extent of injury (with the least level of motor control), the worse expected recovery outcome. This does not even consider those suffering from strokes, who form a much larger population. Individuals with severe motor deficits may benefit from technological solutions that can enable functional task performance [1].

Motivation for Electrical Muscle Stimulation

These problems arise largely from losing voluntary control of muscle, and the reduced indpependence this can lead to. One way to counteract this is to use electrical muscle stimulation (EMS). The strength of EMS is its ability to initiate muscle contraction independently from the brain. On the surface, the case for using EMS on paralyzed muscle is obvious: otherwise paralyzed muscles can regain functionality.

Electrical muscle stimulation (EMS) techniques-either in the form of functional electrical stimulation (FES, when used during a functional task) and neuromuscular

electrical stimulation (NMES, when used non-functional task and typically in isometric conditions)-and assistive devices (such as orthotics and exoskeletons) are promising technologies to restore function in SCI patients. EMS injects electrical current to activate muscles by exciting their motor neurons (or more rarely, muscles directly [4] in case of a peripheral nerve lesion). EMS can be performed with surgically implanted electrodes, or with surface electrodes applied to the skin. EMS is a subfield of the electrical stimulation techniques, specifically designed elicit and/or aid skeletal muscle activation. Other electrical stimulation techniques can be used to influence other electrophysiological tissues like heart (pacemakers), brain (deep brain stimulation), or be used for sensory feedback [5]. Recent work has also indicated that, in the right circumstances, applying electrical stimulation to injured spinal cords directly could restore enough nerve excitability to allow voluntary muscle control in otherwise completely paralyzed individuals [6], [7].

Regaining function in otherwise paralyzed muscles could prevent or even reversing muscle atrophy [8] and lead to acute health benefits like increased cardiovascular health, reduced muscle spasticity, and reducing inflammatory markers associated with diabetes [1]. Regardless, using the patient's own muscles could dramatically increase their quality of life by directly increasing their functional capabilities or by making assistive devices more practical. By using their own muscle contractions, it could also help reduce the power consumption and battery weight for assistive devices, making them last longer between charges and weigh less.

EMS Drawbacks

EMS is not ideal, however, because it induces an unnatural muscle fiber recruitment pattern that causes rapid loss of muscle force [9] which hereafter is referred to as muscle fatigue. This is not to be confused with central fatigue, which is caused the brain's inability to maintain constant motor command due to exhaustion or losing focus. Because EMS stimulates motor neurons directly, it makes it easier to directly identify peripheral fatigue, or fatigue originating in either the muscles or motor neurons.

Muscle fatigue is not a simple problem to overcome. Increasing current to counteract the loss of force soon leads to even greater fatigue and we will address some of the possible reasons for this in the subsequent section. Methods to minimize fatigue induced by electrical stimulation is an active area of research. Custom stimulation patterns like using doublets [10] (starting an otherwise constant frequency pulse train with two rapid pulses) or desynchronizing stimulation across multiple sites [11]–[13] have shown promising results to reduce fatigue by spreading activation across different muscle tissue. Nevertheless, rapid muscle fatigue remains a major concern for implementing EMS. Developing new techniques to reduce EMS fatigue will require a thorough understanding of muscle and the molecular basis for fatigue.

Overview of Skeletal Muscle Physiology

Normal Skeletal Muscle Activation

To understand the motivation and methods behind this project, it is necessary to understand how muscles work. From there, we can both form relevant hypotheses of how the muscles will perform under in our experiments and interpret the data generated.

Movements are controlled by the activation and contraction skeletal muscle, providing stability to the internal bone structure, torquing joints to move limbs, eyes, draw breaths, and apply forces to external bodies. Muscles generally use tendons (except certain muscles like in the gluteus) to attach to and pull on bone. Each muscle evolved for their given task by developing custom shapes, pennation/not pennation, fiber makeup, specializations for sensitive movements (motor neuron to muscle fiber ratio)/speed or brute strength/or endurance.

Many chemical and physical factors interact to form skeletal muscle function. On the chemical and biomolecular level, muscle generates force by a process called the sliding filament theory. Under this model, muscle contraction is generated by two contractile proteins: actin and myosin (modulated by tropomyosin and troponin complex/Ca^{2+} ATP-ADP and P_i and Mg^{2+}), though a third contractile protein-titin-has been discovered. Titin's role in muscle structure, signaling, and mechanical function is only partially understood, as there is evidence for several theorized functions that have not yet reached broad scientific consensus [14]. When an action potential reaches the sarcoplasmic reticulum, calcium is released, which sets off a chain reaction where calcium is released. This calcium then exposes the active sites on the actin molecules and allows myosin heads to bind. These heads bind, bend, and pull these fibers together along the direction of the sarcolemma. The myosin head binding and release cycle consumes ATP in the process and continues until calcium levels are insufficient to hold the actin binding sites open. Alternatively, a depletion of ATP will leave the myosin heads bound to the actin. This is believed to be the cause of rigor mortis shortly after death.

Above the molecular scale, muscles are composed of small contractile units called muscle fibers. These fibers come in two broad classes: slow twitch (also referred to as red or type I fibers) and fast twitch (also referred to as white or type II fibers). These fibers both use the same sliding filament mechanism to produce force, but differ in their cross-sectional area, metabolism, blood perfusion, force characteristics, fatigue rates, Ca^{2+} dynamics, and their respective innervating motor neurons. Slow twitch fibers are thinner, primarily run on aerobic metabolism and contain more mitochondria, are subsequently more highly vascularized (hence 'red' fibers), slower and weaker compared to fast twitch fibers, fatigue relatively slowly, have slower Ca^{2+} dynamics, consume ATP more slowly, and are innervated by thinner motor neurons compared to those of fast twitch fibers. Fast twitch fibers generally have the opposite characteristics, being thicker, running primarily on anerobic metabolism with fewer mitochondria, are less highly vascularized (hence 'white' fibers), contract more quickly and with more force, fatigue relatively quickly, have faster Ca^{2+} dynamics, consume ATP more quickly, and are innervated by thicker motor neurons. Further, fast twitch fibers are broken down into several subgroups with varying levels of each characteristic (IIa fast fatigue resistant, IIx fast intermediate, and IIb fast fatiguing), but it is common in the literature to only refer to these as fast twitch fibers, without distinction as to which subtype or relative quantities thereof. The differences between slow and fast twitch (all subtypes) play a major role in the development of macro-scale muscle force and fatigue as that we will examine subsequent chapters.

Each muscle's macroscale structure and distribution of fiber types are related to their functional tasks (fine manipulation, weight bearing, etc.). Further, the orientation of fibers with respect to the muscle is another variable that affects its performance. There are two broad categories of fiber orientation, being either aligned with the muscle's line of action or at an angle (pennate muscle). Pennate muscles can be classified as unipennate, bipennate (containing two sets of fibers oriented oppositely), or multipennate containing a multitude of pennate orientations. Beyond that, the labels for more complex parallel-structures vary between sources. Some of these labels include parallel, fusiform, convergent/triangular, sphincter/circular types amongst others. Fiber orientation is important because it determines how the fibers convert contraction on the fiber into macro-scale muscle dynamics. Parallel muscle fibers run and contract along the length of the muscle, allowing longer sarcomeres and hence faster muscle movement and greater displacement [15]. Pennate muscle fibers on the other hand are oriented at an angle (φ, the pennation angle) with respect to the muscle's line of action. As such the muscle moves slower [15] and converts only a portion (Equation 1) of the muscle fibers' contraction force (F_{Fiber}) to the overall muscle force (F_{Muscle}). The tradeoff is that, even though only a fraction of the fiber force is translated into muscle force, pennation allows more fibers to fit into the same volume compared to parallel fibers for the same space, which allows the muscle to produce more force overall.

Equation 1. Pennate muscle force

$$F_{Muscle} = F_{Fiber} * cos(\varphi)$$

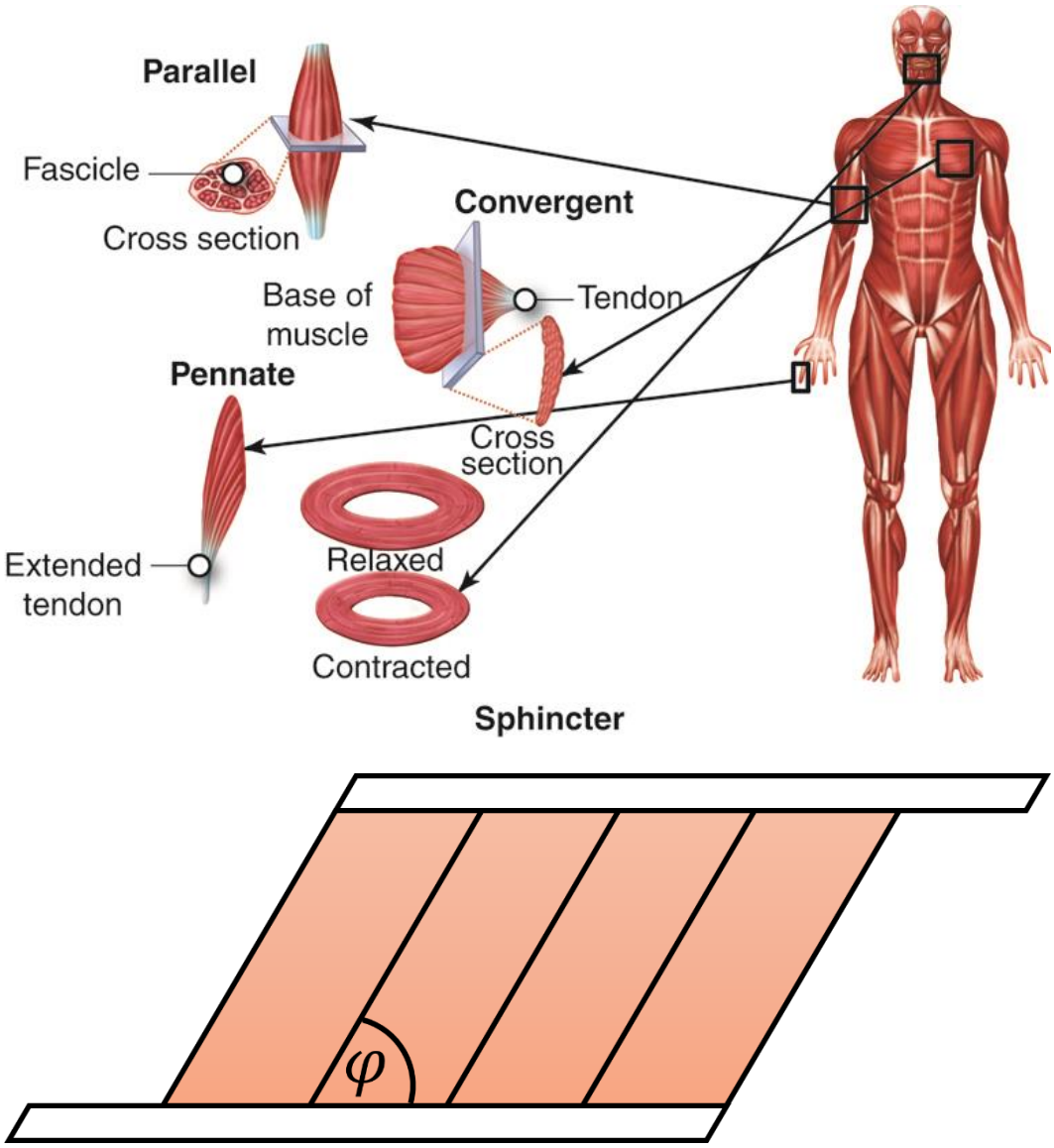

Figure 1-1. Top: Several macroscale fiber orientation variants from [16]. Bottom: Schematic of a bipennate muscle acting on an aponeurosis on the top and bottom of the muscle fibers.

One motor neuron innervates several muscle fibers, the ratio of which affects the precision of the muscle's movement. The higher the number of fibers to a single motor neuron, the less the precision of movement.

Understanding muscle activation at the biomolecular level as discussed previously is key to understand performance and the breakdown of muscle function (muscle fatigue),

which impairs the muscle's ability to generate force. We will focus on this in the next section.

Muscle Fatigue Overview

It is important to establish the meaning of 'fatigue' and how it relates to electrical stimulation. Unless otherwise noted, I refer to peripheral fatigue, or fatigue resulting from a breakdown in either the ability for peripheral motor neurons to excite muscles or in muscles themselves. This is not to be confused with central fatigue, which is more a measure of the brain's ability to generate the underlying motor commands resulting from mental exhaustion, distraction, etc. Peripheral fatigue is the breakdown between motor commands from the central nervous system or external stimulation such as EMS and the contractile force the muscle generates. Both of these effects are relevant with voluntary movements, which makes it difficult to determine their relative contributions. However, EMS induced peripheral muscle fatigue is driven directly by the overactivation of the muscles and motor nerves. It is believed that stimulating peripheral motor neurons at very high frequency (>100Hz) can drive them beyond their ability to form and release acetylcholine [17]. Otherwise, peripheral fatigue is breakdown of excitation-contraction coupling (ECC) within the muscle itself [18], where the muscle receives the proper motor commands but fails to contract at the desired level of force and consequently less joint torque.

Muscle fatigue occurs in multiple stages. During early 'high frequency' muscle fatigue, calcium release is actually higher than in the unfatigued state, but the muscle is less sensitive to it[19]. Later, calcium levels drop dramatically which becomes the

dominating factor. Further, a series of problems are also introduced by the accumulation of inorganic phosphate (P_i) generated from using ATP, including P_i (at high concentrations) and Ca^{2+} binding and dropping out of solution all together[19]. These mechanisms taken together form 'high frequency' muscle fatigue, which forms and recovers in the range of minutes. Prolonged activation can lead to 'low frequency' muscle fatigue, where the reduced force/torque can last hours or even days, and is believed to be related to the damage/breakdown and recovery of the proteins involved in generating contraction[20]. Our investigation in Chapter 4 will focus primarily on the calcium mechanisms in fast frequency fatigue.

Generally, fatigue is viewed in a negative light as a flaw in muscle. Interestingly, a 2018 review [19] points out that the breakdown of calcium dynamics that hamper muscle contraction may not be a failure of the muscle at all, but a feature to prevent the depletion of ATP during energetically demanding levels of muscle contraction. If ATP was significantly depleted in the muscle, a series of catastrophic failures would occur [19]: actin/myosin cross bridging would cease to cycle and remain locked in rigor, Ca^{2+} pumping would cease and lead to an uncontrolled release in cytolic Ca^{2+} levels, and likewise Na^{+}/K^{+} gradient pumps would fail leading to a breakdown of action potential propagation down the sarcolemma and the inability to excite muscle fibers entirely. This should inform the strategy of EMS stimulation, not to minimize the disruption Ca^{2+} dynamics while maintaining the same amount of muscle activation (and ATP consumption), but to attempt to minimize the metabolic cost of activation all together. Successfully activating muscles continuously without this negative feedback could

indeed lead to this breakdown of the muscle electrophysiology and contraction dynamics all together due to the depletion of ATP. The optimal strategy if possible, minimizing metabolic cost, would ideally avoid disrupting Ca^{2+} dynamics by making the mechanism unnecessary rather than disabling this feedback and powering through contractions without it.

Natural Muscle Recruitment vs EMS

The recruitment pattern (order, frequency, and timing) are very different between natural activation and EMS induced activation. During voluntary muscle contraction, motor units are activated asynchronously [21], providing intermittent resting periods for muscle fibers, with a discharge rate proportional to the desired level of contraction [22]. However, EMS elicits unnatural activation, recruiting many fibers simultaneously [11] proportional to the stimulus (based on pulse width and/or stimulus current) [23], without providing rest periods as with natural muscle recruitment.

In natural muscle recruitment, thinner slow twitch (and slower fatiguing) fibers are recruited first, before fast twitch (and fast fatiguing) fibers are recruited [24]. By relying on more slowly fatiguing fibers first, fatigue is minimized for normal activities. EMS stimulation, however, preferentially targets the thicker motor neurons which innervate fast twitch fibers, reversing the recruitment order and relying on the faster fatiguing fibers first [24]. Because the faster fatiguing fibers are recruited comparatively more, and the slower fatiguing fibers less, the overall fatiguing characteristics of the muscle favor faster muscle fatigue when compared to the natural recruitment pattern.

In natural recruitment, prolonged sub-maximal contractions can fatigue a subset of fibers, which can be compensated with the recruitment of additional fibers [25], [26]. To an extent, it is theoretically possible to do the same with EMS. However, the higher the stimulus, the faster the rate fatigue is produced, which limits the utility of recruiting additional fibers.

Further, there are gender-based differences in muscle fatigue and fatigue recovery with males fatiguing more and taking longer to recover [27]. This could be due to higher intramuscular pressure during contraction leading to less perfusion in males [27], and it has been shown that testing females in ischemic conditions eliminates the gender discrepancy in fatigue rates [27].

Current Technology for Estimating Muscle Activation and Fatigue

Surface Electromyography

Surface electromyography (sEMG) is the current gold standard in measuring muscle activation and detecting muscle fatigue. sEMG works by recording electrical signals created by muscle via skin mounted electrodes. From there, a series of electronics, filters, and digital signal processing techniques convert these electrical signals into a form that can be interpreted by a medical professional or a machine, such as a prosthetic device. This process works because muscles create electrical signal when they activate (recall, there is a prolonged calcium release that drives the actin/myosin cross bridge cycling).

Detecting and quantifying muscle force/fatigue through indirect, noninvasive means has been a topic of study since at the 1950's [26]. Surface electromyography

(sEMG) is currently the gold standard for noninvasively measuring electrical activity from muscle, which is used across a wide variety of applications from controlling powered prosthetics to biomechanics and motor control research. sEMG electrodes placed on the skin can record the electrical activity generated by contracting muscles beneath. However, sEMG lacks depth resolution and suffers from poor SNR [28]. Despite its limitations, sEMG can be used in certain situations to detect muscle fatigue from voluntary contraction. For instance, submaximal voluntary contraction generates progressively greater electrical activity as the muscle fatigues, which is likely from increased fiber recruitment to compensate for partial fatigue [25], [26], [29]. This can be somewhat limited for detecting fatigue because the subject is only activating a subset of motor neurons and can therefore compensate for fatigue by generating additional efferent muscle commands to recruit additional, unfatigued fibers to assist. Although higher sEMG signal amplitude can be a sign of fatigue, this is because sEMG becomes increasingly decoupled with muscle activation. Unlike submaximal contraction, a maximum voluntary contraction recruits as many fibers as possible and cannot recruit additional fibers to compensate for fatigue. Specifically, at maximum voluntary isometric contraction (MVIC), measured force will drop with time but the high amplitude sEMG signal will remain essentially constant [30]. One implication of this is that sEMG amplitude alone would have trouble differentiating between a fatigued muscle maintaining a lower force by recruiting additional fibers and an unfatigued muscle maintaining greater force. For these reasons, detecting muscle fatigue with sEMG generally requires frequency analysis, which can be hampered by its intrinsically low

SNR and/or any external electrical interference. For this reason, sEMG frequency analysis is severely compromised when paired with EMS, as EMS can severely corrupt the sEMG signal with artifacts and may completely saturate the recording entirely. For comparison, EMS can be hundreds of volts [31] whereas the passive biological signal is less than 100 millivolts. It may be possible to use a non-causal filtering scheme to decode swamped sEMG signal between stimulation periods, but this is not truly real-time, and it is not possible at all if the signal saturated. Overall, sEMG is poorly suited for detecting muscle fatigue concurrently with EMS and another approach is necessary.

Human-machine interfaces designed to make physiological measurements span a huge range of invasiveness ranging from indirect contact (e.g. optical, electromagnetic) to requiring surgical implantation. Generally speaking, the more invasive, the more detailed or localized information the communication. Invasive, surgically implanted peripheral nerve electrodes can provide highly localized recordings or stimulation [5] and require significantly less current [32] compared to transdermal stimulation electrodes. However, implantable electrodes come at a cost, not only requiring surgery, but also the risk of infection, often lose quality and or fail completely over time [33], as well as lower stimulation thresholds for causing damage by exceeding the water window [32]. The implanted nature of these devices also runs the risk of becoming obsolete and creating a barrier for implanting newer technology should it become available and patients can be left with nonfunctional devices if the manufacturer goes out of business or abandons the product line as is the case with the Argus II epiretinal implants [34]. Because of the infection risks, immune rejection/electrode failures, surgical requirements, invasiveness,

and difficulty to change/remove if something goes wrong or if the manufacturer stops supporting the device or a newer better device comes along, not to mention the significantly high barrier to perform experiments required to develop the technology, it is difficult to justify an implanted device if there is a noninvasive, easily removable/replaceable alternative. Thus, I focused on noninvasive methods of both stimulating muscle and estimating muscle fatigue.

Alternative Methods for Monitoring Muscle Activation and Fatigue

It is important to note that direct measurements of muscle contraction strength in the literature come as either force (tension) or torque, and these are not necessarily interchangeable. It is generally not feasible to directly measure muscle force in humans because it requires isolating the muscle and tendons from the rest of the body. This is why direct muscle force measurements come almost exclusively from animal studies where muscles can be surgically isolated and measured. This is not to be confused with ground reaction forces or other measured applied forces such as when measured from a force plate/strain gauge. These are the *net* reactionary forces acting upon an outside body that can result from combinations of muscles, joint angles, gravity, etc. and are not direct measurements of the tension a muscle is producing. Human data is often reported as joint torque because high end commercial human dynamometers like the Biodex System 4 (Biodex Medical Systems, Upton, NY) or Humac Norm (CSMi Solutions, Stoughton, MA) are designed to directly measure rotational torque around isolated movement patterns. In isometric cases, where the length of muscle-tendon complex and joint angle

is fixed, force can be directly inferred from torque measurements if the muscle contracting is isolated.

Mechanomyography (MMG) is an umbrella term for a class of mechanical alternatives to sEMG, which record muscle mechanical activity like acceleration, velocity, displacement. Several variants exist from measuring muscle radial displacement (tensiomyography, TMG) [35], measuring movements with accelerometers [36], to passively recording soundwaves generated by muscle contractions (acoustic myography, AMG, also called phonomyography, PMG) [30], though some argue that AMG is distinct from MMG [37]. Because these techniques measure mechanical signals (as opposed to electrical signals), they provide a meaningful measure of active muscle contractions that is not dependent on ECC [30]. MMG should be significantly less susceptible electrical artifacts induced by EMS, and there have been recent advancements in the lab setting toward creating wearable, noninvasive muscle monitoring using MMG [38] and AMG [37]. These methods are promising, but they provide limited spatial resolution and like sEMG, lack depth resolution.

The Case Medical Ultrasound for Monitoring Muscle Fatigue

We believe that ultrasound imaging could have great utility in noninvasive fatigue monitoring and may address the issues and shortcomings of the other methods mentioned in the previous section. In this section, I will describe our motivation for using ultrasound to study muscle architecture and movements related to EMS induced muscle contractions, fatigue, and recovery.

What is Medical Ultrasound?

To understand the rational for using medical ultrasound in this dissertation, we must first discuss what ultrasound is and how is it used presently.

Brief Medical Ultrasound and Physics Overview

Ultrasound has long been used for noninvasive medical imaging in clinical practice. It gets its name from the fact that high frequency acoustic waves are inaudible, hence it is above hearing (ultra-sound). Acoustic waves are longitudinal compression waves (who vibrate along their direction of travel) that require a medium to propagate, unlike electromagnetic wave like light. Medical ultrasound specifically refers to measuring biological tissue rather than sensing an open space in the air or nondestructive testing like other forms of ultrasound.

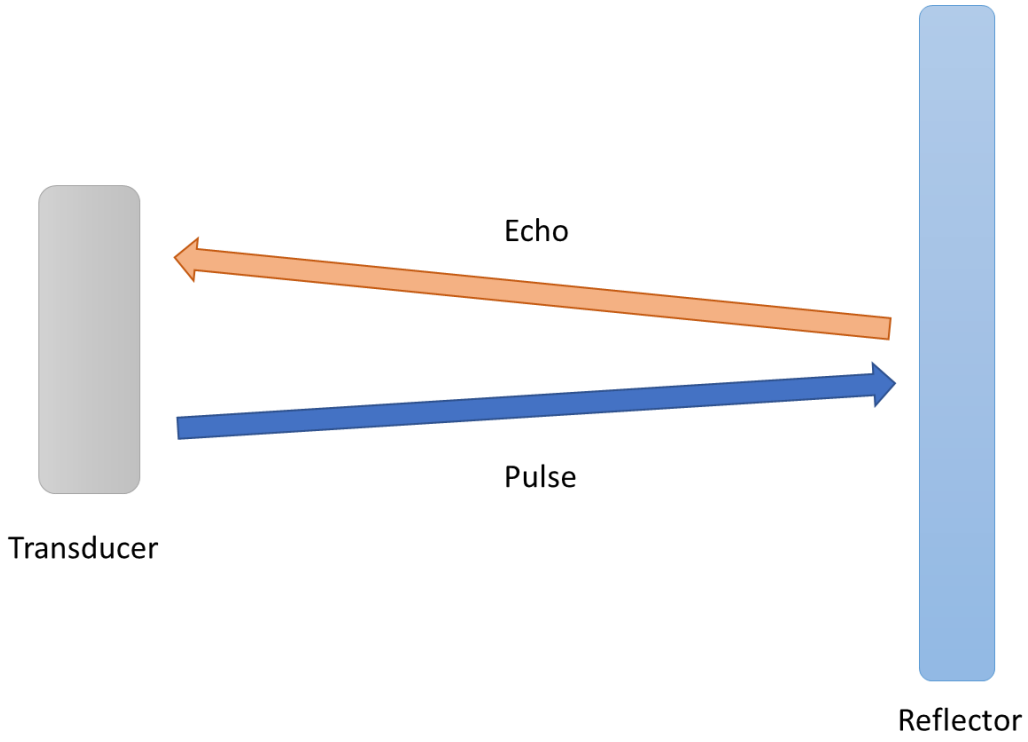

Figure 1-2. Schematic of an ultrasound transducer performing a simple pulse echo procedure.

In the simplest form of conventional brightness mode (B-mode) pulse-echo ultrasound imaging (Figure 1-2), an acoustic pulse of center frequency f_c and wavelength λ (Equation 2) is transmitted by a transducer, which then switches to a listening mode to record any reflected echoes. λ is also the resolution of the system, meaning no object smaller than λ can be resolved independently. If the speed of sound (c) in a medium is known, then we can tie the delay between the transmission and receive signals (τ) directly to the depth of the reflector (sometimes referred to as the 'range' in other modalities) by Equation 3. Note the divide by two to account for the wave having to travel both to and from the transducer. From there, additional beams are transmitted, received, and processed as scan lines to form an image. The image can be used as a medical diagnostic or analyzed for information.

Equation 2. Wavelength Equation for Given Speed of Sound and Center Frequency

$$\lambda = \frac{c}{f_c}$$

Equation 3. Imaging Depth by Transmission and Reception Delay

$$depth = \frac{\tau * c}{2}$$

Medical Ultrasound and its Utility for Studying Muscle

Recently, medical ultrasound imaging has gathered more attention in research for numerous applications to quantify both nerve muscle architecture and activity. These have included estimating muscle force and fatigue using muscle architecture like fiber pennation angle, cross sectional area, and tissue motion tracking [39]–[44], detecting passive and active muscle activation using fast M-mode or TDI approaches [45]–[47], and for controlling prosthetics [48]–[50], remotely modulating [51] and recording neural activity, either directly from scattering [52] or indirectly by increased blood flow [53], [54]. among others. Muscle activation also affects the acoustics of ultrasound propagation including speed of sound [55], [56] and echogenicity [57], [58], which have been used to estimate joint torque [59]–[62]. Muscle radius identified by ultrasound imaging has also been used as indicators of muscle force [41], [44] and fatigue [25]. Radial muscle velocity and velocity derivative metrics like strain and strain rate have shown promise in studying both muscle fatigue [42], [43] and muscle force [63]. Black box convolutional neural network techniques to predict joint torque from ultrasound images are also under development [64]. Ultimately US could provide a measure of muscle mechanics localized in three dimensions to subsections of individual muscles unlike MMG and like techniques or sEMG, with high SNR. Moreover, US could be used to compliment the electrical sensitivity of sEMG to measure excitation and activation separately.

Bringing it All Together

At present, there is still an open need for a wearable, reliable, real time muscle fatigue monitor that is compatible with EMS. We believe ultrasound could provide the solution. In this work, we test the hypothesis that Doppler ultrasound is sensitive to mechanical signs of muscle fatigue which will serve as the foundation for a wearable fatigue monitoring system.

This chapter has centered around the big picture problems we wish to address, EMS and its drawbacks, brief overviews on muscle physiology, current technology for studying muscle fatigue, and the case for using medical ultrasound as a muscle force and fatigue monitor. The subsequent chapters will focus on our hypotheses and the experiments we performed to help understand and interpret the observed muscle performance (Chapters 2 and 3) and how this can inform muscle dynamic system modeling (Chapter 3) to help us better predict muscle function for real world us such as closed loop electrical muscle stimulation applications like closed loop EMS exercise or shared robotics controls. Finally, it concludes with an interpretation of the main findings if this study and potential investigational paths for future work.

CHAPTER TWO: TOWARDS A WEARABLE MONITOR OF LOCAL MUSCLE FATIGUE DURING ELECTRICAL MUSCLE STIMULATION USING TISSUE DOPPLER IMAGING

Joseph A. Majdi,[1,2] Samuel A. Acuña,[1,2] Parag V. Chitnis,[1,2] and Siddhartha Sikdar[1,2]*

[1]Department of Bioengineering, George Mason University, Fairfax, VA, USA

[2]Center for Adaptive Systems of Brain–Body Interactions, George Mason University, Fairfax, VA, USA

*Corresponding author: ssikdar@gmu.edu

At the time of this dissertation submission, this work was submitted and accepted to the Wearable Technology journal [65]. I would like to thank Samuel Acuña for his assistance with statistical analysis, figure design, and manuscript revisions.

ABSTRACT

Introduction/Aims:

Electrical muscle stimulation (EMS) is widely used in rehabilitation and athletic training applications to generate involuntary muscle contractions. However, this stimulation leads to rapid muscle fatigue, which limits the amount of force a muscle can produce over prolonged use. Stimulation protocols would benefit from methods that monitor localized muscle fatigue and recovery, but most approaches to assess muscle fatigue are either incompatible with electrical stimulation (e.g., surface electromyography, sEMG) or cannot be used on freely moving subjects. Ultrasound is an alternative modality that has previously shown potential for monitoring fatigue. The

purpose of this study was to examine whether Doppler ultrasound imaging can assess changes in stimulated muscle twitches that are related to muscle fatigue from electrical stimulation.

Methods:

We stimulated isometric muscle twitches in the medial and lateral gastrocnemius using isolated, biphasic pulses in healthy subjects. Tissue Doppler imaging (TDI) of medial gastrocnemius muscle recorded tissue velocities before and after a 60-second EMS protocol designed to elicit fatigue. We extracted features of the average muscle tissue velocity waveforms during muscle twitch and compared them to the isometric ankle torque before the stimulation and during recovery.

Results:

Features of the average tissue velocity waveforms changed following the fatiguing stimulation protocol (*peak velocity*: decreased by 38%, $p = 0.022$; *time-to-zero velocity*: increased by 8%, $p = 0.050$) in 13 subjects. We observed that the tissue velocity features showed a return towards baseline during the rest period for five stimulated muscle twitches following induced fatigue. The normalized *peak velocity* significantly increased from the first muscle twitch to the fifth (+23%, $p = 0.022$, $d = 1.413$) muscle twitches. The normalized *peak tissue strain rate* significantly increased from the first muscle twitch to the fifth muscle twitch (+14%, $p = 0.011$, $d = 1.118$). This pattern was similar to that of the normalized ankle torque, which significantly increased from the first to the fifth (+42%, $p < 0.001$, $d = 3.434$) muscle twitch. We also found that features of

the average tissue velocity waveform could significantly predict the ankle torque for each participant (R^2 = 0.255–0.849, $p < 0.001$).

Discussion:

Doppler ultrasound imaging can detect changes in muscle tissue during isometric muscle twitch that are related to muscle fatigue, fatigue recovery, and the generated joint torque.

Conclusion:

This work helps establish feasibility for using Doppler ultrasound to monitor muscle fatigue during EMS, and could be utilized for design of future wearable ultrasound feedback devices for fatigue monitoring.

Keywords:

Feedback devices; Performance characterization; Exoskeletons; Human-robot interaction

INTRODUCTION

Electrical muscle stimulation (EMS) is an increasingly popular approach to train, rehabilitate, and evaluate muscle contraction using electrical impulses. EMS (which encompasses both functional electrical stimulation and neuromuscular electrical stimulation) is widely used in a variety of applications, such as a strength training tool to improve athletic performance [66], [67], as a rehabilitative tool to improve motor function for individuals with motor deficits [4]–[7], [68], [69], and as a research tool to investigate muscular function in vivo [70], [71]. A typical EMS system generates patterns of electrical impulses and delivers them to muscle fibers via electrodes, which are commonly adhered to skin over the targeted muscle motor points. The target muscles involuntarily contract in response to the stimulation pattern, thus providing a user extensive control over the timing and amplitude of the generated induced muscle forces. However, most EMS systems use open-loop control of their stimulation patterns and fail to account for real-time changes in muscle performance, such as muscle fatigue.

Muscle fatigue, the decreased capacity of a muscle to generate force after exercise [72], is a primary consideration for EMS because stimulated muscles tend to fatigue very rapidly [9], [73], [74]. During voluntary muscle contraction, motor units are activated asynchronously [21] with a discharge rate proportional to the desired level of contraction [22]. However, EMS elicits unnatural activation and discharge of the motor units, causing stimulated muscles to fatigue faster [75]. This remains a major limitation for many applications of EMS, such as during strength training [76] or physical rehabilitation [9]. Further, without adequate rest to recover from fatigue, overworked muscles are at risk for

injury and lead to muscle soreness and pain [77]. Attempts to mitigate EMS-induced muscle fatigue often involve spatially distributing the stimulation [73], [78], [79] and modifying the stimulation parameters (e.g., timing and waveforms) [80], [81]. However, these open-loop approaches do not attempt to evaluate or characterize the induced muscle fatigue throughout the stimulation protocol. EMS protocols would greatly benefit from methods to monitor muscle fatigue and recovery within individual muscles.

Due to the ease of implementation and abundance of signal features, surface electromyography (sEMG) has emerged as the primary method to assess localized muscle activity and fatigue [25], [26], [29], [82], [83]. However, sEMG is poorly suited for monitoring muscle fatigue during EMS because in addition to interference and crosstalk from adjacent muscles, sEMG is extremely sensitive to electrical interference [84]. sEMG records electrical activity during muscle contraction via electrodes placed on the skin, which are by necessity near the electrodes used in EMS. EMS impulses can severely corrupt the sEMG signal with artifacts [85]. For example, EMS can deliver impulses on the order of 100 V while sEMG attempts to record muscle signals that are on the order of <100 mV with an inherently low SNR. Although advanced signal processing methods to remove stimulation artifacts from sEMG signals are emerging [86]–[88], working with sEMG signals during EMS has remained challenging. Thus, muscle fatigue monitoring during EMS would greatly benefit from a robust alternative to sEMG.

Various non-invasive techniques have attempted to quantify localized muscle fatigue using methods that are not as susceptible to electrical interference [29], such as mechanomyography [89], near-infrared spectroscopy [90], and sonomyography [58].

Mechanomyography can be considered the mechanical equivalent of sEMG by recording low-frequency (i.e., 2-200 Hz) surface vibrations produced by muscle fibers during contraction [91], but it has limited utility due to its sensitivity to acoustic/vibrational interference during movement [92]. Near-infrared spectroscopy can provide a measure of oxygenation in a fatiguing muscle but is also very sensitive to movement and is therefore mainly used as additional information to complement sEMG [29], [93]. Sonomyography uses ultrasound imaging to describe localized morphological changes in muscle and remains an active area of research [28], [29], [48], [94], [95]. Ultrasound imaging is a common, non-invasive clinical tool compatible with EMS and has shown utility for quantifying muscle architecture [46], [50], [96], mechanical activation [28], [40], [48]–[50], force [41], [56], [60], [61], and fatigue [25], [42], [43], [97]. Ultrasound imaging can also distinguish between deep and superficial muscles, whereas sEMG signals contain the summation of any electrical muscle activity beneath the electrode. Previous technical limitations (e.g. large form factor of hand-held ultrasound probes with tethered cables, need for custom holders to stabilize probes during ambulatory tasks, real time data processing and transmission, etc.) have inhibited its use in freely moving subjects, but recent developments have shown remarkable potential for wearable devices capable of sonomyography [48], [63], [98]. Thus, monitoring real-time changes in localized muscle fatigue during EMS might be possible using sonomyographic data.

Although sonomyography has typically been used to track muscle motion using B-mode (2 dimensional image sequences) and M-mode images (one scan line over time), tissue Doppler imaging (TDI) is another ultrasound mode for quantifying tissue motion

[95]. This approach extracts tissue velocities and associated metrics such as strain rate by measuring the phase shift of the ultrasonic reflections in rapid (kHz) succession. Unlike computationally intensive post-processing motion analyses like speckle tracking using B-mode images, RF data, analytical signals etc. [42], [96], TDI can quantify local tissue velocities in real time with sub-mm detail with conventional Doppler processing methods. TDI has proven to be very sensitive to the motion of myocardial structures, and thus this approach is commonly used clinically to assess myocardial dysfunction [99]. However, only a few studies have explored using TDI to assess the dynamic functions of skeletal muscle [100], [101]. For example, TDI can reliably detect the mechanical onset of muscle activity [45]. TDI can also distinguish muscle contraction from passive muscle motion [47]. However, the use of TDI to quantify changes to skeletal muscle experiencing fatigue due to EMS remains unexplored.

Our ultimate goal is to develop a wearable, real-time monitor of EMS-induced muscle fatigue to characterize time-varying EMS/muscle performance. Our overarching hypothesis is that TDI is sensitive to the mechanical signs of muscle fatigue during EMS and has potential to monitor muscle fatigue and recovery in real time. As a first step, the purpose of this study was to examine whether TDI can assess changes in stimulated muscle twitches that are related to muscle fatigue from electrical stimulation. We used TDI to extract gastrocnemius muscle tissue velocities during isometric muscle twitches before and after a fatiguing EMS protocol. We first hypothesized that muscle tissue velocities during stimulated muscle twitches would decrease after the fatiguing EMS protocol, and then gradually increase during fatigue recovery. Our second hypothesis was

that changes to the muscle tissue velocities would be related to increases in isometric muscle torque during fatigue recovery.

METHODS

Participants

We recruited healthy adults to participate in the study. The self-reported inclusion criteria were: 1) 18–60 years old, 2) able to consent and participate in this study, 3) able to walk independently, and 4) did not use a pacemaker or any other implanted electronic device. We excluded participants with any previous history of stroke, cerebral palsy, multiple sclerosis, or any other neuromuscular disorder. We also excluded participants with a history of cardiovascular disease, lower extremity surgery or injury, diagnosis of an unstable spine, unhealed limb of pelvic fractures, recurrent fractures, or osteoporosis. Any participants who currently had active pressure sores, open wounds, or an infection were also excluded. The experimental protocol was approved by the George Mason University Institutional Review Board, and each research subject provided written informed consent before participating in the study.

Experimental Setup

We performed our assessments of muscle fatigue on subjects instrumented with a Biodex II dynamometer (Biodex Medical Systems, Upton, NY) retrofitted with a Humac interface (CSMi Solutions, Stoughton, MA). Subjects were placed in either a prone or seated position with either their right or left leg fit into the Biodex, chosen at random by coin flip. The Biodex was configured such that subjects could perform isometric plantar flexion with the chosen leg. To prevent lateral ankle movement, the ankle was secured at

90˚ using a foot plate. For subjects in the prone position, we recorded the ankle torque from the Biodex using LabView (National Instruments, Austin, TX). For subjects in the seated position, we recorded ankle torque from a load cell (Futek Inc., Irvine, CA) affixed to the platform under the applied center of pressure.

Subjects were instrumented with a 38 mm wide L 14-5 MHz ultrasound probe with a center frequency of 6.66 MHz, attached to a SonixOne ultrasound system (BK Analogic, Richmond, BC) with a sample rate of 40 MHz, beamformed across 32 channels. The probe was placed as close as possible to the center of the muscle belly from the distal side of the medial gastrocnemius muscle belly (Figure 2-1). The probe was oriented over the muscle to allow for an optimal image of medial gastrocnemius fiber orientation. A custom 3D-printed mount held the probe perpendicular to the muscle, using a neoprene cuff secured around the calf. Ultrasound data was collected in the pulse-wave TDI mode. The upper and lower boundaries of the Doppler gate, which define the depths of interest along the TDI scan line (see Figure 2-1C), were set to cover the entire thickness of the medial gastrocnemius along the scan line at both rest and during voluntary flexion. We set the pulse repetition frequency to 10 kHz, but if the gate depth was small enough to permit the buffer to use a higher pulse repletion frequency (PRF), we increased the frequency to 12.5 kHz. Due to memory limits on the ultrasound machine, we chose not to image regions of the soleus. We also did not account for soleus activation or movement because the gastrocnemius has distinct innervation zones from the soleus and thus could be activated independently during stimulation [102].

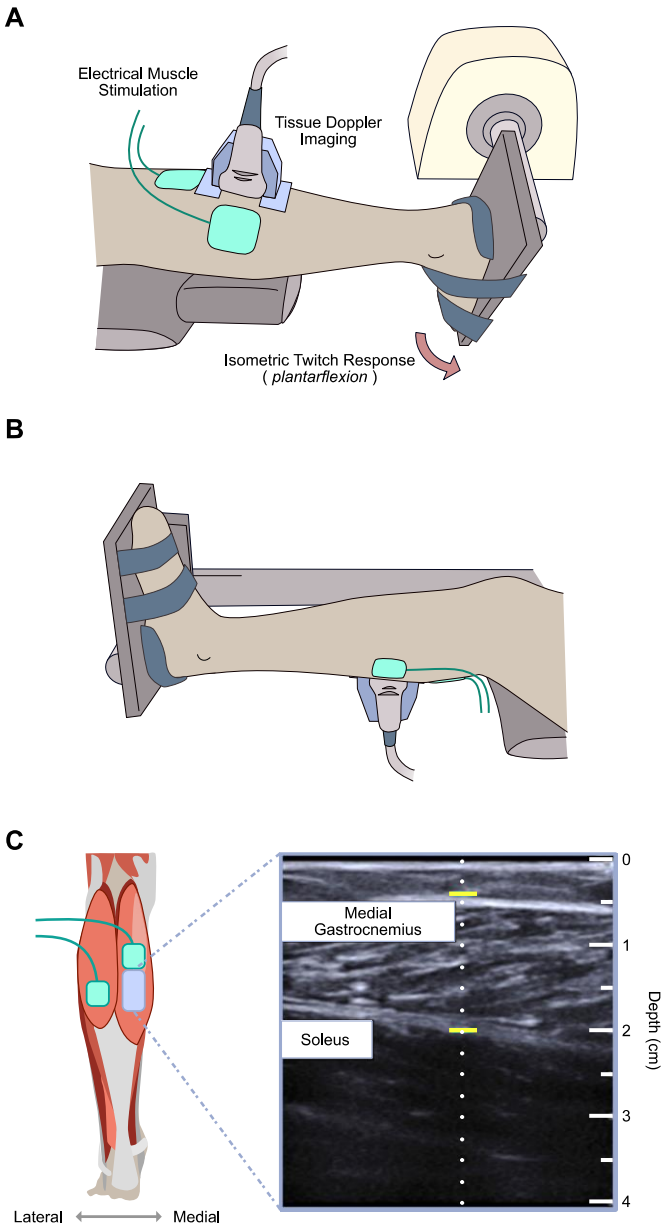

Figure 2-1. We used tissue Doppler imaging to examine gastrocnemius muscle tissue velocities during stimulated isometric muscle twitches before and after electrical muscle stimulation. Our experimental setup for (A) participants in a prone position and for (B) participants in a seated position. (C) An example longitudinal view B-mode ultrasound image of the medial gastrocnemius used during placement and orientation of the ultrasound probe. We adjusted the probe to create an optimal image of gastrocnemius muscle fibers. The thin dotted line in the middle of the B-mode image represents the scan line (where the beam is directed during the rapid TDI pulsing). The two horizontal yellow lines define the gating depth (i.e., the zone measured) and were set to cover the gastrocnemius muscle tissue. The major tick marks to the right of the image represent 1 cm, with minor tick marks at the 0.5 cm midpoints. The total image is just over 4 cm deep and 3.8 cm wide.

We placed two electrodes for an EMS system (Rehastim2, Hasomed GmbH, Magdeburg, GE) over the heads of the gastrocnemius in accordance with the manufacturer's guidelines (Figure 2-1). The first electrode was placed over the medial gastrocnemius proximal to the ultrasound probe (at approximately the middle of the muscle belly). The second electrode was placed over the distal end of the lateral gastrocnemius. We stimulated both heads of the gastrocnemius to minimize unnatural lateral shifting of the muscle belly. We controlled the EMS system using a custom Matlab/Simulink interface (MathWorks Inc., Natick, MA).

Experimental Protocol

We established a normalized stimulation intensity (I_{20}) for each subject. First, we instructed subjects to generate a maximum voluntary isometric contraction (MVIC) during plantar flexion. We then electrically stimulated the gastrocnemius with pulse trains of increasing current (starting from 5mA) until we determined the current necessary to stimulate the gastrocnemius to produce an isometric ankle torque at 20% of the MVIC torque (I_{20}). All EMS used biphasic, constant current pulses with 100 μs pulse width per phase and 100 μs delay between phases. Fatiguing stimulation used 50 Hz pulse trains (20 ms main pulse interval) whereas muscle twitch stimulation used individual pulses.

We then recorded ankle torque and TDI muscle velocity during electrically stimulated muscle twitches before and after a fatiguing EMS protocol (Figure 2-2). We first established baseline (i.e., pre-fatigue) muscle twitch behavior by stimulating the

gastrocnemius at least five times with single pulses at the stimulation intensity I_{20}. Subjects then received a time varying stimulation train intended to emulate cyclic stepping and induce muscle fatigue, lasting a total of 60 seconds per fatiguing period. The stimulation train included 60 cycles (i.e., 60 steps). For each stimulation cycle, current was ramped up from zero to I_{20} over 0.12 s, held at I_{20} for 0.5 s, and then ramped down to zero for 0.12 s, followed by 0.26 s rest, for a total period of 1 s. After the fatiguing stimulation train, we assessed muscle twitch as the muscle recovered by electrically stimulating the medial gastrocnemius with single pulses at stimulation intensity I_{20} approximately once every 20 s over two minutes of rest. Due to memory limits of the ultrasound machine, we could only record for approximately 3 to 5 s at a time depending on the size of the Doppler gate (which depended on the thickness of the muscle measured) and pulse repetition frequency, plus approximately 10 s to save.

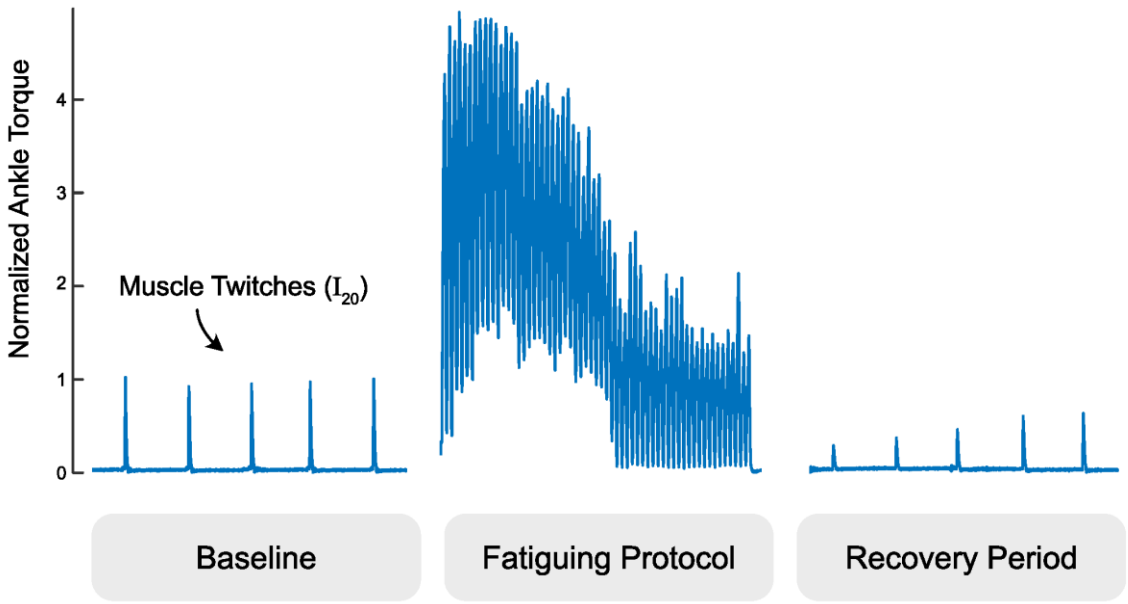

Figure 2-2. We examined tissue Doppler images before and after a fatiguing stimulation protocol pictured. The gastrocnemius is intermittently twitched to establish a baseline, intentionally fatigued with a one minute electrical muscle stimulation protocol, and intermittently twitched during a period of at least two minutes to evaluate fatigue recovery. Ankle torque is normalized to the average of the pre-fatigue twitch values and times are scaled for easier viewing.

After we started collecting data using the fatiguing EMS protocol, we decided to examine how the TDI muscle velocities might change after multiple rounds of the fatiguing EMS protocol. For the subjects recruited after this decision was made, we included four additional rounds of the fatiguing EMS protocol separated by two-minute periods for rest.

Data Analysis

For each TDI imaging period, we generated the average TDI velocity waveform over the thickness of medial gastrocnemius tissue (i.e., across the Doppler gate) using an autocorrelation method [103]. Briefly, TDI is collected as a beamformed scanline

acquired in rapid succession (kHz range). Scanlines are converted to their complex in-phase and quadrature components via a Hilbert transform, and an estimate of velocity is determined by comparing the relative change in phase angle between pulses via conjugate multiplication for every sample along the imaging depth defined by the Doppler gate. Using the change in phase angle vector ($\emptyset$), the velocity (v) for a given time (t), pixel depth (d), and period between pulses (T) can be calculated with the following equation:

Equation 4 TDI Velocity

$$v(t,d,T) = \Delta\theta(t,d,T) * \frac{c}{\mathbf{4}\pi f_c T}$$

where c is the speed of sound and f_c is the center frequency of the transducer. Note that T can either be the pulse repetition period (the inverse of the pulse repetition frequency), or an integer multiple thereof in the case of adding a delay to emphasize lower frequencies. The resulting velocity field image is similar to an M-mode image, except each data point reflects the estimated velocity at a given depth and time point, rather than echo intensity. The data were downsampled to 1 kHz to emphasize low tissue velocities, and then averaged across depth to create a 1D velocity waveform for further analysis.

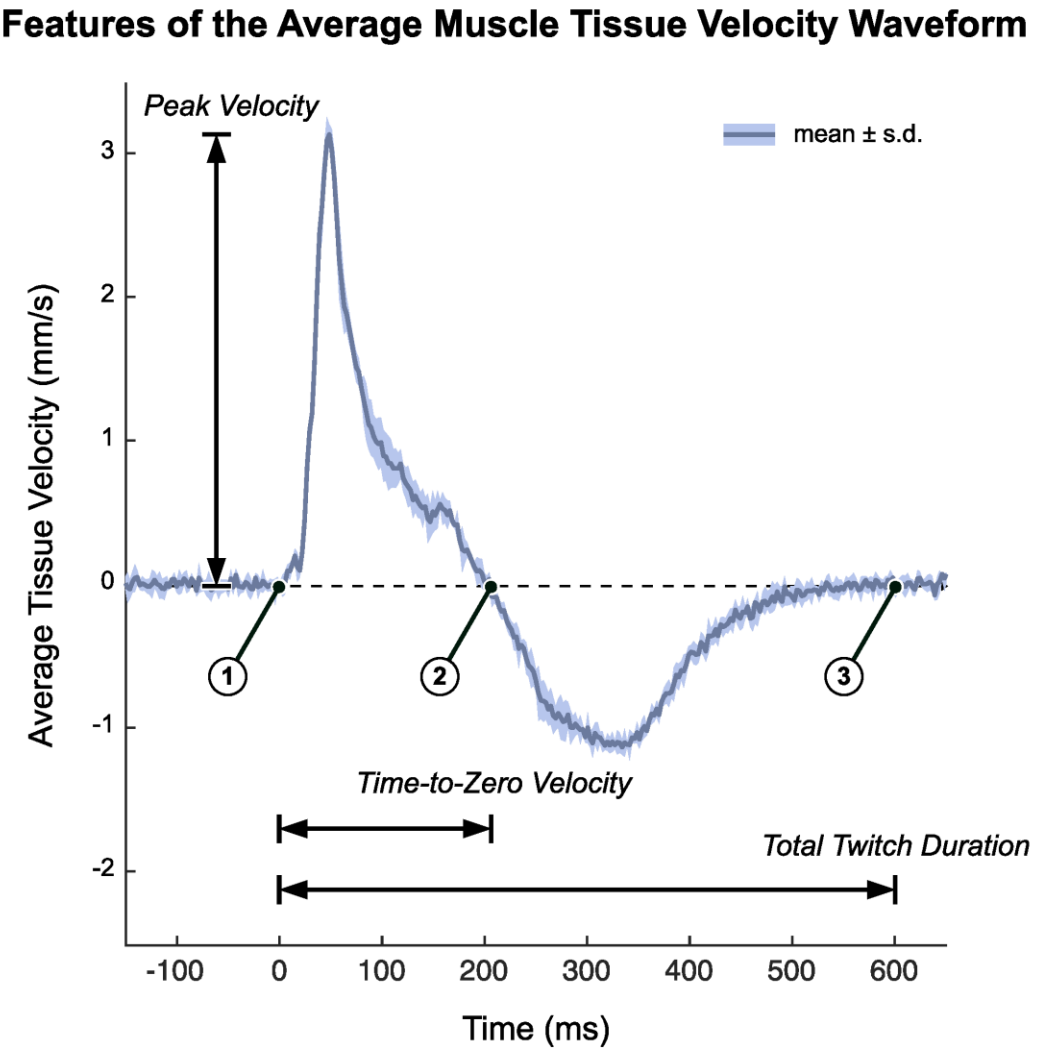

Figure 2-3. We quantified tissue Doppler imaging during a stimulated muscle twitch by extracting key features of the average muscle tissue velocity waveforms. Time point 1 is the onset of muscle twitch, time point 2 is the zero-crossing of tissue velocity waveform, and time point 3 is the end of muscle twitch. Several waveform features were used in this analysis. Time-To-Zero velocity is defined as time point 2 minus time point 1. We interpret this as the period of net expansion along the cross section of the muscle during a muscle twitch. Total twitch duration is defined as time point 3 minus time point 2. Peak Velocity is the maximum absolute velocity during the initial expansion phase (from time point 1 to time point 2). The Peak Velocity-Time Integral (Peak VTI) is the integral of the average tissue velocity waveform, whose peak occurs at time point 2 (Peak VTI is not shown on the figure). Data plotted as the mean ± standard deviation of the recorded tissue velocities of a representative twitch response (pre-fatigue).

Average velocity waveforms were manually divided into three time points: 1) the onset of muscle twitch, 2) the zero-crossing of tissue velocity (i.e., from positive to

negative velocity or vice versa), and 3) the end of muscle twitch (i.e., when the velocity returns to zero). For the end point (point 3), spectral entropy [104] with a 164 sample window and cutoff of -0.7 was used to help guide the manual segmentation. During the first time interval, the velocity profile represents a net velocity measured through the muscle thickness which we interpret as the time during which the muscle undergoes net cross sectional expansion. Conversely, we interpret the second time interval as the time during which the net expansion stops and the musculotendon unit passively contracts to baseline which necessarily is of opposite sign as the expansion period. Several features were then extracted from the average tissue velocity waveforms (Figure 2-3). The *peak velocity* was calculated as the maximum absolute velocity during the net (active) cross sectional expansion (i.e., between the first and second time points). The *time-to-zero velocity* was calculated as the difference between the first and second time points. The *total twitch duration* was calculated as the difference between the first and third time points. The *peak velocity-time integral* (*VTI*) was calculated as the maximum value of the integral of the average velocity waveform, which occurs at the second time point, and represents the accumulation of net cross section velocity as the muscle expands and releases. Unlike *peak velocity*, which depends on the fibers firing in synchrony, we believe the *peak VTI* to record the cumulative effects of fibers firing and more robust to any variations in electromechanical delay in the fibers. We also approximated the *peak tissue strain rate* by first smoothing the pixel-by-pixel velocities using a 1.925 mm (100-sample) moving average and then calculating the average spatial gradient over the depth of the gating window (which varied by subject). In nonisometric conditions, the muscle

body could possibly shift towards or away from the probe as the lever arm changes. We believe that *peak tissue strain rate* would in theory be more robust than *peak velocity* in these conditions and should perform similarly in isometric conditions because the lever arm is fixed.

Statistical Analysis

To test our first hypothesis, we compared the features of the tissue velocity waveforms before and after the first fatiguing EMS protocol. We collected data for five stimulated muscle twitches before and after the fatiguing protocol. We then normalized the data to their average pre-fatigue value (i.e., baseline). To assess any initial changes after the fatiguing protocol, we first compared the pooled pre-fatigue features with the features extracted during the first stimulated muscle twitch using paired t-tests. To assess subsequent changes to these waveform features, we then used a repeated measures analysis of variance (rmANOVA) to compare the features extracted over the five muscle twitches following the protocol. We confirmed assumptions of normality using a Shapiro–Wilk test. When we found significant differences, we focused post-hoc comparisons on changes from the first muscle twitch using paired t-tests with a Holm-Bonferroni correction. Because changes to the waveform features over time might present a subtle pattern of recovery that is not readily captured by an rmANOVA, we also attempted to fit a monotonically increasing trend to the waveform features over time. We chose to use a power regression model, $\ln(y) = \ln(b_0) + b_1 \ln(x)$, to depict a trend because this model exhibited the best fit to our data (e.g., highest R^2 values) when compared to the other curve fitting models we considered (e.g., linear, logarithmic,

exponential, etc.). For the subset of participants who completed the four additional rounds of the fatiguing protocol, we also examined any patterns of recovery after each round by attempting to fit a trend to the resulting waveform features over time.

To assess if and how the waveform features might change over multiple rounds of the fatiguing protocol, we averaged the normalized feature values following each round (five twitches per round) for the subset of participants who completed the four additional rounds. An rmANOVA tested for differences in these pooled features over the five total rounds. We confirmed assumptions of normality using a Shapiro–Wilk test. When we found significant differences, we focused post-hoc comparisons on changes from the first round using paired t-tests with a Holm-Bonferroni correction.

To test our second hypothesis, we examined the relationship between the torques generated during stimulated muscle twitches and the features of the tissue velocity waveforms. We computed a stepwise multiple linear regression model with the recorded ankle torque as the dependent variable, and the features of the tissue velocity waveforms as covariates. Starting with a constant model, the waveform features were added ($p < 0.05$) and removed ($p > 0.10$). Stepwise linear regression iteratively updates a regression model to combine and remove variables systematically to eliminate highly correlated variables and statistically insignificant variables to ensure the data only contains variables with only useful, unique information. To account for any between-subjects variability in the data, we did not normalize the extracted waveform feature values and chose to calculate a separate stepwise regression for each participant. For the participants who completed the four additional rounds of the fatiguing EMS protocol, we

included features values from muscle twitches over the five total rounds in their regression analysis.

We performed the statistical analyses using JASP Version 0.16 (JASP Team, Amsterdam, NL) and SPSS Version 27.0 (IBM Corp., Armonk, NY), and defined significance a priori as $p < 0.05$.

RESULTS

We recruited thirteen participants (9 male, 4 female), and data from nine of these adults included four additional rounds of the fatiguing EMS protocol. We collected data from a total of 479 muscle twitches.

We confirmed the onset of fatigue following the first application of the EMS protocol (N = 13 participants), in which the normalized ankle torque was significantly reduced during the first stimulated muscle twitch (-38%, $p < 0.001$, Cohen's $d = 2.367$) and then recovered over subsequent muscle twitches (Fig. 4). The normalized ankle torque significantly changed over the five muscle twitches ($F = 28.845$, $p < 0.001$, $\eta_p^2 = 0.828$). Normalized ankle torque significantly increased from the first muscle twitch during the second (+19%, $p = 0.002$, $d = 1.561$), third (+31%, $p < 0.001$, $d = 2.575$), fourth (+41%, $p < 0.001$, $d = 3.354$), and fifth (+42%, $p < 0.001$, $d = 3.434$) muscle twitches. Throughout the five muscle twitches during the recovery period, the normalized ankle torque exhibited a monotonically increasing trend that fit a power regression model ($b_0 = 0.614$, $b_1 = 0.236$; $F = 14.504$, $R^2 = 0.305$, $p = 0.001$).

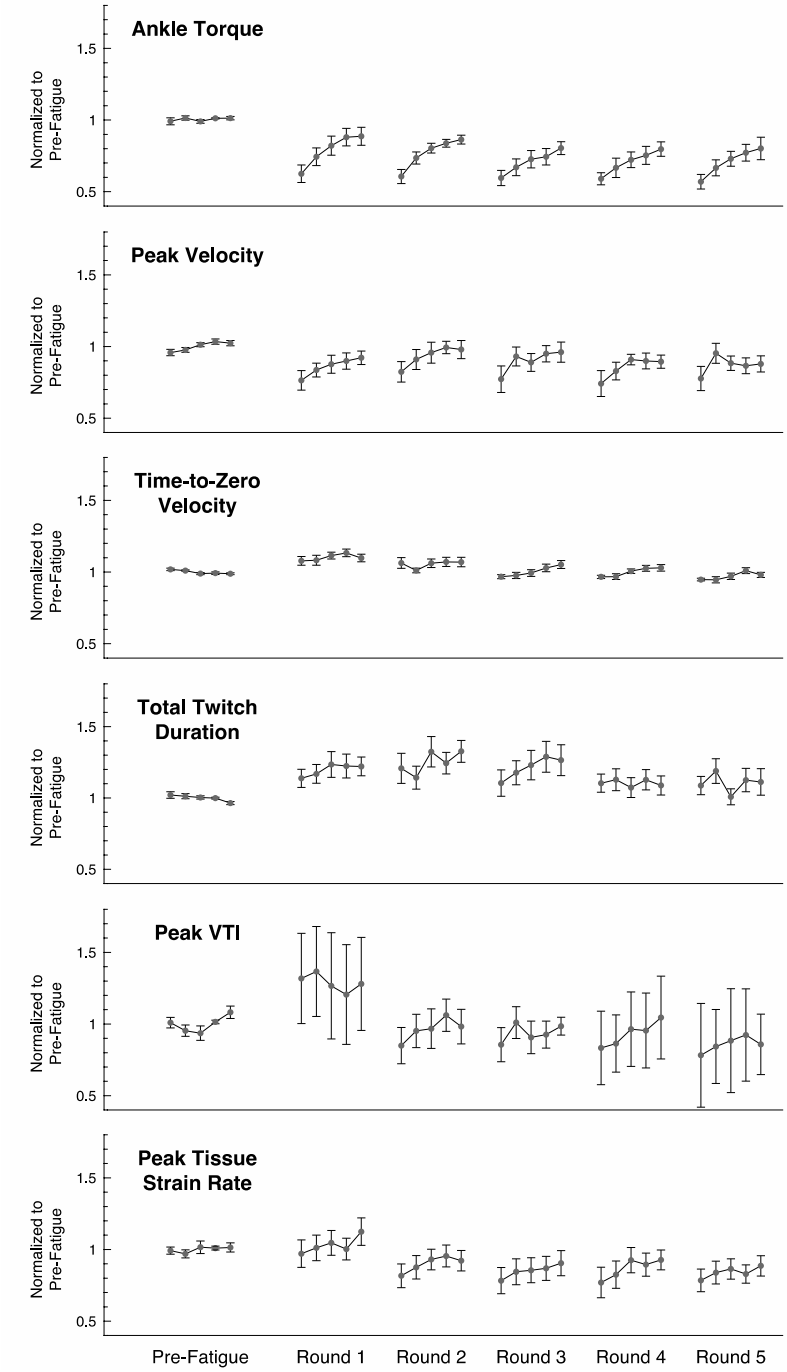

Figure 2-4. The ankle twitch torque and extracted features of the average muscle tissue velocity waveforms after repeated rounds of the fatiguing stimulation protocol, all normalized to their average pre-fatigue value. Data plotted as mean ± standard error. Data for 13 subjects are included in the plotted values for pre-fatigue and round 1; data for 9 subjects are included in the plotted values for rounds 2 through 5. Note that round 1 refers to the initial application of the fatiguing stimulation protocol, and not the first repetition of the fatiguing stimulation protocol. VTI: Velocity-Time Integral.

We found evidence that normalized features of the tissue velocity waveforms also changed following the fatiguing EMS protocol for the 13 participants (Figure 2-4). The average feature values generally appeared to follow a similar pattern to the changes in ankle torque, in which the feature values gradually increased from the first stimulated muscle twitch during subsequent muscle twitches. The normalized *peak velocity* was significantly reduced from baseline during the first stimulated muscle twitch (-24%, $p = 0.022$, $d = 1.156$), and the rmANOVA revealed significant changes over the five muscle twitches ($F = 4.787$, $p = 0.007$, $\eta_p^2 = 0.489$). The normalized *peak velocity* significantly increased from the first muscle twitch to the fourth (+23%, $p = 0.022$, $d = 1.435$) and fifth (+23%, $p = 0.022$, $d = 1.413$) muscle twitches, but the values for the second ($p = 0.843$) and third ($p = 0.060$) muscles twitches were not significantly different. Similar to the normalized ankle torque, the normalized *peak velocity* exhibited a monotonically increasing trend that fit a power regression model. ($b_0 = 0.741$, $b_1 = 0.132$; $F = 4.328$, $R^2 = 0.119$, $p = 0.046$). The normalized *time-to-zero velocity* was significantly increased from baseline during the first stimulated muscle twitch (+8%, $p = 0.050$, $d = 0.671$), but the rmANOVA did not reveal any significant changes over the five muscle twitches ($F = 2.022$, $p = 0.115$), nor did the data exhibit a significant monotonically increasing trend ($F = 1.128$, $R^2 = 0.022$, $p = 0.293$). The normalized *total twitch duration* was not significantly different than baseline during the first stimulated muscle twitch (+14%, $p = 0.064$), the rmANOVA did not reveal any significant changes over the five muscle twitches ($F = 1.136$, $p = 0.355$), and the data did not exhibit a significant monotonically increasing trend ($F = 1.109$, $R^2 = 0.019$, $p = 0.297$). The

normalized *peak VTI* was also not significantly different than baseline during the first stimulated muscle twitch (+32%, $p = 0.202$), the rmANOVA did not reveal any significant changes over the five muscle twitches ($F = 0.061$, $p = 0.993$), and the data did not exhibit a significant monotonically increasing trend ($F = 0.211$, $R^2 = 0.004$, $p = 0.648$). The normalized *peak tissue strain rate* was not significantly different than baseline during the first stimulated muscle twitch (-3%, $p = 0.734$), but the rmANOVA did reveal significant changes over the five muscle twitches ($F = 3.954$, $p = 0.009$, $\eta_p^2 = 0.305$). The normalized *peak tissue strain rate* significantly increased from the first muscle twitch to the fifth muscle twitch (+14%, $p = 0.011$, $d = 1.118$), but the values for the second ($p = 0.999$), third ($p = 0.316$), and fourth ($p = 0.257$) were not significantly different. However, the data for the *peak tissue strain rate* did not exhibit a significant monotonically increasing trend ($F = 1.467$, $R^2 = 0.026$, $p = 0.231$).

For the subset of participants who completed five total rounds of the fatiguing EMS protocol (N = 9 subjects), the average waveform features exhibited a similar pattern of recovery after subsequent rounds (Figure 2-4). The normalized ankle torque during the recovery periods following each round all exhibited a monotonically increasing trend that fit a power regression model ($R^2 = 0.216–0.507$, $p < 0.010$). The normalized *peak velocity* also exhibited this monotonically increasing trend during the recovery periods after the first, third, and fourth round ($R^2 = 0.118–0.143$, $p < 0.046$), but not the second or fifth round ($R^2 = 0.040–0.087$, $p = 0.068–0.266$). The normalized *time-to-zero velocity* only exhibited a monotonically increasing trend that fit a power regression model during the recovery periods following the third and fourth rounds ($R^2 = 0.144–0.172$, $p < 0.019$),

but not after the first, second, or fifth rounds (R^2 = 0.007–0.092, p = 0.085–0.600). During the recovery periods after all five rounds, the data for the normalized *total twitch duration* (R^2 = 0.001–0.052, p = 0.119–0.925), *peak VTI* (R^2 = 0.004–0.089, p = 0.069–0.648), and *peak tissue strain rate* (R^2 = 0.007–0.092, p = 0.085–0.600) did not exhibit any significant monotonically increasing trends.

We did not observe strong evidence that waveform features would substantially change after multiple rounds of the fatiguing protocol (Figure 2-4). For example, the rmANOVA did not detect significant changes in the average normalized ankle torque over the five rounds (F = 1.506, p = 0.238, η_p^2 = 0.231). However, an rmANOVA did reveal that the average normalized *time-to-zero velocity* significantly changed across the five rounds (F = 17.461, p < 0.001, η_p^2 = 0.744). Post-hoc comparisons found that the average values from the second (p = 0.012, d = 1.310), third (p < 0.001, d = 2.080), fourth (p < 0.001, d = 2.402), and fifth rounds (p < 0.001, d = 2.846) were all significantly lower than the first round. Similarly, an rmANOVA revealed that the average normalized *peak VTI* significantly changed across the five rounds (F = 3.065, p = 0.036, η_p^2 = 0.338), but post-hoc comparison only found that the average values from the fifth round were significantly lower than the first round (p = 0.039, d = 1.205). The rmANOVA did not detect any significant changes across the five rounds for the average normalized *peak velocity* (F = 0.296, p = 0.877, η_p^2 = 0.056), the average normalized *total twitch duration* (F = 1.202, p = 0.332, η_p^2 = 0.147), or the average normalized *peak tissue strain rate* (F = 1.363, p = 0.272, η_p^2 = 0.163).

Table 1. Stepwise linear regression to predict ankle torque. Although we found that features of the velocity tissue waveforms could significantly predict the recorded ankle torque, the significant waveform features identified by stepwise regression were not consistent across subjects. (VTI: Velocity-Time Integral)

Model Terms	**Subject 1** (R^2 = 0.752)			**Subject 2** (R^2 = 0.849)			**Subject 3** (R^2 = 0.784)		
	Estimate	Std Error	*p*	Estimate	Std Error	*p*	Estimate	Std Error	*p*
Intercept	2.807	2.169	0.212	13.331	1.171	< .001	−6.400	3.119	0.052
Peak Velocity									
Time-to-Zero Velocity	61.29	8.307	< .001						
Total Twitch Duration							6.774	3.205	0.046
Peak VTI				52.114	4.159	< .001			
Peak Tissue Strain Rate							10.32	1.173	< .001

	Subject 4 (R^2 = 0.577)			**Subject 5** (R^2 = 0.477)			**Subject 6** (R^2 = 0.749)		
	Estimate	Std Error	*p*	Estimate	Std Error	*p*	Estimate	Std Error	*p*
Intercept	0.857	0.299	0.008	−35.046	10.616	0.002	−7.097	1.154	< .001
Peak Velocity				1.351	0.312	< .001			
Time-to-Zero Velocity				356.045	63.822	< .001	76.875	9.506	< .001
Total Twitch Duration				−13.134	3.739	0.001			
Peak VTI	1.912	0.315	< .001						
Peak Tissue Strain Rate				−8.026	3.427	0.024	2.596	0.266	< .001

	Subject 7 (R^2 = 0.666)			**Subject 8** (R^2 = 0.613)			**Subject 9** (R^2 = 0.255)		
	Estimate	Std Error	*p*	Estimate	Std Error	*p*	Estimate	Std Error	*p*
Intercept	6.193	1.192	< .001	1.232	1.897	0.519	5.08	1.454	< .001
Peak Velocity							3.654	0.828	< .001
Time-to-Zero Velocity				30.514	11.823	0.013			
Total Twitch Duration	6.168	0.809	< .001						
Peak VTI				−10.621	2.949	< .001			
Peak Tissue Strain Rate	2.805	0.618	< .001	10.944	1.168	< .001			

The stepwise linear regression analysis revealed that features of the velocity tissue waveforms could significantly predict the recorded ankle torque for each individual subject (Table 1). The fit of the regression models varied between subjects (N = 9 participants), ranging from $R^2 = 0.255$ to $R^2 = 0.849$ with a mean of $R^2 = 0.635$. We observed that the significant waveform features identified by the stepwise regression were not consistent across the nine participants. The *peak tissue strain rate* emerged as a significant predictor in five of the participant models, the *time-to-zero velocity* emerged in four of the participant models, the *peak VTI* and *total twitch duration* emerged in three participant models, and the *peak velocity* emerged in two participant models.

DISCUSSION

In this study, we examined whether TDI could assess changes in stimulated isometric muscle twitches that are related to muscle fatigue following EMS. We extracted features from the average medial gastrocnemius tissue velocities and found that the *peak velocity* and *time-to-zero velocity* during the first stimulated muscle twitch after a fatiguing EMS protocol had changed significantly from their pre-fatigue values. We also observed that the *peak velocity*, *time-to-zero velocity*, and *peak tissue strain rate* for five stimulated muscle twitches after the protocol followed the pattern of fatigue recovery exhibited by the isometric ankle torque. We also found that features of the average tissue velocity waveforms could significantly predict the ankle torque for each participant using stepwise linear regression (Table 1). We interpret these results to suggest that TDI can detect changes in muscle tissue during isometric muscle twitch that are related to muscle fatigue, fatigue recovery, and the generated joint torque. Thus, Doppler ultrasound approaches may have utility for monitoring changes to muscle fatigue during applications of EMS and could be considered in the design of future wearable ultrasound feedback devices.

Tissue Velocity Waveform Features Change After Fatiguing Protocol

In support of our first hypothesis, we found that features of the average tissue velocity waveforms during stimulated muscle twitches had significantly changed after the fatiguing EMS protocol. We used TDI ultrasound to measure features of the muscle tissue velocities, which can indicate muscle activation and release. We anticipated that velocity features would change after fatiguing the muscle because prior studies have

found that changes in muscle deformation detected via ultrasound are correlated to isometric output torques [105], [106]. This is understandable due to the varying number of fibers being activated, the nonlinear elastic stretching properties of the tendons in series with the contractile muscle elements [40], and the interaction of complex muscle geometries [15], [39], [107]. However, we only observed that the normalized *peak velocity* and normalized *time-to-zero velocity* exhibited any significant change from their pre-fatigue value. It may have been that a single round of our fatiguing EMS protocol was not sufficient to evoke detectable changes in the other waveform features, but they could be detected after experiencing an increased level of muscle fatigue. This may explain why subsequent rounds of the protocol exhibited waveform feature values drifting farther away from their pre-fatigue values (e.g., the *peak tissue strain rate*). We also observed that the *peak velocity*, *time-to-zero velocity*, and the *peak tissue strain rate* over the five stimulated muscle twitches exhibited a pattern of fatigue recovery similar to the ankle torque. Although not significant, we noticed that the other waveform features exhibited a generally similar pattern of gradual increase following a round of stimulation (Figure 2-4). Again, this pattern of fatigue recovery might be more prominent for the other waveform features after the muscle reaches a sufficient level of fatigue. For example, a pattern of fatigue recovery in the normalized *peak VTI* might not be fully revealed until after four rounds of the fatiguing EMS protocol. Considering that these velocity waveform changes manifested across subjects and throughout repeated rounds of the EMS protocol, we interpret our findings as compelling evidence that TDI has potential to quantify localized changes in muscle fatigue and recovery during EMS

applications.

We observed that the average *time-to-zero velocity* and *peak VTI* significantly decreased over five rounds of the fatiguing EMS protocol, but we did not detect a similar decrease in the average isometric ankle torque. We did expect subsequent applications of the fatiguing EMS protocol to elicit a gradual increase in overall muscle fatigue, but this was not reflected in the measured ankle torque. This suggests that TDI might have the sensitivity to detect quantifiable changes in muscle tissue related to localized muscle fatigue that are not as easily detected using a biomechanical assessment of joint torque, which provides only a gross measure of neuromuscular system output and contributes little insight into fatigue within an individual muscle [108]. Although the average *peak tissue strain rate* appeared to decrease over five rounds of the protocol, this overall decrease was not statistically significant. This might be due to fiber heterogeneity or boundary conditions affecting the approximated strain [43]. We also observed an increased variability in the normalized velocity waveform features compared to their pre-fatigued values, particularly for the *peak VTI* and *total twitch duration* (Figure 2-4). This might be due to individual subject differences in response to the EMS protocol. For example, some participants may have been more susceptible to muscle potentiation, in which a muscle becomes more sensitive to stimulation after a brief, intense activation [109], [110]. As potentiation and fatigue are both influenced by prior muscle activity but have opposing effects on muscle force production, it can be difficult to quantify either process independently and are thus thought to coexist after initiation of contractile activity [111], [112].

Tissue Velocity Waveform Features Predict Twitch Torque During Fatigue Recovery

In support of our second hypothesis, we found that features of the average muscle tissue velocity waveforms during twitch could predict changes in the isometric ankle torque. We were surprised to find that the tissue velocity waveform features identified as significant predictors in the regression were not consistent between subjects. We had anticipated that the *peak tissue strain rate* and the *peak VTI* would emerge as consistent predictors, because they result from net cross-sectional expansion (*peak tissue strain rate* being an indicator of the rate of change of muscle thickness robust to any muscle shifts due to lever arm movement and the *peak VTI* being dependent on the total change in muscle thickness which would be robust to the synchronicity of muscle fiber contractions). The observed between-subjects variability might have been due to anatomical and physiological variations such as in muscle fiber composition, activity level, resting foot progression angle, muscle thickness, length, stiffness, or motor points. We cannot exclude the possibility that our observed relationship between tissue velocities and ankle torque are dependent on the specific orientation and location of the transducer probe. The gastrocnemius is a pennate muscle and thus the tissue location we were measuring was inherently anisotropic. Complicating this further, the pennation angle of the muscle fibers changes during contraction (although it is possible that features related to the time-duration of muscle contraction may be more robust to variations in probe placement). Considering that muscle fiber length may vary with fatigue [113], we are encouraged that even our relatively simple measures of tissue velocities were sensitive to

the changes after EMS, and future studies should consider methods to overcome this between-subjects variability. The strength of this technique is that subject specific combinations of tissue velocity waveform features can still be used to accurately predict muscle twitch torque during fatigue recovery, despite the varying biological factors or experimental conditions such as probe placement. This is important because twitch torque has been found to mirror tetanic force fatigue levels during short durations (<5 minutes) of fatigue recovery [114], [115].

Practical Considerations and Potential Applications

The primary motivating factor for investigating ultrasound in EMS applications is that EMS is generally incompatible with the current gold standard for studying voluntary muscle activation, sEMG. This, however, does not limit ultrasound to EMS applications only. In fact, velocity and anatomical information provided by ultrasound is independent of, and complementary to, the electrophysiology information provided by sEMG, which means ultrasound could be used either with or in place of sEMG. Unlike sEMG, ultrasound measurements are depth-resolved, and therefore the specific muscle and its depth are identifiable. A phased array ultrasound beam can be steered, so the source of movement along different directions or depth within the imaging field can be localized. A limitation is that measurements are performed within the probe's field of view (generally a plane, or a single scan line), which can make it difficult when stimulating muscle groups that are spread farther apart than the field of view, and could possibly require multiple probes. Conversely, the data from an sEMG electrode are not depth-resolved, which means they cannot differentiate signals from multiple overlying muscles, making it

difficult to attribute components to their respective source(s). This is particularly a concern in EMS applications because the large stimulus artifacts produced by stimulation can severely corrupt the comparatively small signals generated by the muscle. Because ultrasound provides detailed physiological information without the same susceptibility to EMS artifacts, we believed that it would be an ideal candidate for EMS applications, such as hybrid EMS exoskeletons [58], [97], [116].

Our results support our overarching hypothesis that Doppler ultrasound imaging is sensitive to the mechanical signs of muscle fatigue during EMS. More specifically, our results suggest that TDI can detect changes in muscle tissue that are related to muscle fatigue, fatigue recovery, and the generated joint torque. The present study examined a single muscle undergoing isometric contraction due to EMS. Applications of EMS typically include limb movement involving multiple stimulated muscles, and future studies should consider the effect of these potential confounding factors on the recorded muscle tissue velocities. Future studies should also investigate the feasibility of using TDI to monitor changes in muscle fatigue during a fatiguing EMS protocol, instead of limiting the analysis to observed changes during recovery periods following an EMS protocol.

The potential for TDI to monitor muscle fatigue during EMS brings about unique opportunities in biomechanics, rehabilitation, and sports performance. EMS parameters such as timing, duration, and intensity are commonly controlled without any feedback from the targeted muscle [105], [117]–[119], though finding real time feedback to close the loop for human-robot interaction is an active area of research [116], [120]. By

integrating muscle fatigue as feedback, EMS protocols can be better refined to optimize the desired stimulation outcomes. This might be particularly useful for stimulating muscles effectively over a prolonged period, such as when using a powered exoskeleton coupled with functional EMS [121]. By gauging the level of fatigue recovery between bouts of EMS, stimulation could be limited to periods when the muscle has recovered enough to generate the sufficient torque. Measures of local muscle fatigue might also inform modifications to stimulation parameters (i.e., timing and waveforms), which may increase their effectiveness at reducing EMS-induced fatigue [10], [80], [81].

Desynchronizing stimulation across multiple sites can be used to mitigate EMS-induced muscle fatigue [11]–[13]; thus there is potential for TDI to inform stimulation strategies strategically applied to a set of muscles such that fatigued muscles have sufficient time to recover. There is also potential for TDI to optimize the application of EMS based on the spatial distribution of activated muscle fibers within a muscle. Electrode placement restricts which fibers are activated during EMS, and thus poor electrode placement can lead to accelerated fatigue in certain fibers while leaving other fibers underutilized [122]. Incorporating TDI to characterize EMS/muscle performance might help identify which muscle fibers are activated by certain electrodes to avoid redundant or underutilized placement that would over stimulate, over activate, and prematurely fatigue these fibers. Additionally, by using multiple stimulation sites across a muscle, stimulation protocols could be designed to minimize the demand on the local muscle fibers under each electrode while maintaining a net force from the muscle. Spatially distributed stimulation protocols might be also used to intermittently excite

subsets of fibers, which could mimic the natural rest and recruitment patterns of muscle fibers.

We envision future wearable feedback devices can use ultrasound to monitor EMS-induced muscle fatigue in real time. Wearable ultrasound is still an emerging technology [48], [98], and we are optimistic that other ultrasound approaches besides TDI may have utility to quantify muscle fatigue [58]. Although TDI provides robust and detailed velocity information, current implementations of TDI typically have high power requirements, impractically large physical forms, extensive computational and memory demands, and are thus generally unsuited for wearable applications. Nonetheless, this study of TDI to quantify muscle fatigue provides a proof of concept that can inform the design of more accessible ultrasound approaches, like continuous wave Doppler imaging [123], which may better serve as the foundation for a real-time, wearable ultrasound system to monitor muscle fatigue. Continuous wave systems can provide velocity estimates from a predefined focal depth. Further, multiple transducers with distinct center frequencies can be used in an array with multiple focal depths to gather depth resolved velocity information, all significantly reduced memory requirements, power consumption, and sample rates. We are particularly encouraged by the development of frequency-modulated continuous wave (FMCW) ultrasound techniques based on FMCW Doppler radar that might provide low-power, depth-resolved velocity waveforms using a single transducer [124], [125].

Study Limitations and Future Directions

The study has some limitations to consider. First, the stimulated muscle twitches

were assessed during a two-minute rest period at an interval of 20 seconds. While the data collected were sufficient to demonstrate the potential of assessing fatigue after EMS, further research is needed to assess how the TDI velocity features may change within shorter time windows (i.e., < 20 s) or during longer recovery periods (i.e., > 2 min). Second, the biomechanical measures of ankle torque in this study represent a measure of the net torque generated at the ankle joint. We stimulated the two heads of gastrocnemius to generate this torque, but only collected Doppler ultrasound images for the medial gastrocnemius. Further work is needed to decompose the individual muscle contributions to the net ankle torque when considering localized measures of muscle fatigue. Third, we did not analyze the effect of subject positioning (prone vs seated). However, our analysis methods did help to mitigate a potential effect of positioning. Whenever we compared values across subjects, we used normalized values so that any observed changes were relative to their pre-fatigue values. During the regression analyses, we did not pool the subject's data together and instead calculated an individual regression for each subject, which kept any positioning effect consistent for that subject. Fourth, because muscle fatigue is a complex, multi-factorial process involving various central and peripheral mechanisms [77], there may be additional underlying factors contributing to our observed changes in ankle torque [112].

Further research should determine if the observed changes in ultrasound imaging is consistent across a variety of stimulation patterns and protocols. Another limitation is that the TDI method only measures the axial component of tissue velocity (center dotted line in Figure 2-1C) while the muscle shortening occurs along the fiber direction. The

true shortening velocity is related to the estimated axial velocity by the cosine of the angle between the ultrasound beam and the fiber direction. The pennation angle observed in ultrasound B-mode images of the medial gastrocnemius muscle at rest provides an initial estimate of the fiber direction, however, the pennation angle changes during the contraction. While the rate of change of the pennation angle may be small during an isometric contraction [126], the relationship between the estimated axial TDI velocity and the true shortening velocity is nevertheless complex. Thus, the *peak velocity* feature needs to be interpreted with caution since it is not directly proportional to peak shortening velocity. We also note that in our study, we did not find that the observed relationship between axial velocity and torque was dependent on the initial pennation angle at rest.

CONCLUSION

In conclusion, we found that tissue Doppler ultrasound imaging during stimulated isometric muscle twitches after EMS can detect changes in muscle fatigue, fatigue recovery, and the generated joint torque. Thus, TDI may have utility to monitor EMS-induced muscle fatigue. These findings support the potential of using TDI approaches with wearable ultrasound to develop a real-time, wearable muscle fatigue monitor compatible with EMS.

ACKNOWLEDGMENTS

We would like to thank Alex Baker for assistance with the instrumentation and Erica King for assistance with data collection. Portions of this research were presented at the annual meetings of the Acoustical Society of America (2019) and the International Symposium on Ultrasonic Imaging and Tissue Characterization (2019).

DATA

The data that support the findings of this study are available from the corresponding author, SS, upon reasonable request.

AUTHOR CONTRIBUTIONS

JM, PC, and SS contributed to conception and design of the study. JM collected the data. JM, SA, and SS contributed to analysis and interpretation of the data. JM, SA, and SS were involved in writing this manuscript. All authors approve of the submitted version.

FINANCIAL SUPPORT

This work was supported by the National Science Foundation, Cyberphysical Systems (grant number 1646204).

COMPETING INTERESTS DECLARATION

JM, PC, and SS used a portion of this work as part of a patent application to the US Patent and Trademark Office. SA declares no competing interests.

ETHICAL STANDARDS

The authors assert that all procedures contributing to this work comply with the ethical standards of the relevant national and institutional committees on human experimentation and with the Helsinki Declaration of 1975, as revised in 2008.

CHAPTER THREE: ESTIMATION OF JOINT TORQUE AND MUSCLE FATIGUE FOR ASSISTIVE TECHNOLOGY APPLICATIONS USING A WEARABLE ULTRASOUND SYSTEM

Joseph A. Majdi[1], Parag V. Chitnis[1], Siddhartha Sikdar[1]

[1]*George Mason University*

Portions of this work were presented at the 2019 and 2020 meetings of the Acoustical Society of America, International Symposium on Ultrasound and Tissue Characterization, as well as in internal meetings at the NSF Cyberphysical Systems group, and the Center for Adaptive Systems of Brain-Body Interaction at George Mason University, and was published as a conference paper at RESNA 2020 [123].

INTRODUCTION

A significant challenge in improving the design of assistive technologies for rehabilitation of individuals with neuromuscular deficits is the limited ability to robustly sense muscle activity and function. For the past 50 years, surface electromyography (sEMG) has been the dominant standard for detecting muscle activity for prosthetics [127] and is also widely used for rehabilitation and biomechanics research. However, sEMG lacks spatial specificity and suffers from poor SNR [28]. Despite these limitations, sEMG has been widely used for estimating voluntary muscle force and fatigue [88]. However, sEMG is generally incompatible with electrical muscle stimulation (EMS), which is often used either as a therapeutic intervention or in conjunction with assistive

technologies, as sEMG signals are typically saturated by current injection during electrical stimulation.

Due to the well-documented limitations of sEMG, alternative biosignal sensing methods for studying muscle activation have been investigated. Mechanomyography (MMG) is a class of mechanical alternatives to sEMG, which record forces and physical energy transfer from muscle activation. Several variants exist from measuring muscle radial displacement (tensiomyography, TMG) [35] to passively recording soundwaves generated by muscle contractions (acoustic myography, AMG) [30], [37]. Because these techniques measure mechanical activity (as opposed to electrical activity), they provide a meaningful measure of active muscle contractions that is not dependent on ECC [30]. Further, they would be significantly less susceptible electrical aberrations induced by EMS current injection. While these methods have some advantages over sEMG, they suffer from their own limitations, including susceptibility to motion artifacts, and the limited sensitivity to deep-seated muscle motion [128].

Recently, the use of ultrasound imaging has gathered more attention in research for numerous applications to detect and quantify muscle activity. These have included estimating muscle force generation using muscle fiber pennation angle, cross sectional area, and tissue motion tracking [39]–[44], detecting passive and active muscle activation using fast M-mode or TDI approaches [45]–[47], and using ultrasound-derived signals for controlling prosthetics [48]–[50] or inform hybrid EMS exoskeleton controllers [58], [116], [129]. Our earlier work [65] detailed in Chapter 2 used a commercial ultrasound machine to perform tissue Doppler imaging (TDI) to identify signs of muscle fatigue and

muscle fatigue recovery. A major challenge with ultrasound systems have been the bulky form factor of the transducers and instrumentation, which is a significant limitation to deploying in a wearable system during free, unconstrained movement. In this paper, we investigated the use of dual-element continuous-wave (CW) Doppler ultrasound systems, which can be deployed in a small form factor for wearable use alongside assistive devices. A comparison between TDI and CW ultrasound methods can be found below in Table 2. A portable CW probe is orders of magnitude cheaper, is portable, requires as little as AAA batteries and has vastly reduced memory and hardware requirements. For instance, our CW data sampled at 100kHz acquired approximately 67 MB/minute of data and could be reduced about five-fold further for audio frequency measurements, compared to the TDI data that acquired approximately at 1.6 GB/minute. The latter figure does not include the fact that this is post-beamforming, meaning that 32 channels (or more for other machines) are acquired at the same rate simultaneously and then delay and sum beamformed, which means the analog to digital sampling rate and bus requirements are actually 32x higher (and can be even greater for other machines). Both the delay and sum beamforming and the higher number of samples overall likewise require more calculations to process them. The tradeoff however is that TDI provides a velocity estimate at every pixel depth where the CW is sensitive to velocities across a given focal depth, which provides localized information but with far less detail than in the TDI case. The hardware benefits are clear, but there remains the open question of the effectiveness of this technique given its reduced capacity to measure velocity at various depths. To demonstrate the value of this method, we investigated its utility in estimating muscle

force production and fatigue during electrical stimulation, a situation where conventional sEMG cannot be utilized.

Table 2. TDI Ultrasound vs. CW Ultrasound Comparison

Design Requirements	Tissue Doppler Imaging (TDI) Ultrasound	Continuous Wave (CW) Ultrasound
Price	$$$ - ✗	$ - ✓
Portability	No - ✗	Yes - ✓
Power	High power - ✗	AAA batteries - ✓
Sample rate	~40 MHz - ✗	44-100 kHz - ✓
Memory requirements	~1.6GB/min - ✗	~67MB/min or less - ✓
Computational requirements	Intense - ✗	Low - ✓
Depth sensitivity	Detailed - ✓	Limited - ✓−
Sensitive to muscle force and fatigue?	Yes - ✓	<?>

METHODS

Experimental Setup

EMS Plantar Flexion

Six healthy male subjects were recruited for the experiments under a protocol approved by the George Mason University Institutional Review Board. Subjects were asked to lie in a prone position, and the isometric plantar flexion torque was measured (Figure 3-1) using a Biodex II dynamometer (Biodex Medical Systems, Upton NY) upgraded with a Humac interface (CSMi Solutions, Stoughton, MA) interfaced with LabView (National Instruments, Austin, TX). Subjects were instrumented with a modified 5Mhz BT-200 Hi-Dop vascular continuous wave Doppler ultrasound probe

(Bistos, Seongnam-si, SK), placed over the muscle body of the medial head of the gastrocnemius. Care was taken to place the probe away from blood vessels so that the movement detected by the probe was from muscle/tissue motion alone. The probe was also shielded in a grounded aluminum enclosure to minimize electromagnetic interference (not shown). Rehastim2 (Hasomed GmbH, Magdeburg, GE) EMS electrodes were placed on the proximal part of the medial head and distal part of the lateral head of the gastrocnemius in accordance with the Rehastim2 manual. EMS was controlled with a custom Matlab/Simulink (MathWorks Inc., Natick, MA) interface. The experimental setup and protocol for these experiments were virtually identical to those in Chapter 2, except done using a continuous wave probe (which was incapable of depth resolved imaging).

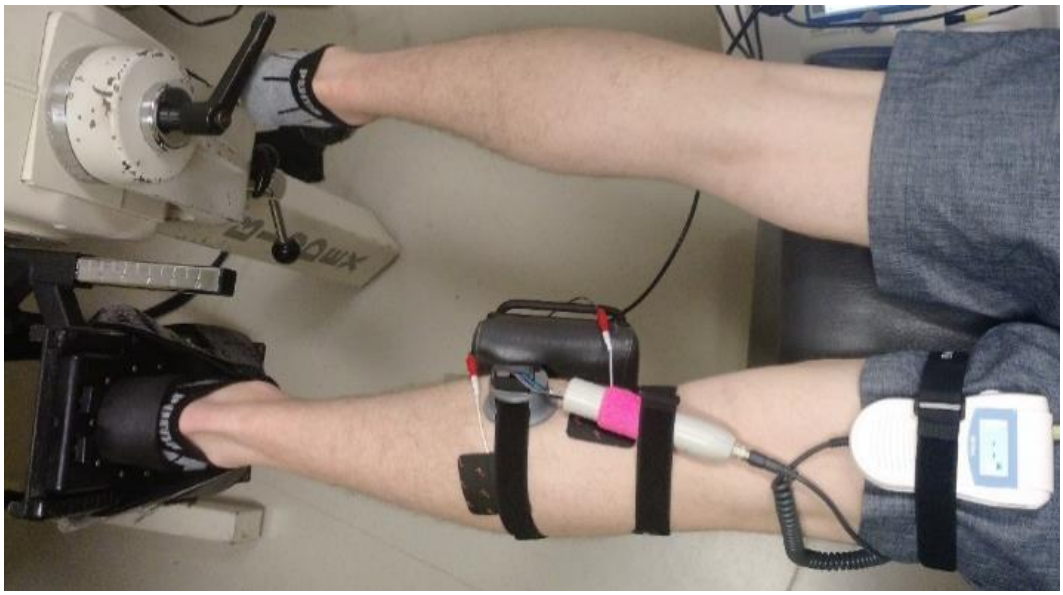

Figure 3-1. A subject is fitted with a modified portable continuous wave (CW) ultrasound probe and stimulation electrodes on a modified commercial Biodex II dynamometer.

Knee Extension Tasks

Because we are unable to test dynamic motion in the plantar flexion setting, we decided to test the robustness of the system on the vastus lateralis (Figure 3-2), which is commonly used in sEMG research of knee extension because it is relatively isolated and provides information about the quadriceps. 2 subjects were set up in the knee extension/knee flexion configuration for the Biodex dynamometer with their legs chosen at random. The CW probe (inside the shielding box, Figure 3-2) was affixed over the vastus lateralis using Velcro straps and a custom 3D printed probe holder.

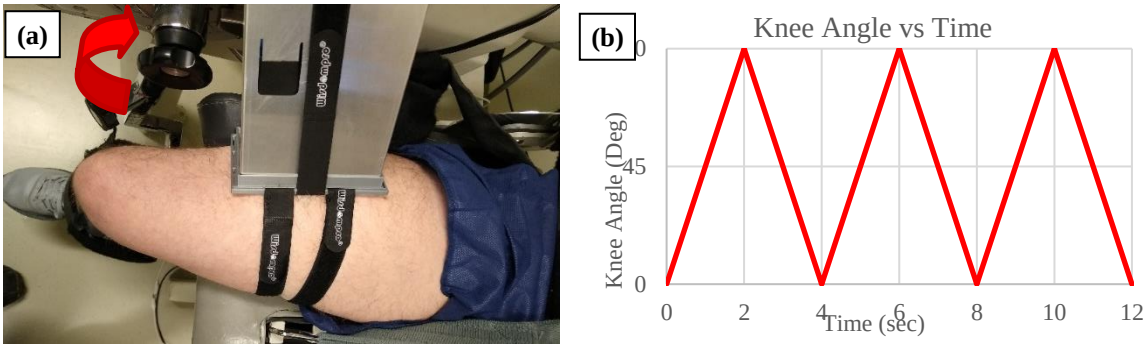

Figure 3-2. Dynamic knee extensions by passive and voluntary actuation. (a) Subjects are fitted with a shielded CW US probe and hooked into a modified Biodex II dynamometer in the knee flexion/extension configuration. The subject's knee joint is then driven by the dynamometer between 0° and 90° (curved red arrow) in the continuous passive motion (CPM, motor driven) mode, or asked to move their leg voluntarily in the same pattern in the isokinetic mode. Isokinetic mode requires the user to use their own voluntary muscle contractions to drive movement, but restricts the movement speed to a constant value. (b) Twelve seconds of the knee movement pattern used in experiments. Knee extension was driven in either fixed velocity CPM (passive, motor driven) or isokinetic (voluntary, muscle driven) modes.

Experimental Protocol

EMS Plantar Flexion

First, subjects were asked to perform voluntary plantar flexion, and the maximum voluntary isometric contraction (MVIC) torque was recorded. We then applied 50 Hz, 100 μs biphasic current at progressively higher amperage, and the current required to

produce approximately 20% of their MVIC was recorded as the stimulation current. A stimulation cycle of 1 second duration was designed as follows: The current during the on phase was ramped up from zero to maximum over 0.12 s, held at maximum current for 0.5 s, and then ramped down to zero for 0.12 s, followed by 0.26 s rest, with a total stimulation period of 1s. We then stimulated the calf for 60 cycles over a period of 60 seconds. The peak torque declined significantly to below 50% of the initial value for all subjects during this 60-second stimulation, indicating the onset of fatigue. The muscle was then allowed to rest for two minutes, and the 60-second stimulation cycles was repeated for a total of five trials. This experimental protocol is identical to that in chapter 2, except audio output from the CW Doppler instrument was recorded continuously throughout the entire experiment, and not just during brief periods when twitching the muscle.

Knee Extension Task

To compare signals generated by voluntary muscle activation and those generated from passive deformation, subjects performed knee extensions and run in both machine driven continuous passive motion (CPM) mode (machine driven) and isokinetic (same force, subject driven). In each configuration, the knee was brought from 0 to 90 degrees back to 0 degrees over 4 seconds, three times and the position and audio signal were recorded continuously for this experiment.

Analysis

EMS Plantar Flexion

We used the CW Doppler audio jack signal to estimate the muscle contraction velocity normal to the muscle's line of action (towards and away from the skin). We calculated the spectrogram (Figure 3-3) and spectral entropy [130] (not shown) of the CW Doppler signal to analyze signal duration at the onset of muscle contraction. As is common with CW Doppler machines, our instrument had a built in high-pass clutter filter (with a cutoff of approximately 500Hz) to suppress slow tissue motion. This inherently creates a nonlinearity, where audio signal represents only movements above a certain velocity, based on the Doppler shift frequency and filter cutoff.

On occasion, multiple activation signals were present (presumably from the two heads of the gastrocnemius activating at different recruitment times, or from fibers having a variable delay caused by varying fatigue levels)[1]. In these cases, only the first part of the signal was used in the analysis. We first hypothesized that there would be a difference in signal duration with muscle fatigue. To test this, we compared the signal duration for the first (least fatigued) and 60th stimulation period (most fatigued) using a paired t-test. To further quantify the relationship between signal duration and EMS induced torque, we calculated the signal duration at the onset of movement and performed a simple linear regression between this signal duration and peak plantar flexion torque for stimulation cycles 1, 11, 21, 31, 41, 51, and 60 for each of the five EMS trials.

[1] The published conference paper attributed this to the gastrocnemius and soleus separately contracting. However, due to their distinct motor points, this was more likely the two heads of gastrocnemius diverging in their fatigue induced electromechanical delay.

We also performed post hoc analysis on existing data to identify any other potential signal metrics to measure muscle force and muscle fatigue. Additional metrics included image decorrelation, curve fitting to estimate fatiguing time constants, sub-band power analysis, and total low frequency (<2kHz) signal power (Figure 3-6).

Knee extension task

The raw position signal generated by the Biodex system was first converted to knee angle via the CMSi's manual, and the audio signal synchronized to it. From there, the audio signal was analyzed manually. The audio signal was played over headphones and qualitatively described to distinguish between signals generated by the dynamometer axel striking the hard stops and actual doppler audio signal. The audio signals of both mechanical striking and Doppler audio signal were then visually compared with the knee angle position to attribute the timing of mechanical striking and times of Doppler signal indicating active muscle movement.

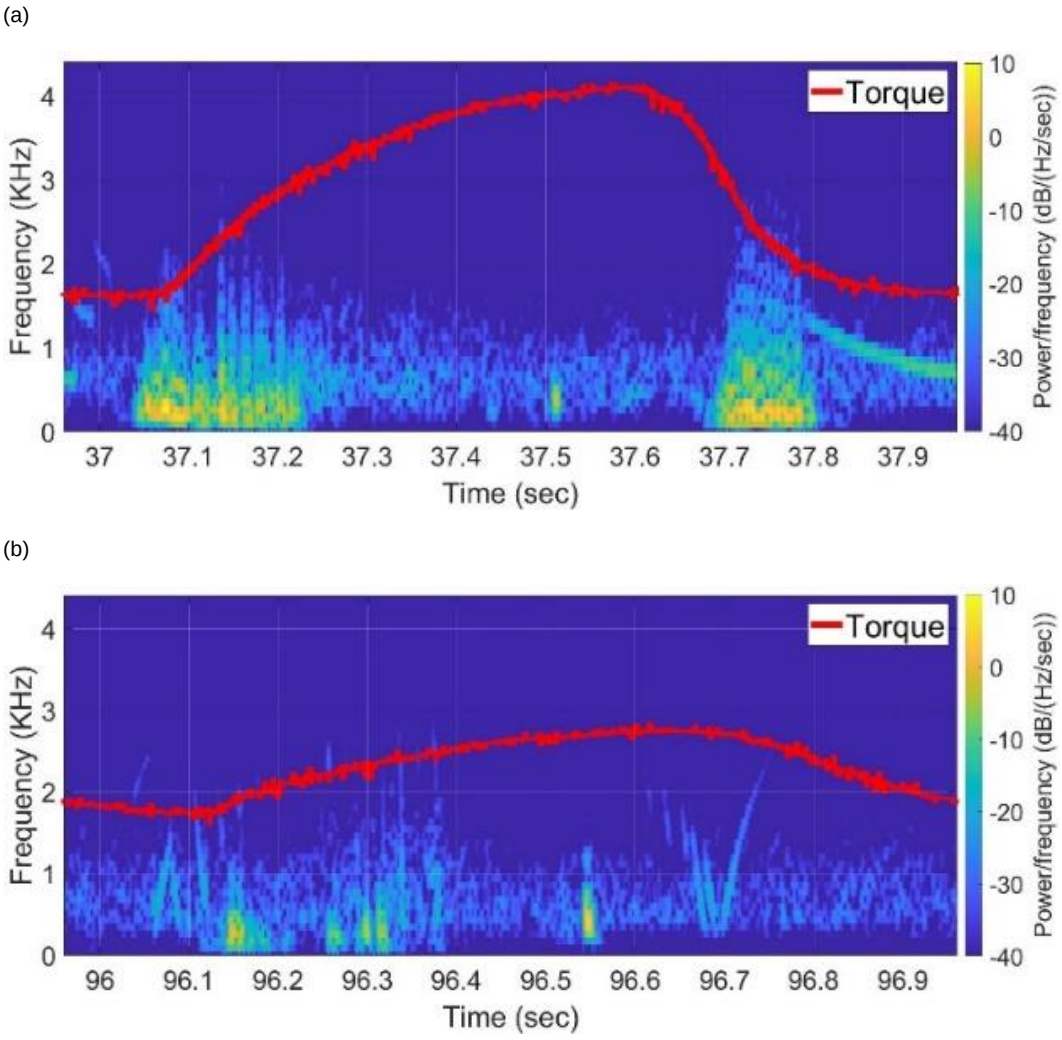

Figure 3-3. Example plantar flexion torque during electrical stimulation (black trace) for the first cycle (a) and the 60th cycle (b) overlaid on the corresponding CW Doppler spectrograms. It can be seen that for the 60th cycle of stimulation, the torque has decreased significantly, and the Doppler spectrogram shows a smaller duration signal.

RESULTS

EMS Plantar Flexion

We found that CW Doppler signals at both the onset phase and release phase of force, were force/fatigue dependent (Figure 3-4). In general, as the muscles fatigued, the

audio signal durations continually shortened during the contraction phase, and tended to drop below detectable levels for the release phase indicating very slow movement.

For the first stimulation period, the contraction signal was on average 133.5ms ± 36.05ms SD. By the 60^{th} stimulation period, the muscle had fatigued and the signal duration dropped to 52.16ms ± 20.24ms. This change was statistically significant ($p = 0.012$, paired 2-tailed t-test). This indicates that the signal duration is correlated with peak plantar flexion torque.

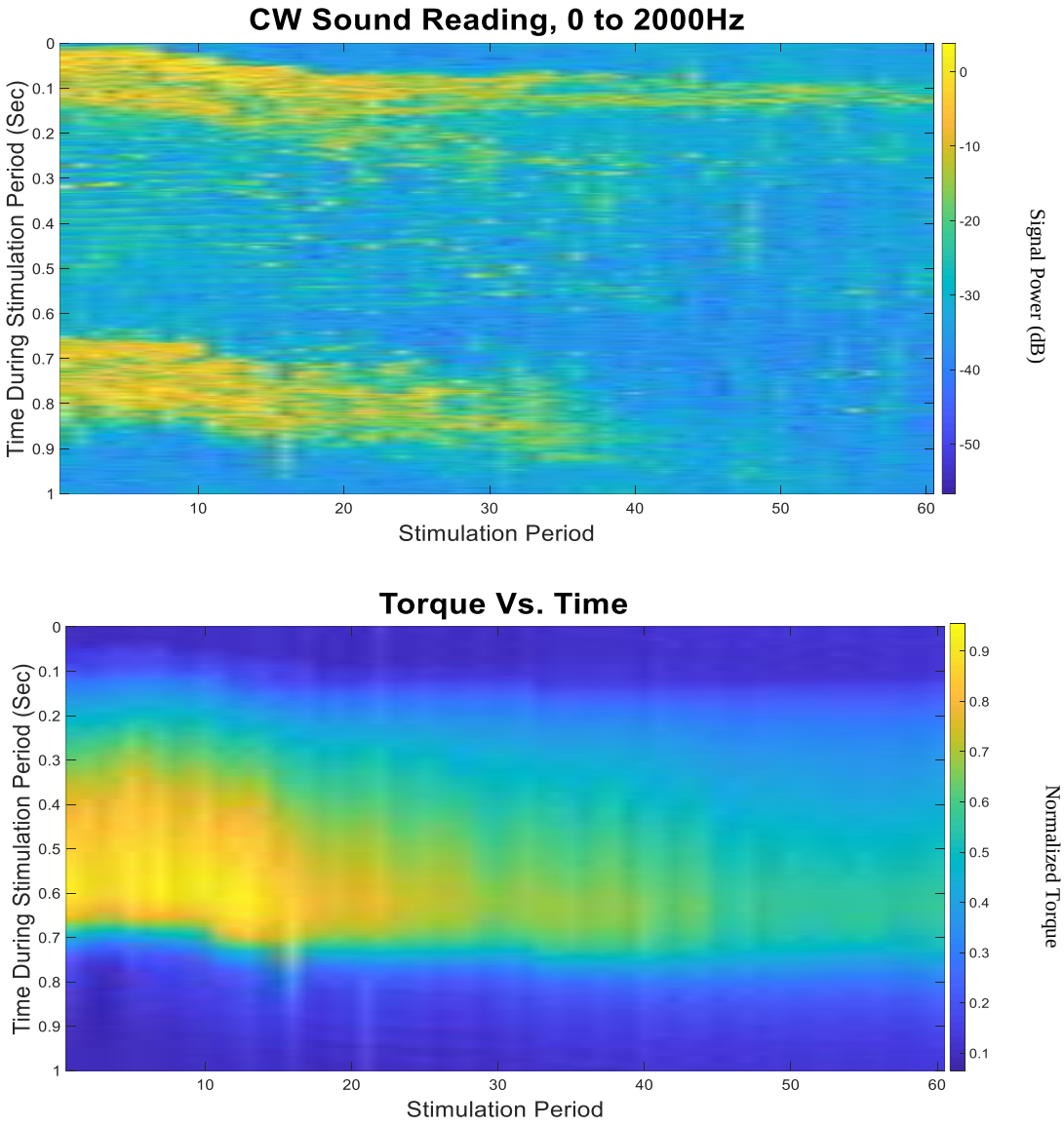

Figure 3-4. Top: The total power of the CW spectrum from 0 to 2kHz (dB) for one subject. Columns represent individual 1sec stimulation periods. Note that the contraction phase becomes thinner and the relaxation phase can drop to undetectable levels. Bottom: The normalized torque trace over the same time periods.

We then performed a simple linear regression between signal duration and peak plantar flexion torque for each subject. We found that if all EMS trials were included, the average R^2 value was 0.504 ± 0.159, meaning that 50.4% of the torque variability could be explained by the signal duration. It was clear, however, that the initial EMS trial did

not follow the same pattern as trials 2-5 (see Figure 3-5 as an example). If trials 2-5 were analyzed without trial 1, the average R^2 increased to 0.661 ± 0.0957, indicating that 66.1% of the torque variability could be explained by the signal duration. This could indicate that the muscle needed a warm-up period before they start producing more consistent results.

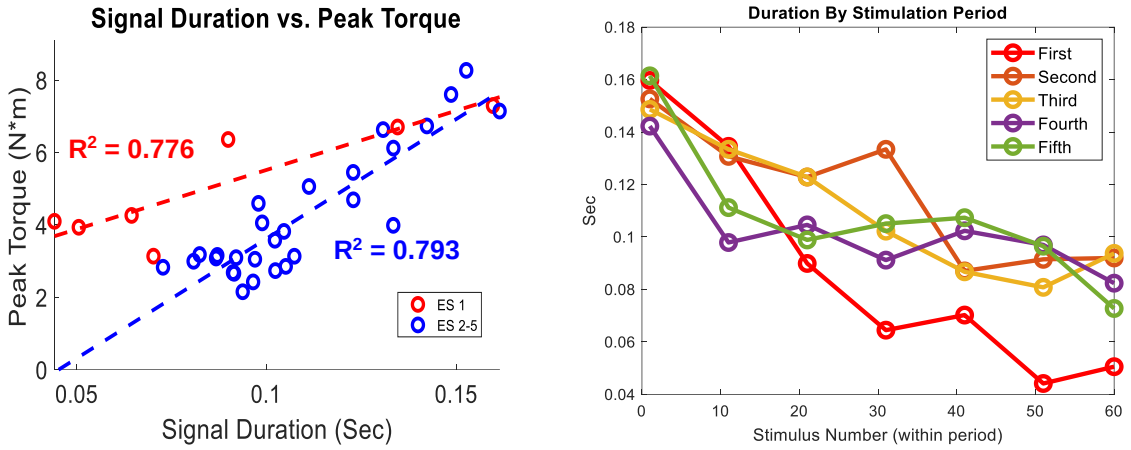

Figure 3-5. Left: An example of signal duration vs peak torque for one subject. Note the difference in slope between the first ES (ES 1) and the subsequent stimulations (ES 2-5). Right: Doppler signal duration with respect to stimulation period for one subject.

Of the post-hoc analyses we performed on the EMS plantar flexion CW audio signal, only signal power analysis revealed any worthwhile connection. Figure 3-6 shows the signal power analysis for two subjects. For the first subject (Figure 3-6a and Figure 3-6b), signal power decreases with decreasing joint torque. However, in another subject (Figure 3-6c and Figure 3-6d) the later stimulations in Figure 3-6d, the power of the signal increases without a co-occurring increase in force. This is likely due to shifts in the muscle fiber orientation or the positioning in the probe. Unlike total signal power, timing metrics such as signal duration should in theory be independent of intensity artifacts.

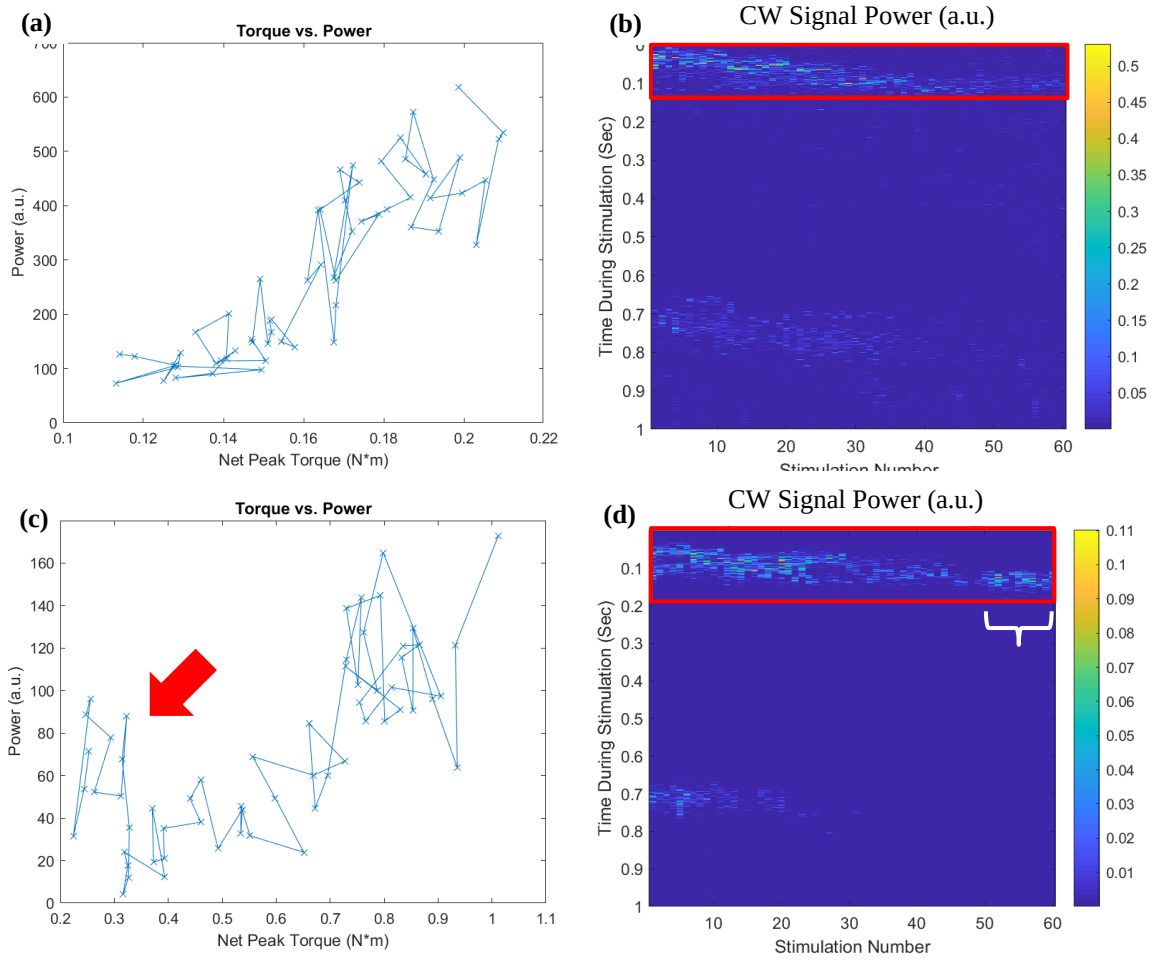

Figure 3-6. Signal power does not always show a consistent trend with respect to joint torque. (a) and (c) show two examples of the measured CW signal power during the initial, force generating phase of FES stimulations (red box in (b) and (d)) and the torque generated by those stimulations as the muscle fatigues. (b) and (d) show the CW signal power throughout the stimulation period, corresponding to (a) and (c) respectively. Each column in (b) and (d) represents a one second simulation. Note that in the final stimulations in (d), the signal power increases (white bracket). Because peak torque did not increase in this period, the power to torque relationship is no longer monotonically increasing (c, red arrow region), and hence this metric alone is an unreliable measure for estimating joint torque.

Knee extension task

For the CPM (machine driven) motions, we observed stark audio signals near the ends of the range of motion (0 and 90 degrees). After listening to the audio signal, it was clear that this was not related to the Doppler signal associated with passive or active

muscle movement, but a telegraphed clanking when the axel of the machine hit its rotational hard stops. No observable Doppler signal was otherwise noted for the machine-driven portion.

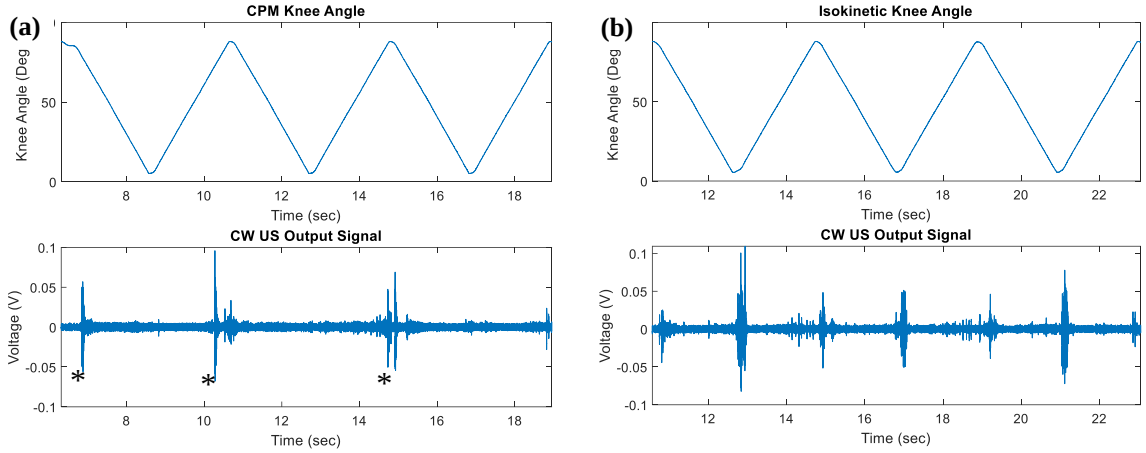

Figure 3-7. CW Doppler ultrasound signal generated in knee flexion and extension. (a) An example of the CW signal recorded by passive (CPM) knee movements controlled by the dynamometer. The large bursts of signal (asterisks) are not from the muscle, but from the dynamometer hitting its hard stop limits and from the RF shielding enclosure contacting the dynamometer. (b) An example of the CW signal recorded from the same subject during voluntary isokinetic knee movement over the sawtooth pattern as in (a). Unlike (a), there are distinct CW signals at both the 0 degree and 90 degree angle inflection points from when the user switches between knee extension and knee flexion. Muscle motion is detectable in (b) which can be used to distinguish manually controlled isokinetic (b) and continuous passive motion (a) knee flexion and extension.

Unlike in the CPM mode, there are Doppler audio signals did occur in the isokinetic motions at the 0 degree and 90 degree transitions (Figure 3-7), where the muscle is motion switches from a knee extension to a knee (flexion). This coincides to the time periods where the quadriceps transitions from the active muscle group to the antagonist muscle and vice versa. This is consistent with the EMS plantar flexion case, where Doppler audio signal can be observed at both the onset of force and at the release.

DISCUSSION

Our results indicate that CW Doppler can be utilized in conjunction with electrical stimulation to infer the muscle force production as well as the onset of fatigue. This method can overcome a major limitation of sEMG, which cannot be utilized in conjunction with EMS.

CW Doppler can be performed with a dual-element transducer with a small footprint, and miniaturized battery-operated electronics, making this technology well-suited for a wearable application. CW Doppler can be sampled at relatively low sample rate (44-100kHz, audio range) and can be analyzed with fast Fourier transform algorithms, which makes real-time analysis possible. We found that the duration of the CW Doppler signal after a high-pass clutter filter, correlated with peak muscle force, throughout five trials of EMS stimulation, fatigue, and recovery. One interpretation of our data is that the muscle shortening velocity decreases as the muscle fatigues, and the measured signal duration that exceeds the clutter filter cutoff of 500Hz decreases with fatigue.

The use of CW Doppler to measure muscle contraction velocities has a significant advantage over conventional ultrasound imaging methods that rely on measurement of muscle architecture features such as pennation angle and cross-sectional area. Image-based measures are highly sensitive to transducer positioning, and out of plane movement that is common during muscle contraction.

Further, if this modality is to be used as a feedback mechanism for a hybrid robotics controller, it is crucial that there be no significant signal generated by passively

moving muscles as the electric motor leads movement, or at least to have that signal well characterized to isolate it from signal from active muscle contractions. For that reason, we experimented with the vastus lateralis in both machine driven (CPM) and user driven (isokinetic) modes, and confirmed that we did not observe any Doppler signal outside of active muscle contraction.

In this study, we utilized a commercial vascular CW probe to demonstrate the feasibility of this approach. The use of a commercial system has limitations. First, this system was designed to measure blood flow and hence has a clutter filter designed to block signal from low velocity tissue movement. However, the Doppler shift due to muscle contractions were sufficiently large to exceed the clutter filter settings. Doppler signals for lower velocities, such as those produced during the relaxation phases can sometimes fall below the clutter filter cutoff, especially after muscle fatigue. Likewise, passive tissue motion in the vastus lateralis was insufficient to create a Doppler signal. Additionally, because we are measuring the audio output alone, we lose the phase and thus directionality of the movement, and instead are left with only magnitude. In future work, we plan to bypass the internal signal processing circuitry and record the in phase and quadrature (I/Q) components to both preserve directionality and bypass the clutter filter to make slower tissue movements detectable. A second limitation is that CW Doppler provides limited information based on the focal depth. We are currently investigating the use of frequency-encoded (FMCW based) methods that can enable depth-specific velocities without significantly increasing the form factor of the transducer and associated instrumentation. Finally, we did experience electromagnetic interference

from the electrical stimulation at times, which is the rational for putting the CW probe inside a shielded aluminum box. However, electromagnetic interference is generally not an issue with properly shielded CW machines, though this particular device seems susceptible, possibly because it lacks shielding internally, which we verified by manually disassembling and reassembling the probe.

CONCLUSION

Continuous wave Doppler ultrasound is portable, low power, and provides real time information about muscle activation, fatigue, and recovery that is compatible with EMS. This could provide a useful wearable biosignal sensing method for use in conjunction with assistive technologies such as hybrid exoskeletons combining EMS and actuators, and therapeutic electrical stimulation. This method overcomes many of the limitations of other sensing modalities.

CHAPTER FOUR: MULTISCALE MODELING OF MUSCLE ACTIVATION FOR ACCURATE ELECTRIC MUSCLE STIMULATION SIMULATION

We have thus far concentrated on establishing the feasibility to apply two existing Doppler ultrasound techniques in novel ways to serve as a new human computer interface to estimate EMS induced muscle fatigue and recovery. The following section is dedicated to capitalizing on these muscle fatigue estimates to improve muscle modeling for end applications like closed loop EMS exercise or hybrid EMS exoskeleton controllers, whose performance degrades without accurate EMS muscle fatigue estimates[129] or become unstable [131].

INTRODUCTION

Dynamic system models form the foundation of controllers, and therefore better muscle modeling will lead to better controller performance. In particular, accurately observing and predicting the efficacy of EMS muscle activation is critical to optimizing real-time interactions between electrical motors and muscle, such as for hybrid EMS/exoskeleton. For such shared controller schemes, the actions of stimulating muscle and running electrical motors must be coordinated so that the system generates the desired torque in time with the functional task's cycle. If a system is relatively simple and governed by linear ordinary differential equations as is commonly found in engineering and robotics, it is possible to incorporate models and inputs (such as electric motors, pneumatic pressure, etc.) to control the system with state-space control theory. However,

biological systems are often too complicated simple controller schemes and require advanced nonlinear modeling to accurately predict their behavior, as it is with the performance of muscles undergoing EMS.

Muscles are highly nonlinear in their input/output characteristics, with time varying properties such as mechanical delay [131], potentiation [110], and muscle fatigue [75]. We chose to start with the multiscale muscle activation model Carriou 2019 [132] for a number of reasons. First, the equations developed for this model are physiologically derived and not just curve fit, so that the information they provide can provide reasonable physiological insights when making predictions. Further, physiologically derived models are more easily modified with additional physiological insights. Because the known phenomena are the basis for model terms and interactions, adding or modifying interactions is straight forward. For a system whose terms are merely derived from data, with no labels for the inner variables, adding an interaction from a known physiological interaction becomes almost impossible. If the phenomena of the model are defined, you can also make inferences from data that was not necessarily collected, such as tuning the initial conditions to match observed data. A physiologically relevant model can help identify missing initial conditions or ones that are not easily measured such as the length tension curve of pennate fibers, which are difficult to measure experimentally. Second, this model utilizes nonlinear viscoelastic properties of muscle and tendon tissue that can be overlooked in simpler models. Third, this model takes into account many individual muscle fibers of varying fiber types (slow twitch, fast intermediate fibers, fast fatigue resistant fibers, and fast twitch fibers) the proportion of which can be adjusted as a

variable, which may help explain subject to subject variability. Not only is this more physiologically accurate, but it has been shown that Hill-type muscle models are improved by taking variable muscle fiber composition and recruitment patterns into account [133]. Fourth, this model takes calcium dynamics, which are critical for fast muscle fatigue, into account as the basis for generating force on a molecular level [19], [77], [112], [134]. For these reasons, we found this model to be a good starting point to help examine our data. However, despite the strengths of this model, two key features need to be added. This model does not consider fatigue dependent electromechanical delay nor muscle pennation angle and therefore we have tried to address these elements when applying it to our dataset.

METHODS

Model Design

The models here were implemented in Matlab 2022a using Euler's method of numerical integration (Equation 5) for simplicity. The chosen step size, $\Delta t = 1\mu s$, is three orders of magnitude smaller than the fastest time constant of our calcium dynamics models, meaning we can expect reasonably close approximations of the model dynamics, at the cost of higher memory requirements and computation time. This fact is critical, because the simulation periods are on the order of minutes, or tens to hundreds of millions of iterations per fiber, which could lead to significant propagation of approximation error, where inaccurate estimates are fed into subsequent steps leading to greater error or even instability issues.

Equation 5. Euler's Method for Estimating Differential Equations

$$y(((n+1)*\Delta t)+t_0) \cong y((n*\Delta t)+t_0) + \dot{y}((n*\Delta t)+t_0)*\Delta t$$

As with any model, approximation error compounds the longer the simulation is run. However, because our active stimulation periods are intermittent and theoretically should return the muscle to 'rest' cyclically, which should serve as a stable/steady state baseline. the accumulation of feed forward approximation errors for the fast dynamic elements, like Ca^{2+} dynamics, is mitigated to periods of active stimulation and does not compound for long periods. However, this remains an issue for variables whose time scale persist beyond a few seconds such as fatigue state. Ultimately, the objective of the ultrasound-based fatigue estimation is to use it as a feedback mechanism to correct (or affirm) the model estimates if fatigue estimates become excessively inaccurate due to A) accumulation of approximation error, B) oversimplification or inaccuracy of the model design, or C) imperfect tuning of model parameters.

Table 3. Calcium Dynamics Parameters

Parameter (symbol)	**Value (unit)**
Time delay response (τ_D)	5 (ms)
SMU resting Ca^{2+} concentration ($U_{r,S}$)	5 (μmol/L)
FRMU resting Ca^{2+} concentration ($U_{r,FR}$)	5 (μmol/L)
FIMU resting Ca^{2+} concentration ($U_{r,FI}$)	7 (μmol/L)
FFMU resting Ca^{2+} concentration ($U_{r,FF}$)	8 (μmol/L)
SMU rise slope ($\tau_{1,S}$)	4 (ms)
SMU descent slope ($\tau_{2,S}$)	20 (ms)
SMU amplitude Ca^{2+} dynamics (R_S)	16 (unitless)
FRMU rise slope ($\tau_{1,FR}$)	3 (ms)
FRMU descent slope ($\tau_{2,FR}$)	17 (ms)
FRMU amplitude Ca^{2+} dynamics (R_{FR})	16 (unitless)
FIMU rise slope ($\tau_{1,FI}$)	1.3 (ms)
FIMU descent slope ($\tau_{2,FI}$)	13 (ms)
FIMU amplitude Ca^{2+} dynamics (R_{FI})	14.5 (unitless)
FFMU rise slope ($\tau_{1,FF}$)	1 (ms)
FFMU descent slope ($\tau_{2,FF}$)	8 (ms)
FFMU amplitude Ca^{2+} dynamics (R_{FF})	20.0 (unitless)

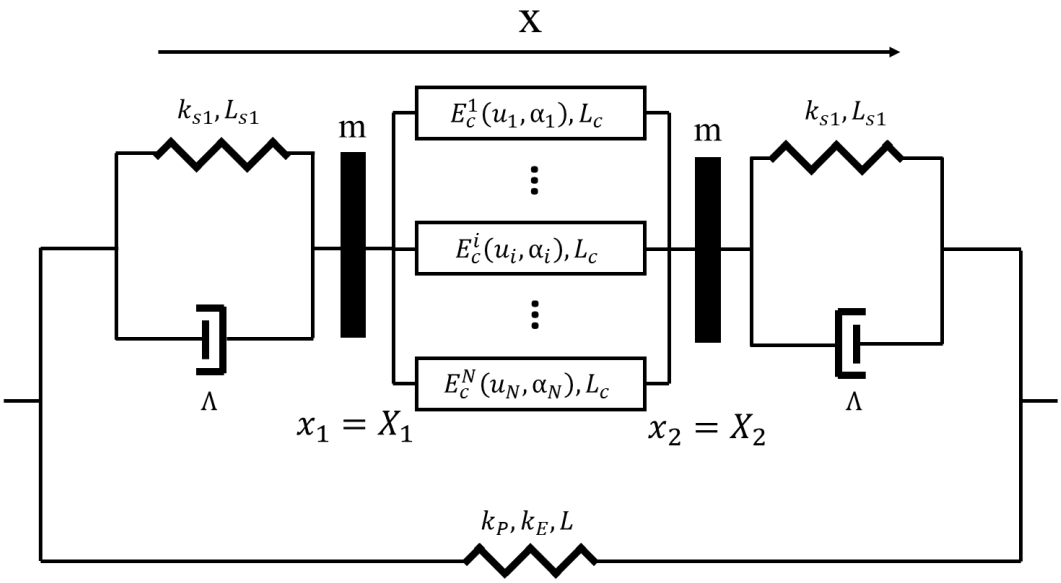

Figure 4-1. Mechanical rheological model of the muscle.

Table 4. Calcium Activation Thresholds

Concentration activated threshold	Value (unit)
SMU Ca^{2+} ($U_{c,S}$)	10 (μmol/L)
FRMU Ca^{2+} ($U_{c,FR}$)	11 (μmol/L)
FIMU Ca^{2+} ($U_{c,FI}$)	14 (μmol/L)
FFMU Ca^{2+} ($U_{c,FF}$)	15 (μmol/L)

The rheological model of the muscle (Figure 4-1) was originally derived in El Makssoud et al., 2011 [23] and later modified by Carriou et al., 2019 [132] to account for individual motor units (MUs) with varying fiber types with their own calcium dynamics and mechanical properties. The rheological model (Equation 6 through Equation 15) constants (Table 5) were derived in or found in literature, see [132] for more details. Likewise, the physiological constants (Table 3 and Table 4) used in the calcium dynamics (Equation 8, Equation 9, Equation 16, Equation 17) and their derivations were also identified in [132]. More detailed explanations for many of these equations can also be found in [23], [135].

Table 5. Muscle Parameters

Parameter	Value (unit)
Maximal Stimulation Intensity (i_{max})	3.15 (mA)
Stimulation Intensity (i)	1.73 (mA)
Elicited Recruitment Parameters (c_1, c_2, c_3)	1.15, 8.12, 0.75 (unitless)
Optimal Muscle Length for Greatest Contraction Force (L_{c0})	0.0918 (m)
Resting Muscle Length (L_c^0)	0.0100 (m)
Velocity Contribution Parameter (a)	1.0 (unitless)
Force–Length Parameter (b)	0.54 (unitless)
[2]Tendon Viscosity (Λ)	19.0 ($kg*s^{-1}$)
Muscle Mass (m)	0.5 (kg)
Maximal (Whole Muscle) Force (F_{max})	300 (N)
Maximal (Whole Muscle) Stiffness (k_{max})	100,000 (N/m)
Tendon Stiffness (k_{s1})	120,000 (N/m)

Equation 6. Strain of the bulk contractile element

$$\ddot{\varepsilon}_c = -\frac{\Lambda}{m}\dot{\varepsilon}_c - \frac{k_{s1}}{m}\varepsilon_c + \frac{k_{s1}}{m}\varepsilon_c^0 - \frac{2F_c}{mL_{c0}}$$

Equation 7. Force of the elastic element

$$\ddot{F}_e = -\frac{\Lambda}{m}\dot{F}_e - \frac{k_{s1}}{m}F_e + \frac{\Lambda}{m}\dot{F}_c + \frac{k_{s1}}{m}F_c$$

Equation 8. Stiffness for individual motor units

$$\dot{k}_{c,i} = -(u_i(t) + a|\dot{\varepsilon}_c(t)|)k_{c,i}(t) + \alpha_i(t)k_{max,i}(t)\Pi_{c,i}(t)U_{c,i}$$

Equation 9. Force for individual motor units

$$\dot{F}_{c,i}(t) = -(u_i(t) + a|\dot{\varepsilon}_c(t)|)F_{c,i}(t) + \alpha_i(t)F_{max,i}(t)\Pi_{c,i}(t)U_{c,i} + \omega(F_{c,i}(t))k_c(t)L_{c0}\dot{\varepsilon}_c(t)$$

Equation 10. Force correction factor for individual motor units

$$\omega(F_c) = \begin{cases} 1, & if\ F_c > 10^{-4} \\ 0, & otherwise \end{cases}$$

Equation 11. Force for bulk contractile element

$$F_c = \sum_{i=0}^{N} F_{c,i}$$

The literature cited use lower case lambda (λ), but to avoid confusion with wavelength, I have changed this to capital lambda (Λ).[2]

Equation 12. Stiffness for bulk contractile element

$$k_c = \sum_{i=0}^{N} k_{c,i}$$

Equation 13. Maximum force for individual motor units

$$F_{max,i}(t) = F_{max,i} f_l(\varepsilon_c)$$

Equation 14. Maximum stiffness for individual motor units

$$k_{max,i}(t) = k_{max,i} f_l(\varepsilon_c)$$

Equation 15. Length-tension factor for motor unit force and stiffness

$$f_l(\varepsilon_c) = e^{-\frac{\varepsilon_c^2}{b}}$$

Equation 16. Calcium dynamics for individual motor units

$$u_i(t) = \begin{cases} U_{r,i} & if\ t < \tau_D \\ R_i * \left(1 - e^{\frac{-(t-\tau_D)}{\tau_{1,i}}}\right)^5 * e^{\frac{-(t-\tau_D)}{\tau_{2,i}}} + U_{r,i} & if\ t > \tau_D \end{cases}$$

Equation 17. Activation threshold for individual motor units

$$\alpha_i(t) = \begin{cases} 1 & if \quad u_i(t) \geq U_{c,i} \\ 0 & otherwise \end{cases}$$

Equation 18. Muscle Recruitment Equation for Stimulus Intensity

$$\alpha(i) = \frac{c_1}{1 + \mathrm{e}^{c_2 * \left(c_3 - \frac{i}{i_{max}}\right)}}$$

Pennation angle was measured at the start of the experiments, but during Doppler measurements, only one scanline could be recorded at a time. Therefore, we added a pennation angle approximation from Scott and Winter 1991 [136] to the model (Equation 19). Given the initial muscle length, L_c^0, optimal muscle length, L_{c0}, initial pennation angle, φ_0, the change in muscle length, $\Delta L(t)$, the pennation angle, $\varphi(t)$, can be estimated with the following:

Equation 19. Pennation Angle Estimate

$$\theta(t) = \tan^{-1} \frac{L_c^0 \sin \varphi_0}{L_c^0 \cos \varphi_0 - \Delta L(t)}$$

We estimated the radial muscle velocity by approximating the muscle as a cylinder of 2cm radius of 2cm, and length L, using the strain rate ($\dot{\varepsilon}$) integrated from Equation 6 to estimate $\dot{L}$ and subsequently the instantaneous change in radius. All velocity estimates assumed constant volume of the cylinder. All stimulus trains were 50 Hz unless otherwise stated. To account for the action potential velocity, we added a time delay for every fiber assuming equal distribution throughout the diameter of the muscle assuming a nerve velocity of 56.5m/s. This delay was incorporated in every model unless otherwise stated.

Variable Stimulation Delay

Simplified Calcium Inhibition Fatigue Model

Electromechanical delay is the delay between the electrical activity of a muscle and muscle contraction. This is closely related to the stimulation delay, can be viewed as the time between an electrical stimulus and muscle activity, which can be measured three ways: by the timing of the induced electrical activity (sEMG), by the timing of muscle movement (US, possibly MMG or AMG), or by the timing of the force/torque generated though these times phenomena do not occur simultaneously [46], [102]. For closed loop hybrid motor/EMS controllers, the most relevant of these three measures is the delay to force onset as they can become unstable if they do not take time varying EMD into account [131].

The model in [132] assumes constant electrical delay regardless of previous excitation effects (not accounting for either potentiation which would decrease stimulation delay or fatigue that would increase stimulation delay, or their mixed effects

if both coexist simultaneously[111], [112]). The model stimulation delay (τ_D) is defined by the time between stimulation and the initiation of calcium dynamics, which should most closely match with the start of sEMG signal because it reflects the electrical activity in the muscle.

However, any variations in the calcium dynamics should automatically induce a fiber-specific stimulation delay in both the muscle force and movement without accounting for any other desynchronizing effects mentioned above. This model treats the actin/myosin cross bridge formation as a binary event where calcium levels are either sufficiently high to create new cross bridges or it is not. If fatigue or at least a component of fatigue is due to inhibited calcium release, should in theory automatically increase the delay between the neural drive and the generation of muscle force. This is because any decrease in ascending slope in the calcium transient will result in longer time to reach the fiber-specific critical calcium levels ($U_{c,i}$ in Equation 17) to induce a contraction within the fiber if it reaches it at all. To show that even the most simplistic models of impaired calcium dynamics would cause increased EMD in muscle force and movement with all other factors remaining the same, we implemented a muscle twitch model with a varying the Ca^{2+} scaling factor (R_i value in Equation 16) with a linear 'fatigue' scaling from 0.6 (reducing the active Ca^{2+} transient by 40%) to 1.0 (no reduction in Ca^{2+}) in 0.05 (5%) increments for 50 scaled slow twitch and 50 scaled fast twitch fibers.

Fixed and Ramped Intensity Stimulus Trains

In EMS applications, it is not uncommon to apply stimulus trains with a gradual ramp up to maximum intensity to reduce the shock on the muscle. Our experiments in

Chapters 2 and 3 for instance used both an up and down slope at the beginning and ending of the stimulus train. For this simulation, we used the fiber recruitment model in Equation 18, and the standardized parameter fit from [132] for simplicity and proof of concept, attempting to activate 20% of the MU at peak, similar to what we used in our real-world experiments to examine how changing the recruitment pattern affected the muscle dynamics with respect to the fixed intensity stimulus train of equal duration. The model muscle was set to be predominantly fast twitch fibers (375 fast twitch/125 slow twitch) similar to the distribution found in the gastrocnemius [137].

Variable Muscle Composition

Next, we decided to estimate the effect of muscle fiber composition, which we theorized to be behind some of the variability we observed in chapter 2. Here we simulated two 500 MU muscles undergoing intermittent, variable intensity stimulus trains as we used in our physical experiments. The first muscle was composed of 75% (375) fast twitch and 25% (125) slow twitch fibers, which is a typical gastrocnemius fiber composition [137]. To contrast this, we also simulated a muscle with an equal split of slow (250) and fast (250) twitch fibers.

RESULTS

Variable Stimulation Delay

Simplified Calcium Inhibition Fatigue Model

As expected, any decrease in calcium dynamics delayed the activation of the muscle unit (Figure 4-2). Because the fast twitch and slow twitch fibers had different slopes calcium thresholds, the stimulus delay varied by fiber type. We observed that slow

twitch fibers would be more susceptible to a depletion of calcium, because the relative difference between its resting and activated state is smaller compared to the fast twitch fiber. Because we do not observe this in nature, it implies that either the model is inaccurate in this regard, or that the fact that slow twitch fibers have a lower metabolic demand and thus do not typically experience as much disruption in their calcium dynamics for this to be observed in the real world.

For a comparison with real world data, Figure 4-3 and Figure 4-4 compare the predicted values with continuous wave (CW) data from Chapter 3. In Figure 4-3, we can see that as fatigue increases in the real world, so too does the delay between stimulation and muscle movement. Likewise, in Figure 4-4, we see that we do in fact see shortening of muscle movement duration as well. However, this is not an apples-to-apples comparison in Figure 4-4 because the top portion compares muscle twitch movement duration and the bottom portion is during a stimulus train. Nevertheless, we do see the same phenomenon in both cases. Although Figure 4-3 also compares a muscle twitch to a stimulus train, it should result in a comparable twitch delay.

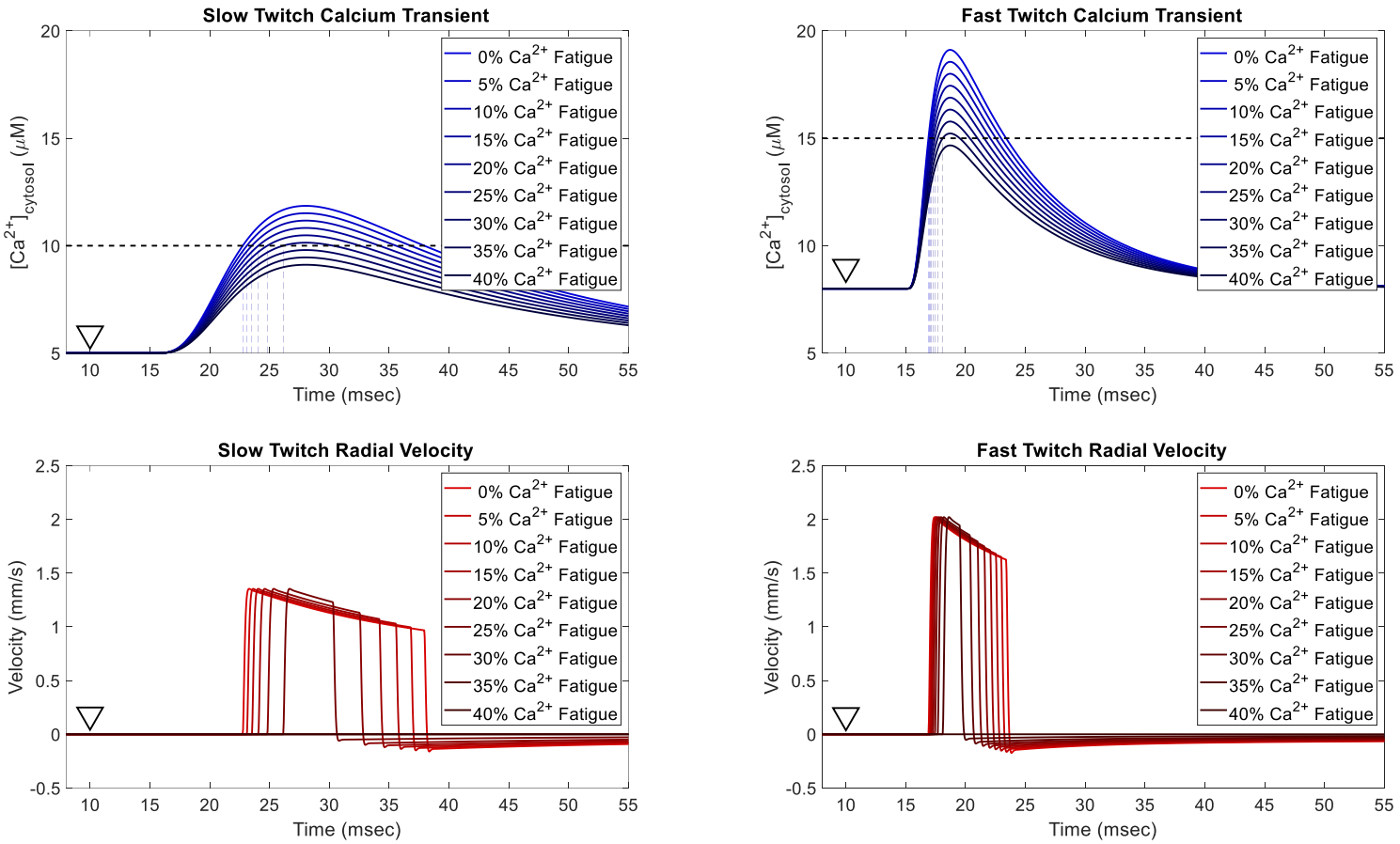

Figure 4-2. Electromechanical delay for simplified fatigue dynamics simulated for 50 slow (left) and 50 fast (right) twitch fibers. Top Left: Slow twitch fiber calcium scaling results in increased time (thin dashed lines) to critical calcium concentration (dashed horizontal line) after a stimulus pulse (triangle). Note that reducing the calcium concentrations by 30% or more fails to contract (bottom left). Bottom Left: Increasing delay to critical calcium level translates into EMD in muscle movement. Top Right: Fast twitch fiber calcium scaling also results in increased time (thin dashed lines) to critical calcium concentration (dashed horizontal line) after a stimulus pulse (triangle). Note that reducing the calcium concentrations by 40% or more fails to contract (bottom right). Bottom Right: Increasing delay to critical calcium level translates into EMD in muscle movement. Note that with this model, calcium fatigue scaling does not affect the peak velocity, but does affect both EMD and duration of movement.

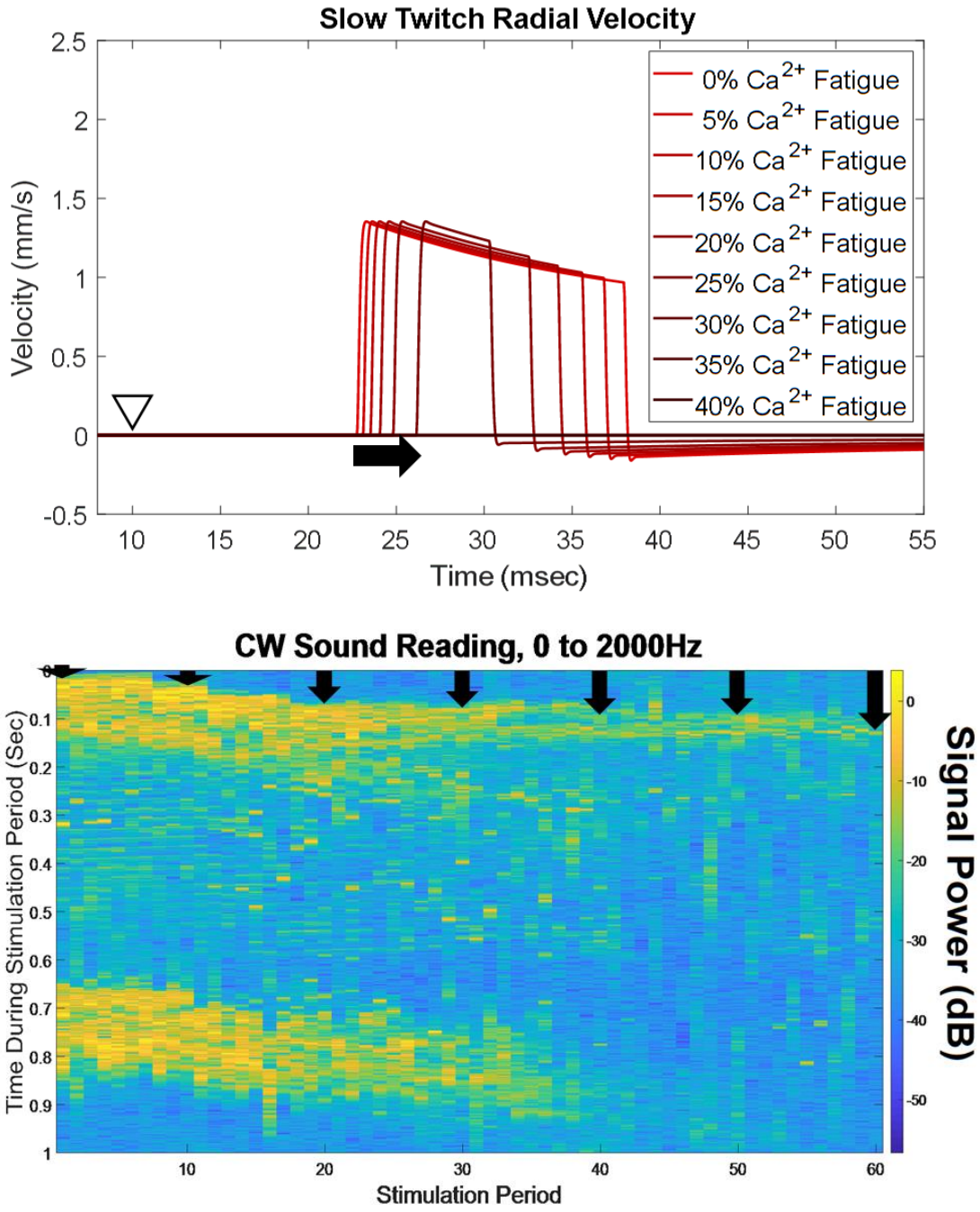

Figure 4-3. Simplified Calcium Fatigue Model and Mechanical Delay. Top: Simulated twitch velocity trace on slow twitch fiber with varying levels of fatigue. Upside down triangle indicates stimulus time. Note that the delay between stimulus onset and the start of movement. Bottom: Likewise, with increasing muscle fatigue, we observed a delay in the onset of movement in our CW experiments (black arrows). Note: Although the top is a twitch and the bottom is a stimulus train, the delay between movement onset and stimulus should be comparable.

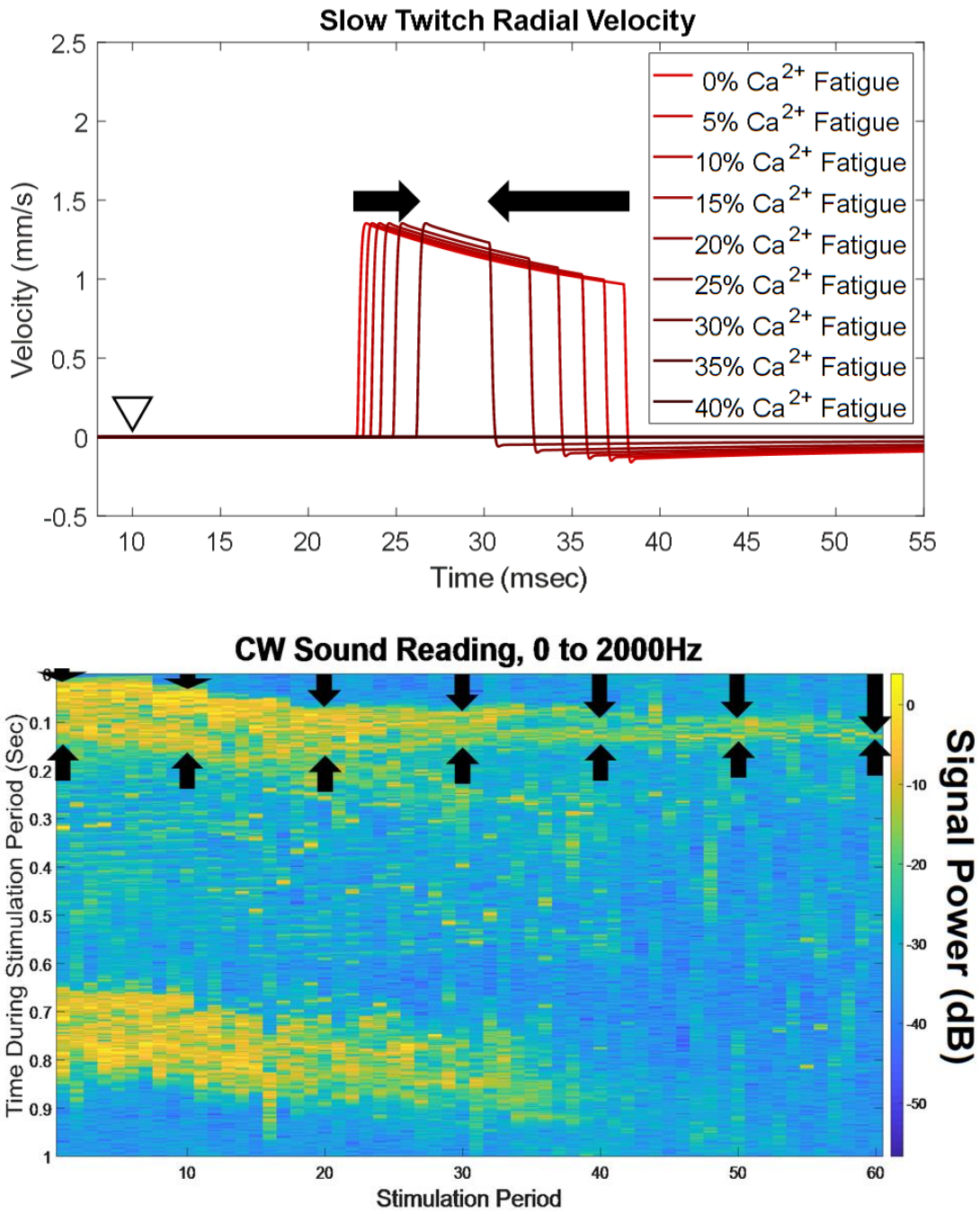

Figure 4-4. Simplified Calcium Fatigue Model and Shorter Duration Movements. Top: Simulated twitch velocity trace on slow twitch fiber with varying levels of fatigue. Upside down triangle indicates stimulus time. Note that the duration of fast velocity movement gets shorter with more fatigue (black arrows). Bottom: Likewise, with increasing muscle fatigue, we observed a reduction in the movement duration in our CW experiments (black arrows). Note: this is not a direct comparison, as the top is muscle twitch and the bottom is a stimulus train.

Fixed and Ramped Intensity Stimulus Trains

Ramping the edges of the pulse train creates a nonlinear recruitment pattern, especially towards the center of the stimulation intensity range. In Figure 4-5 (top left), low stimulus, even as high as 25% of the fully saturated current, only 1.95% MUs are recruited, whereas at 75% of the fully saturated current, 57.5% of MUs are activated by the stimulation. The nonlinear effect is most pronounced in the ramp up/ramp down regions at the start and stop of the pulse train for the middle current intensities, creating a beveled effect. This means that edge-case MUs are activated several more times compared to the adjoining fibers.

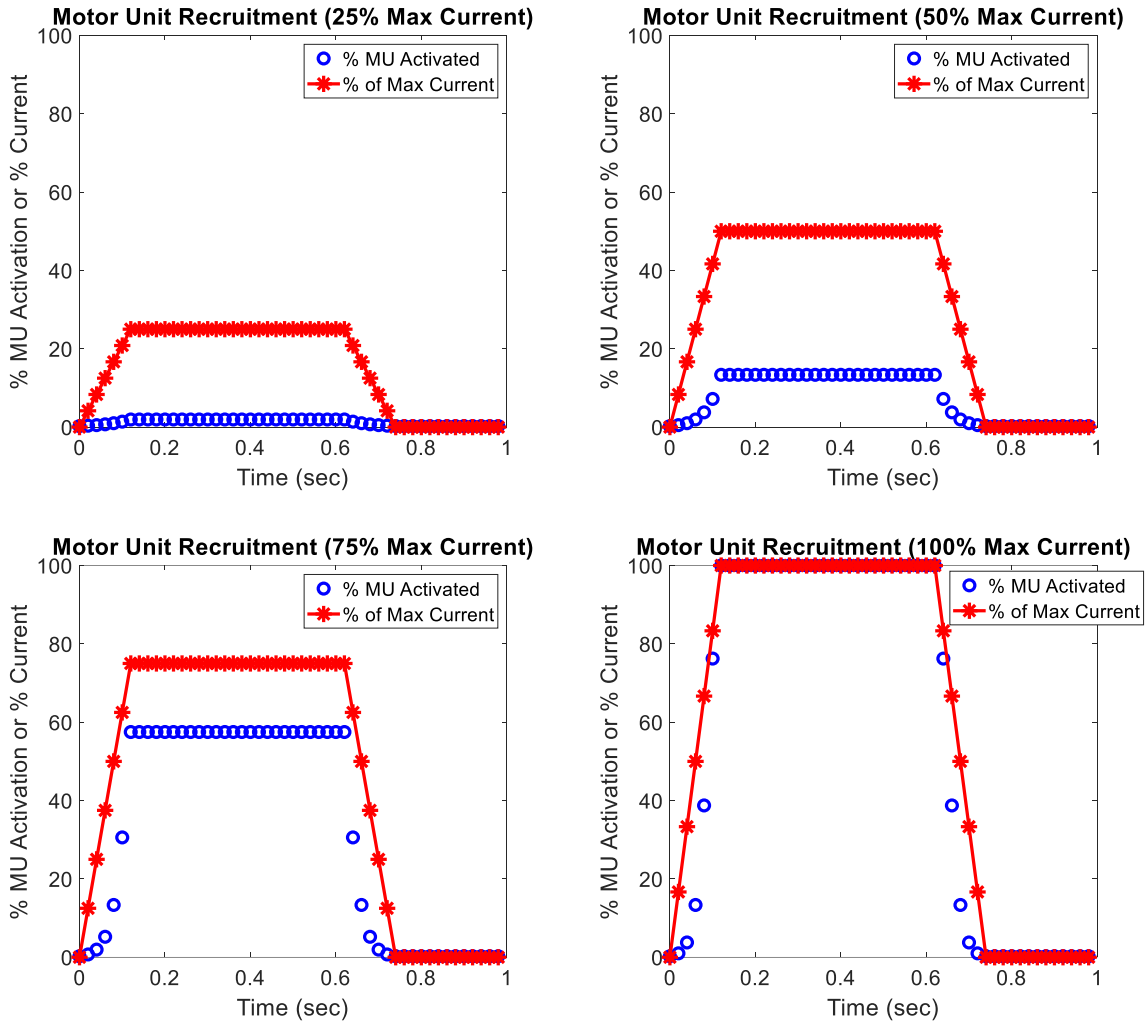

Figure 4-5. Motor Unit Activation by Stimulation Current. Motor unit recruitment is nonlinear, meaning the periods where current is being ramped up and down, the motor units show a more rounded recruitment pattern.

In the fixed intensity pulse train, Figure 4-6 (top half), all fibers that will be recruited by given stimulus will fire and cease to fire completely in synchrony.

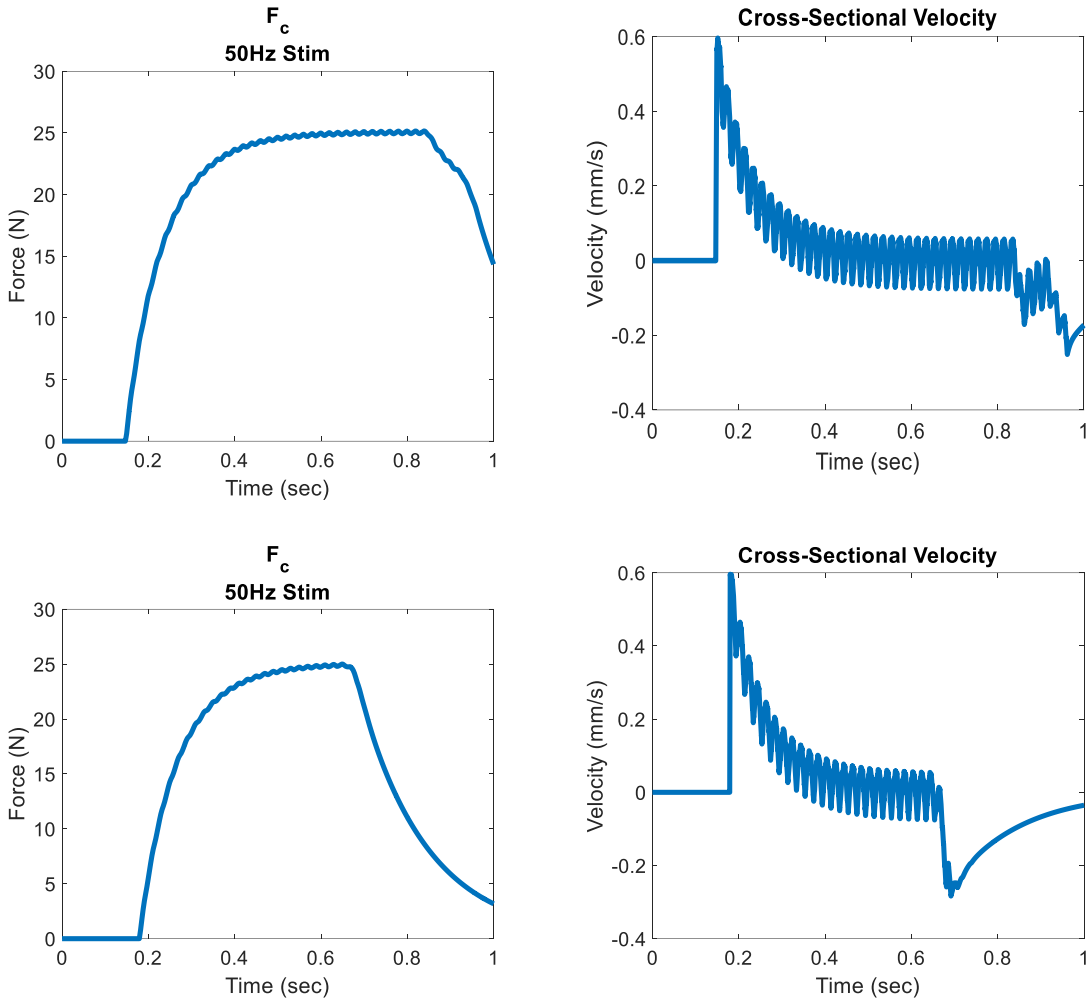

Figure 4-6. Fixed Pulse Train Intensity Vs. Varying Pulse Train Intensity. Top Left: The fixed intensity pulse train holds onto the desired force until the end of the stimulation period, and holds greater than 50% of it more than 200ms after the stimulation has stopped. Top Right: The fixed intensity pulse train velocity trace has a jagged area towards the end. Bottom Left: The ramped intensity pulse train releases force well before the fixed intensity pulse train. However, it releases more orderly than the fixed pulse train. Bottom Right: The velocity trace for the ramped intensity pulse train behaves more like the pulse velocity traces we observed in Chapters 2 and 3.

Variable Muscle Composition

The 125 slow/375 fast twitch muscle demonstrated less fused tetanus, which resulted in lower overall force produced.

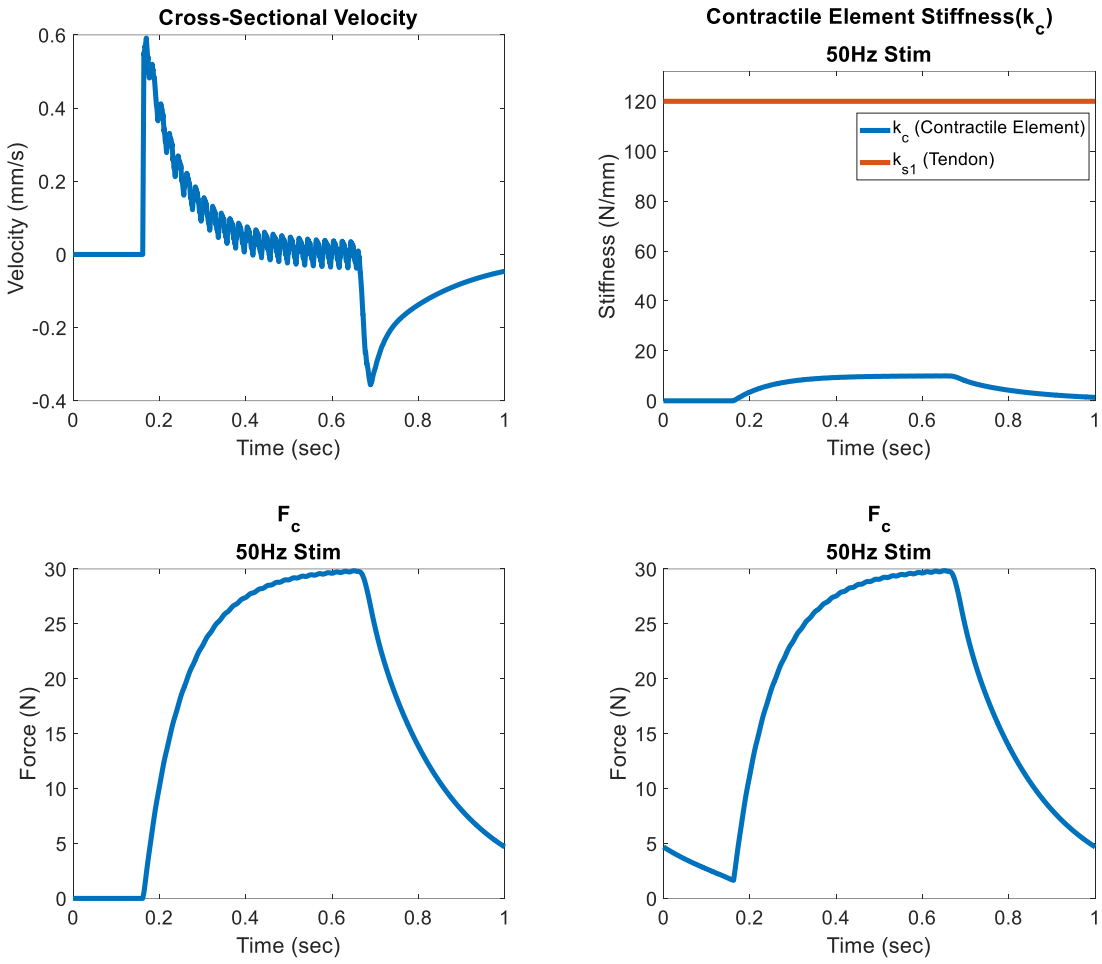

Figure 4-7. Mechanical Performance of Simulated Muscle Model with 250 Slow Twitch and 250 Fast Twitch Muscle Fibers. Top Left: 1 second simulation of radial velocity trace using muscle model stimulated with a shifted, ramped stimulation. Top Right: Simulated time-varying contractile element stiffness overlaid with the constant tendon stiffness for the same period. Bottom Left: Simulated force trace for half/half muscle model for 1 second. Bottom Right: Simulated force trace for half/half muscle model in the subsequent second of stimulation. Note that the force lingers from the first stimulation despite the fact that stimulation ended entirely at 0.8s.

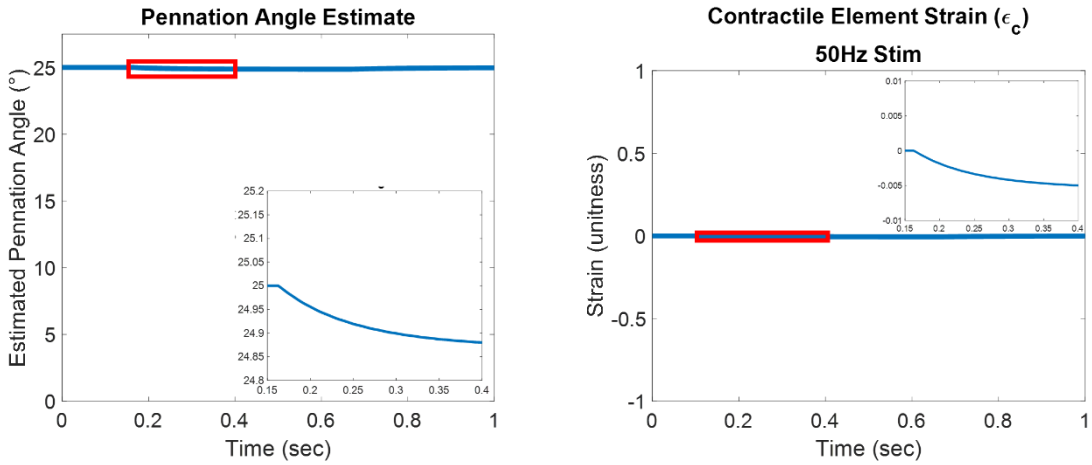

Figure 4-8. Minute changes in the structural characteristics in the 250 slow/250 fast twit fiber model. Left: The pennation angle barely changes due to the almost negligible change in contractile element (muscle) length. Right: The strain resulting from contraction is almost negligible. Note, however, this was enough to cause a radial velocity change in Figure 4-7.

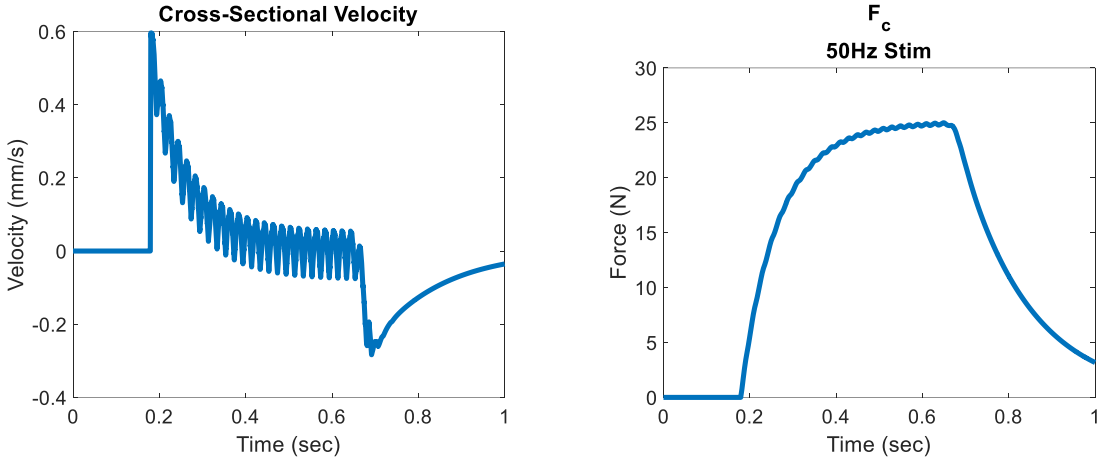

Figure 4-9. Mechanical Performance of Simulated Muscle Model with 125 Slow Twitch and 375 Fast Twitch Muscle Fibers. Left: 1 second simulation of radial velocity trace using muscle model stimulated with a shifted, ramped stimulation. Note that with fewer slow twitch fibers to fuse the twitches, the up and down, the simulated velocity whips back forth during stimulation. Right: Simulated force trace for 125 slow/375 fast twitch muscle model for 1 second. Note that the less fused tetanus of the fast twitch fibers results in lower overall force than compared to the mixed 250 slow/250 fast twitch muscle.

DISCUSSION

General Comments on Muscle Model

For simplicity, and the fact that we do not possess most of the real-world model parameters to properly tune our model, we used primarily parameters used previously in [132], which were a combination of real world and literature based measurements. A third possibility is to tune the parameters in the model post hoc to match real world data. Estimating parameters with these methods is not purely for minimizing the error between predicted and experimental values, but this can provide estimates of the actual muscle states and variables that are difficult, destructive, or otherwise unmeasurable in a real-world setting such spring, mass, or viscosity constants of the muscle, resting ionic distributions, or relative fast and slow twitch muscle fiber composition. Essentially this is running the model in reverse to run a diagnostic estimate of muscle state. For a controller scheme, this is a required step, as most muscle state variables must be estimated as the controller progresses. Ideally, the estimator could make accurate predictions, but there would be a feedback mechanism to improve the system performance when accumulation of error or outside perturbation inevitably decrease the accuracy and validity of the model parameters. Starting a model with accurate parameters is better for the model, but it will end up out of sync with real world values eventually without a corrective feedback mechanism [129].

The estimates of radial muscle velocity are based solely on the assumption of being a constant volume, purely elastic cylinder. Although this is a problem, the purely elastic assumption is mitigated somewhat by the fact that the muscle strain used to derive

the cylinder deformation is derived from more physiologically accurate viscoelastic deformation. Additionally, real world muscle more complicated in structure, and pennate muscle like the gastrocnemius exhibits a variable gearing ratio [15] which affects how the muscle cross-section behaves. Given the fact that we predicted our isometric contraction to have minimal strain and pennation angle changes, it is possible that this effect is minimal.

Variable Delay Twitches

Simplified Calcium Inhibition Fatigue Model

We observed that slow twitch fibers would be more susceptible to a depletion of calcium than the fast twitch fibers, because the relative difference between its resting and activated state is smaller compared to the fast twitch fiber. Because we do not observe this in nature, it implies that either the model is inaccurate in this regard, or that the slow twitch fibers are more resistant to impaired calcium dynamics which is observed in muscle fatigue. Further, the alpha activation term defined in Equation 17 and its subsequent use in Equation 8 and Equation 9 create a noticeably jagged rise and fall for individual twitches due to the binary nature of the thresholding, particularly with respect to the simulated radial velocity (see Figure 4-2, bottom row). This is somewhat of an inconsistency with prior models who treated the term as a fractional value (considering the muscle as one whole unit). By introducing individual motor units, and the authors in [132] decided to create a binary threshold at the reported critical calcium values to initiate cross-bridge formation in literature. We believe it would be more accurate to model this

with a sigmoid or similar function whose transition period occurs around the threshold, rather than a binary threshold.

Fixed and Ramped Stimulus Intensity Trains

The difference in activation between these two models was striking, though perhaps this was more related to the nonlinear activation function than anything else. We observed far more activation with the fixed amplitude stimulation trains than we did with the variable stimulation trains, though this discrepancy may be reduced if we used a higher stimulus intensity. Further, we also saw discontinuity on the release, which we believe is related to the difference in slow and fast muscle fibers when released, as they all released in unity, unlike the variable amplitude trains.

Variable Muscle Composition

Muscle can produce more force the more individual twitches can fuse into a tetanic stimulation, so it is unsurprising to see that the unfused 125 slow/375 fast twitch muscle produces less force when it shows less tetanus and given that the model assumed equal strength between fast and slow twitch fibers. Incorporating more realistic forces for the fibers would likely increase the amount of force the muscle can produce. Further, it is a known phenomenon that with fatigue and recovery, twitch duration can shorten after 5 minutes of recovery, making it more difficult to effectively stimulate the muscle to a tetanic response [115], so this behavior may have some realistic basis even if it is not in the unfatigued context.

CONCLUSION

We have identified several areas of weakness in the original model from [132] and attempted to address them by adding a variable nerve conduction velocity delay, which ended up smoothing results induced by the model's assumptions about calcium dynamics. We also evaluated the effects of a simplified calcium fatigue model and how this would automatically induce stimulation delay, and explored the accuracy of its representation of mixed fiber muscles, highlighting the characteristics generated by the model. We believe our modifications have increased the model accuracy with relevant biological phenomena, which could already predict some real-world situations we observed with our experiments in Chapters 2 and 3.

CHAPTER FIVE: MAIN FINDINGS AND FUTURE DIRECTIONS

Summary of Main Findings

Tissue Doppler Imaging Twitch Recovery Monitor

Tissue Doppler imaging (TDI) was able to accurately predict electrical muscle stimulation (EMS) induced muscle fatigue from EMS induced muscle twitches, but at significant cost and lacks portability. Further, stepwise linear regression revealed that results were subject specific, which likely means that the underlying tissue in the subjects studied varied and thus needs to be taken into account for muscle modeling and hybrid EMS controllers.

Wearable Continuous Wave Force Monitor

Continuous wave (CW) Doppler can provide a cheap, portable fatigue monitor which is primarily sensitive to muscle activity and not passive movements. The current CW design lacks directionality and is only sensitive to a limited range of depth. However, both of these can be addressed with hardware modifications such as implementing I/Q demodulation and making an array of transducers.

Multiscale Muscle Modeling

The model as published could provide reasonably accurate estimates of muscle activation, but lacked several key features that we tried to incorporate, such as a variable action potential propagation delay that we believe has improved the realism of the model.

Lessons Learned

Feasibility Study

This dissertation was conducted in three stages to create a wearable, noninvasive system for monitoring muscle fatigue induced by EMS. The first stage of the study was a feasibility study to conclude that there were physical signs of muscle fatigue and that Doppler ultrasound techniques could detect them, which we confirmed. In doing so, we found that there was a substantial inter-subject variability that we attributed to variations in the subjects' anatomy and physiology. It is possible that this would be less pronounced in those suffering from an extended period of paralysis, as their muscle composition becomes more uniformly fast twitch fibers.

As a feasibility study, it was critical to reduce the number of variables and obtain the clearest data to establish the fundamentals of the technique. This means that this stage was designed to collect the highest quality velocity data (TDI, full depth resolution at the sub-mm scale and velocity estimates at every depth with sub-millisecond resolution) and mechanical data (commercial dynamometer) in the most controlled environments (isometric configuration) and well controlled muscle activation (EMS). We used EMS because it activates the same tissue consistently, and because variability would have been introduced by inconsistent motor commands if subjects were allowed voluntary control their own muscles (mental fatigue, pain avoidance, etc.). Likewise, isometric conditions restricted the movement of muscles which helped isolate the effect on the muscle alone, removing the complications caused by varying joint angles. This of course may be a

critical factor to incorporate into a final design. In this study, the focus was to establish the fundamentals of the technique and therefore we restricted it to isometric conditions.

Portability Study

Our second study was to address the lack of portability in the feasibility study and expanded our experimental conditions into more realistic scenarios. We wanted to know if the fundamentals of the TDI technique translated into a portable system. We found that, as our CW technique lacked directionality as well as clear depth resolution, not all of the same variables could be measured, and therefore we needed a different approach. We were fortunate in that the memory and sampling requirements were so much lower for this technique that we were able to record for the entire experiment (written directly to the hard drive in real time) so we could record for the actual stimulation periods, not just intermittently during muscle twitches. This allowed us to develop a duration of movement metric that strongly correlated to EMS induced force during induced fatigue. Further, we examined what effects voluntary muscle control and free limb movement (isokinetic, same velocity regardless of force) had on the CW signal and compared that to both our isometric EMS stimulation as well as passive constant velocity movements driven by the dynamometer motors alone. In the former case, we observed that muscle movement at both the onset and release of contractions generated CW signal, similar to the isometric EMS case. In the latter case, we established that we saw minimal if any signal generated from passive movements of the dynamometer. This is a crucial finding, as a real-world hybrid controller would need to distinguish between passive movements generated by the electric motor and the active movements caused by simultaneous muscle

contraction. We did not, however, study these two movement mechanisms simultaneously, which will need to be addressed in a future study.

Modeling Study

Finally, we concluded with a muscle modeling study to compare to our real world data in an attempt to A)help explain variations observed in the feasibility study and B)improve muscle modeling. The latter is a critical issue, because a model of muscle activation is required as a sub-component of any hybrid controller scheme to predict the muscle contribution to the hybrid system movement. We observed that varying muscle composition would in fact affect the estimated force and velocity traces, which reenforced that these models need to be generated on a subject-specific basis, possibly by using a systems identification or adaptive filter-based approaches. We also observed that reducing calcium levels in the model, which occurs during muscle fatigue, both reduces the duration of a muscle twitch and automatically increases the delay between the stimulus and the onset of muscle motion. We then used our real-world data from our CW experiments which supported these predictions. We also added a more realistic spread in the delay between stimulus and individual fiber activations to account for the propagation speed of action potentials down motor neurons which we believe improved the model by smoothing the output velocity and force values, which were unnaturally un-tetanized in the model without this addition.

Future Directions

Voluntary Muscle Control Applications

Because the target population for this technique is those suffering paralysis, the fact that we tested these techniques in able bodied subjects (in isometric conditions) is viewed as a drawback of the study. This was done to evaluate the techniques in the most ideal conditions (young healthy able-bodied subjects, advanced human dynamometer, isometric conditions). However, these techniques have applications beyond the scope of paralysis and would be perfectly suited for rehabilitation, sports science, or as a human-machine interface.

Other Portable Ultrasound Implementations

In this work, we reported evaluating two forms of Doppler ultrasound, tissue Doppler imaging and continuous wave Doppler ultrasound, though we experimented with more in other contexts. Tissue Doppler imaging was selected because of it is well established, commercially available, and provides rich depth resolved information, but has high computation, memory, cost, and form factor requirements. For these reasons, we also explored a simple vascular continuous wave Doppler ultrasound approach. Although it does not have the same level of time and spatial resolution, it is cheap, low power, easy to process, and portable. If we were to expand this direction further, we could attempt to rectify the limitations of CW ultrasound by using a depth resolved CW technique like frequency modified continuous wave (FMCW) techniques, like the one developed by Kunita et al., [124] previously or standard FMCW radar techniques that require rapid

successive chirps. Either way, this would require custom hardware design, unlike conventional TDI and CW which are readily available.

Alternatively, we could develop a multi-depth CW US array using different center frequencies for every transducer pair, with IQ for directionality. After all, the TDI information we used in chapter 2 only requires three transducer pairs to get all the info necessary to perform the average velocity waveform calculations (average overall velocity, and the velocity at top and bottom at bottom to calculate strain).

sEMG

As mentioned in chapter 4, the stimulus delay between electrical, movement, and force can all be different, and are related to muscle fatigue, and that the most important of these for a robotic controller is force. Since the other two methods (electrical and movement) are compatible with one another, it may be possible to use these two techniques together to try to predict the muscle force delay. Unlike model with traditional feedback, the information would come before the desired event occurs, which may prevent error from occurring outright. Not only that, but we established that the CW method is more than enough to detect the onset of muscle activity and that it is completely compatible with sEMG. Given this fact, it may be possible to make preemptive updates before error has ever occurred.

Acoustic Myography

We briefly mentioned acoustic myography (AMG) in the text as an alternative method to measure muscle activity. Like ultrasound, it uses acoustic waves. Unlike ultrasound, however, the acoustic signal measured is generated by the muscle itself at

sub-audible frequencies [30], [37]. Both of these facts are important. Because the acoustic signal is intrinsically generated by the muscle itself, it doesn't require a setup to emit acoustic waves thus saving energy power and requiring less electronics. Further, ultrasound emitted into the body travels twice as far as the target depth because it must penetrate, reflect, and then return, whereas AMG signals only travel one direction, reducing attenuation. I should note, however, that the amplitude of ultrasound waves is controlled by the user, and therefore can be much higher intensity than that of AMG signals. To the second point, the lower frequencies emitted by AMG will allow for simultaneous ultrasound/AMG measurements without interfering with one another, meaning both can be performed simultaneously to compliment one another, even at the same location. This may be useful when trying to differentiate passive movements visible to ultrasound from active muscle contractions visible to both ultrasound and AMG. Further, both of these signals are compatible with sEMG and all three could be performed simultaneously.

Variations on Stimulation Parameters and Electrode Placement

On multiple occasions, we mentioned desynchronized multi-site stimulation. This is because we believe this has the greatest utility to reduce EMS induced muscle fatigue. By allowing different fibers to share the load intermittently, the other fibers are guaranteed a small rest period, allowing them to recover and reduce the accumulation of phosphates that are related to muscle fatigue [19]. At present, this technique is performed blind, so results are likely suboptimal. Plane wave ultrasound imaging would be extremely valuable for electrode placement with this technique. Plane wave strain

imaging can identify which parts of the muscle are contracting based on which electrode is firing, and thus identify any redundant stimulation zones or underutilized tissue, and re-place the electrodes accordingly. Because the plain wave imaging only needs to be performed during electrode placement, it does not require portability. Further, it may be possible to use a less computationally intensive Doppler Ultrasound technique to achieve the same results. Likewise, the same techniques could be used to study how muscle contracts for custom stimulation waveforms, which could also lead to better fatiguing characteristics.

Improved Modeling and Prediction:

The simulations we performed in chapter 4 were computationally inefficient, and chosen for simplicity and the available data. However, there are more advanced techniques such as sigma point Kalman filters (SPKF) which can approximate nonlinear model states [23] up to a 2^{nd} order Taylor series expansion, and converge very quickly. This does require, however, that the inputs and outputs are time synchronized. Because we had poor control of the start of our stimulator, we might benefit from tuning our parameters with repetitive simulations to minimize the mean squared error [137]. Both of these methods are potentially useful for not only predicting muscle function, but also for identifying unobservable system dynamics.

APPENDIX

APPENDIX A: Tissue Doppler Imaging

Clinical ultrasound (US) Doppler imaging is most commonly used to measure blood flow, which is considerably faster than tissue movements. For example, blood measurements can be many hundreds of cm/s for certain diseases and stenosis [138], whereas the peak twitch velocity-normal to the muscle's line of action-in Figure 2-3, which is representative of our muscle twitch experiments, is only in the range of 3 mm/s. Blood Doppler ultrasound processing usually contains a low pass filter (hardware or digital) designed to suppress high intensity, slow tissue movements. Tissue Doppler imaging (TDI) on the other hand focuses on these relatively slow-moving tissues as the quantity being measured.

In the TDI sections of this work, we used an autocorrelation pulse wave technique based on the method found in [103], and the derivation of its signal processing can be found in APPENDIX B: TDI Velocity Calculation Derivation. Our TDI measurements are performed by pulsing ultrasound waves into the tissue, receiving over an array of ultrasound elements, beamforming down to a one-dimensional signal, and comparing phase shifts between successive US pulses to estimate muscle velocity at every measured pixel depth. Whenever US waveform reaches an interface with a mismatch in acoustic impedance, part of the waveform reflects back to the transducer. This means that highly

reflective, slow moving tissue (muscle, fat, skin, connective tissue like tendons, etc.) as well as relatively less reflective, fast moving blood cells can all contribute to the receive signal ($R_x(t)$). If you wish to focus on muscle, you can adjust probe placement and the Doppler gate (the depths of interest) to only record from muscles of interest and to avoid blood flow and/or tissues we are not concerned with such as skin and fat layers.

For our experiments, we assumed the signal came exclusively from muscle movement, but there are many complicating factors that could have led to variability in the measurements. This could include the accidental inclusion of blood flow, tissue moving in and out of the imaging plain, interreference with off axis reflections, measurement noise affecting the phase estimates, speckle interference, aliasing of very fast signals (which should be minimal given the fast pulse repetition frequency (PRF)), frequency/depth dependent attenuation, variable speed of sound throughout the tissue, nonlinear acoustical propagation effects, the suboptimal assumption of a narrow band transmit signal ($T_x(t)$), quantization error in the analog to digital sampling, or other effects. Each of these sources of variability would affect the received signal and velocity estimates. We generally neglected these effects, but is possible that these experiments could be improved by taking them into account when feasible.

APPENDIX B: TDI Velocity Calculation Derivation

First we consider our transmitted ultrasound pulse waveform signal, $T_x(t)$, to be a sine wave with a center frequency, f_c, and a real valued envelope, A(t) of the ultrasound signal pulse. The center frequency of the transducer used in this work was 6.66 Mhz.

$$T_x(t) = A(t) * cos(2\pi * f_c * t)$$

As the transmitted ultrasound waveform hits reflectors in the medium, time delayed versions bounce off and propagate back to the transducer array and are recorded digitally. These 'receive signals', $R_x(t)$, are time delayed version of transmitted signal $T_x(t)$, whose delay, τ, is dependent on the depth of the reflector, D, and the speed of sound, C. The calculations all the calculations performed here assume the speed of sound to be a constant, uniform 1540 m/s throughout the tissue. For simplicity's sake, this derivation only considers one reflector. In reality, biological tissues contain many reflectors and the true reflected signal is in fact the summation of many delayed versions of the transmitted signal.

$$R_x(t) = A(t-\tau) * cos(2\pi * f_c * (t - \tau))$$

$$\tau = 2 * D/C$$

For the signal acquisition period, we pulse many of these waves in rapid (kHz) succession, the frequency of pulse being our pulse repetition frequency or PRF. Each return signal is now considered by their own respective timeframe (t) relative to the time that each was pulsed so that we can directly compare changes in the reflections as changes in the tissue itself. If delay between pulses sufficiently small such that the envelopes are essentially the same between two $R_x(t)$ signals, $A(t - \tau_2) \sim A(t - \tau_1)$, we can differentiate the position of the reflector on the change in phase instead Δ_{Phase}, which we can convert into a change in distance Δ_D:

$$2\pi * f_c * \Delta\tau = \Delta_{Phase}$$

$$2\pi * f_c * \left(\frac{2 * \Delta_D}{C}\right) = \Delta_{Phase}$$

$$\Delta_D = \frac{\Delta_{Phase} * C}{4\pi * f_c}$$

To determine the phase change (Δ_{Phase}), use the Hilbert transform to break into in-phase (I) and quadrature (Q) components, multiply by the conjugate of the next pulse, and transform back into angle:

$$IQ_{R_x(t)} = Hilbert\{R_x(t)\}$$

$$\Delta_{Phase} = \tan^{-1}(IQ_{R_{x1}(t)} * conj[IQ_{R_{x2}(t)}])$$

Plug in for Δ_{Phase},

$$\Delta_D = \frac{\Delta_{Phase} * C}{4\pi * f_c}$$

As $Velocity = \frac{distance}{time}$, divide by the time between pulses to get velocity estimate:

$V_{SampleDepth} = \frac{\Delta_D}{\Delta t_{Rx}}$ or $V_{SampleDepth} = \Delta D * PRF$

Because there is a lot of high frequency noise in this signal, you can add an integer multiple delay of PRF, $n * PRF$, to serve as a de facto low pass filter. In the case of using the PRF alone, set n = 1. With the distance traveled calculated from the change in phase and the time between pulses set by the PRF or any added integer multiple, we can calculate the velocity estimate at every pixel depth.

$\therefore$

$V_{SampleDepth} = \frac{\Delta_{Phase} * C}{4\pi * f_c * \Delta t_{Rx}}$ or $\frac{\Delta_{Phase} * C * n * PRF}{4\pi * f_c}$

REFERENCES

[1] S. Luo, H. Xu, Y. Zuo, X. Liu, and A. H. All, "A Review of Functional Electrical Stimulation Treatment in Spinal Cord Injury," *Neuromol Med*, Jan. 2020, doi: 10.1007/s12017-019-08589-9.

[2] S. L. James *et al.*, "Global, regional, and national burden of traumatic brain injury and spinal cord injury, 1990–2016: a systematic analysis for the Global Burden of Disease Study 2016," *The Lancet Neurology*, vol. 18, no. 1, pp. 56–87, Jan. 2019, doi: 10.1016/S1474-4422(18)30415-0.

[3] J. H. Patrick and M. R. McClelland, "Low energy cost reciprocal walking for the adult paraplegic," *Spinal Cord*, vol. 23, no. 2, pp. 113–117, Apr. 1985, doi: 10.1038/sc.1985.19.

[4] E. Rossato *et al.*, "Rise2-Italy Project: Muscle FES after peripheral nerve lesion," *Basic Appl Myol*, vol. 19, pp. 169–172, 2009.

[5] E. D'Anna *et al.*, "A somatotopic bidirectional hand prosthesis with transcutaneous electrical nerve stimulation based sensory feedback," *Scientific Reports*, vol. 7, no. 1, Dec. 2017, doi: 10.1038/s41598-017-11306-w.

[6] C. A. Angeli, V. R. Edgerton, Y. P. Gerasimenko, and S. J. Harkema, "Altering spinal cord excitability enables voluntary movements after chronic complete paralysis in humans," *Brain*, p. awu038, Apr. 2014, doi: 10.1093/brain/awu038.

[7] L. Spieker, C. Wiesener, A. Niedeggen, N. Wenger, and T. Schauer, "Motor and sensor recovery in a paraplegic by transcutaneous spinal cord stimulation in water," *Proceedings on Automation in Medical Engineering*, vol. 1, no. 1, Feb. 2020, doi: 10.18416/AUTOMED.2020.

[8] J. C. Baldi, R. D. Jackson, R. Moraille, and W. J. Mysiw, "Muscle atrophy is prevented in patients with acute spinal cord injury using functional electrical stimulation," *Spinal Cord*, vol. 36, no. 7, pp. 463–469, Jul. 1998, doi: 10.1038/sj.sc.3100679.

[9] M. O. Ibitoye, N. A. Hamzaid, N. Hasnan, A. K. Abdul Wahab, and G. M. Davis, "Strategies for Rapid Muscle Fatigue Reduction during FES Exercise in Individuals with Spinal Cord Injury: A Systematic Review," *PLoS ONE*, vol. 11, no. 2, p. e0149024, Feb. 2016, doi: 10.1371/journal.pone.0149024.

[10] S. A. Binder-Macleod and T. Kesar, "Catchlike property of skeletal muscle: Recent findings and clinical implications," *Muscle Nerve*, vol. 31, no. 6, pp. 681–693, Jun. 2005, doi: 10.1002/mus.20290.

[11] R. Nguyen, K. Masani, S. Micera, M. Morari, and M. R. Popovic, "Spatially Distributed Sequential Stimulation Reduces Fatigue in Paralyzed Triceps Surae Muscles: A Case Study," *Artificial Organs*, vol. 35, no. 12, pp. 1174–1180, 2011, doi: 10.1111/j.1525-1594.2010.01195.x.

[12] M. Laubacher, A. E. Aksöz, R. Riener, S. Binder-Macleod, and K. J. Hunt, “Power output and fatigue properties using spatially distributed sequential stimulation in a dynamic knee extension task,” *Eur J Appl Physiol*, vol. 117, no. 9, pp. 1787–1798, Sep. 2017, doi: 10.1007/s00421-017-3675-0.
[13] A. J. Bergquist, V. Babbar, S. Ali, M. R. Popovic, and K. Masani, “Fatigue reduction during aggregated and distributed sequential stimulation,” *Muscle & Nerve*, vol. 56, no. 2, pp. 271–281, 2017, doi: 10.1002/mus.25465.
[14] W. Herzog, “The multiple roles of titin in muscle contraction and force production,” *Biophys Rev*, vol. 10, no. 4, pp. 1187–1199, Aug. 2018, doi: 10.1007/s12551-017-0395-y.
[15] E. Azizi, E. L. Brainerd, and T. J. Roberts, “Variable gearing in pennate muscles,” *Proceedings of the National Academy of Sciences*, vol. 105, no. 5, pp. 1745–1750, Feb. 2008, doi: 10.1073/pnas.0709212105.
[16] CCCOnline, *Anatomy & Physiology*.
[17] I. V. Kovyazina, A. N. Tsentsevitsky, E. E. Nikolsky, and E. A. Bukharaeva, “Kinetics of acetylcholine quanta release at the neuromuscular junction during high-frequency nerve stimulation,” *European Journal of Neuroscience*, vol. 32, no. 9, pp. 1480–1489, 2010, doi: 10.1111/j.1460-9568.2010.07430.x.
[18] D. G. Allen, G. D. Lamb, and H. Westerblad, “Skeletal Muscle Fatigue: Cellular Mechanisms,” *Physiological Reviews*, vol. 88, no. 1, pp. 287–332, Jan. 2008, doi: 10.1152/physrev.00015.2007.
[19] A. J. Cheng, N. Place, and H. Westerblad, “Molecular Basis for Exercise-Induced Fatigue: The Importance of Strictly Controlled Cellular Ca $^{2+}$ Handling,” *Cold Spring Harb Perspect Med*, vol. 8, no. 2, p. a029710, Feb. 2018, doi: 10.1101/cshperspect.a029710.
[20] D. A. Jones, “High- and low-frequency fatigue revisited,” *Acta Physiologica Scandinavica*, vol. 156, no. 3, pp. 265–270, 1996, doi: 10.1046/j.1365-201X.1996.192000.x.
[21] C. S. Bickel, C. M. Gregory, and J. C. Dean, “Motor unit recruitment during neuromuscular electrical stimulation: a critical appraisal,” *Eur J Appl Physiol*, vol. 111, no. 10, pp. 2399–2407, Oct. 2011, doi: 10.1007/s00421-011-2128-4.
[22] A. Del Vecchio *et al.*, “You are as fast as your motor neurons: speed of recruitment and maximal discharge of motor neurons determine the maximal rate of force development in humans,” *The Journal of Physiology*, vol. 597, no. 9, pp. 2445–2456, 2019, doi: 10.1113/JP277396.
[23] H. El Makssoud *et al.*, “Multiscale modeling of skeletal muscle properties and experimental validations in isometric conditions,” *Biol Cybern*, vol. 105, no. 2, pp. 121–138, Aug. 2011, doi: 10.1007/s00422-011-0445-7.
[24] R. Martin, C. Sadowsky, K. Obst, B. Meyer, and J. McDonald, “Functional Electrical Stimulation in Spinal Cord Injury: From Theory to Practice,” *Topics in Spinal Cord Injury Rehabilitation*, vol. 18, no. 1, pp. 28–33, Jan. 2012, doi: 10.1310/sci1801-28.
[25] J. Shi, Y. P. Zheng, X. Chen, and Q. H. Huang, “Assessment of muscle fatigue using sonomyography: Muscle thickness change detected from ultrasound images,”

Medical Engineering & Physics, vol. 29, no. 4, pp. 472–479, May 2007, doi: 10.1016/j.medengphy.2006.07.004.
[26] R. G. Edwards and O. C. J. Lippold, "The relation between force and integrated electrical activity in fatigued muscle," *The Journal of Physiology*, vol. 132, no. 3, pp. 677–681, 1956, doi: 10.1113/jphysiol.1956.sp005558.
[27] D. W. Russ and J. A. Kent-Braun, "Sex differences in human skeletal muscle fatigue are eliminated under ischemic conditions," *Journal of Applied Physiology*, vol. 94, no. 6, pp. 2414–2422, Jun. 2003, doi: 10.1152/japplphysiol.01145.2002.
[28] N. Akhlaghi *et al.*, "Real-Time Classification of Hand Motions Using Ultrasound Imaging of Forearm Muscles," *IEEE Transactions on Biomedical Engineering*, vol. 63, no. 8, pp. 1687–1698, Aug. 2016, doi: 10.1109/TBME.2015.2498124.
[29] M. R. Al-Mulla, F. Sepulveda, and M. Colley, "A Review of Non-Invasive Techniques to Detect and Predict Localised Muscle Fatigue," *Sensors*, vol. 11, no. 4, pp. 3545–3594, Mar. 2011, doi: 10.3390/s110403545.
[30] D. T. Barry, S. R. Geiringer, and R. D. Ball, "Acoustic myography: A noninvasive monitor of motor unit fatigue," *Muscle & Nerve*, vol. 8, no. 3, pp. 189–194, Mar. 1985, doi: 10.1002/mus.880080303.
[31] T. Bajd and M. Munih, "Basic functional electrical stimulation (FES) of extremities: An engineer's view," *Technology & Health Care*, vol. 18, no. 4/5, pp. 361–369, Jul. 2010, doi: 10.3233/THC20100588.
[32] D. R. Merrill, M. Bikson, and J. G. R. Jefferys, "Electrical stimulation of excitable tissue: design of efficacious and safe protocols," *Journal of Neuroscience Methods*, vol. 141, no. 2, pp. 171–198, Feb. 2005, doi: 10.1016/j.jneumeth.2004.10.020.
[33] T. Saxena *et al.*, "The impact of chronic blood–brain barrier breach on intracortical electrode function," *Biomaterials*, vol. 34, no. 20, pp. 4703–4713, Jul. 2013, doi: 10.1016/j.biomaterials.2013.03.007.
[34] E. Strickland and M. Harris, "What Happens When a Bionic Body Part Becomes Obsolete?: Blind People with Second Sight's Retinal Implants Found Out," *IEEE Spectrum*, vol. 59, no. 3, pp. 24–31, Mar. 2022, doi: 10.1109/MSPEC.2022.9729945.
[35] L. J. Macgregor, A. M. Hunter, C. Orizio, M. M. Fairweather, and M. Ditroilo, "Assessment of Skeletal Muscle Contractile Properties by Radial Displacement: The Case for Tensiomyography," *Sports Med*, vol. 48, no. 7, pp. 1607–1620, Jul. 2018, doi: 10.1007/s40279-018-0912-6.
[36] D. T. Barry, "Vibrations and sounds from evoked muscle twitches," *Electromyogr Clin Neurophysiol*, vol. 32, no. 1–2, pp. 35–40, Feb. 1992.
[37] A. P. Harrison, B. Danneskiold-Samsøe, and E. M. Bartels, "Portable acoustic myography - a realistic noninvasive method for assessment of muscle activity and coordination in human subjects in most home and sports settings," *Physiological Reports*, vol. 1, no. 2, Jul. 2013, doi: 10.1002/phy2.29.
[38] C. Meagher *et al.*, "New advances in mechanomyography sensor technology and signal processing: Validity and intrarater reliability of recordings from muscle," *Journal of Rehabilitation and Assistive Technologies Engineering*, vol. 7, p. 205566832091611, Jan. 2020, doi: 10.1177/2055668320916116.

[39] R. L. Lieber and J. Friden, “Functional and clinical significance of skeletal muscle architecture,” *Muscle & Nerve*, vol. 23, no. 11, pp. 1647–1666, Nov. 2000, doi: 10.1002/1097-4598(200011)23:11<1647::AID-MUS1>3.0.CO;2-M.
[40] M. Ito, Y. Kawakami, Y. Ichinose, S. Fukashiro, and T. Fukunaga, “Nonisometric behavior of fascicles during isometric contractions of a human muscle,” *Journal of Applied Physiology*, vol. 85, no. 4, pp. 1230–1235, Oct. 1998, doi: 10.1152/jappl.1998.85.4.1230.
[41] M. Bakke, A. Tuxetv, P. Vilmann, B. R. Jensen, A. Vilmann, and M. Toft, “Ultrasound image of human masseter muscle related to bite force, electromyography, facial morphology, and occlusal factors,” *European Journal of Oral Sciences*, vol. 100, no. 3, pp. 164–171, Jun. 1992, doi: 10.1111/j.1600-0722.1992.tb01734.x.
[42] R. S. Witte, D. E. Dow, R. Olafsson, Y. Shi, and M. O’Donnell, “High resolution ultrasound imaging of skeletal muscle dynamics and effects of fatigue,” in *IEEE Ultrasonics Symposium, 2004*, Montreal, Canada, 2004, vol. 1, pp. 764–767. doi: 10.1109/ULTSYM.2004.1417834.
[43] R. S. Witte, K. Kim, B. J. Martin, and M. O’Donnell, “Effect of Fatigue on Muscle Elasticity in the Human Forearm Using Ultrasound Strain Imaging,” in *Conf Proc IEEE Eng Med Biol Soc*, Aug. 2006, pp. 4490–4493. doi: 10.1109/IEMBS.2006.4398449.
[44] O. Stavdahl, A. Gronningsaeter, and K. E. Malvig, “ULTRASOUND BASED ESTIMATION OF MUSCLE CONTRACTION,” *Myoelectric Symposium*, p. 7, 1997.
[45] N. Pulkovski, P. Schenk, N. A. Maffiuletti, and A. F. Mannion, “Tissue Doppler imaging for detecting onset of muscle activity,” *Muscle & Nerve*, vol. 37, no. 5, pp. 638–649, May 2008, doi: 10.1002/mus.20996.
[46] A. V. Dieterich *et al.*, “Spatial variation and inconsistency between estimates of onset of muscle activation from EMG and ultrasound,” *Scientific Reports*, vol. 7, no. 1, Dec. 2017, doi: 10.1038/srep42011.
[47] N. R. Grubb, A. Fleming, G. R. Sutherland, and K. A. Fox, “Skeletal muscle contraction in healthy volunteers: assessment with Doppler tissue imaging.,” *Radiology*, vol. 194, no. 3, pp. 837–842, Mar. 1995, doi: 10.1148/radiology.194.3.7862989.
[48] S. Sikdar *et al.*, “Novel Method for Predicting Dexterous Individual Finger Movements by Imaging Muscle Activity Using a Wearable Ultrasonic System,” *IEEE Transactions on Neural Systems and Rehabilitation Engineering*, vol. 22, no. 1, pp. 69–76, Jan. 2014, doi: 10.1109/TNSRE.2013.2274657.
[49] C. Castellini, G. Passig, and E. Zarka, “Using Ultrasound Images of the Forearm to Predict Finger Positions,” *IEEE Transactions on Neural Systems and Rehabilitation Engineering*, vol. 20, no. 6, pp. 788–797, Nov. 2012, doi: 10.1109/TNSRE.2012.2207916.
[50] J. Shi, J.-Y. Guo, S.-X. Hu, and Y.-P. Zheng, “Recognition of Finger Flexion Motion from Ultrasound Image: A Feasibility Study,” *Ultrasound in Medicine &*

Biology, vol. 38, no. 10, pp. 1695–1704, Oct. 2012, doi: 10.1016/j.ultrasmedbio.2012.04.021.
[51] W. J. Tyler, Y. Tufail, M. Finsterwald, M. L. Tauchmann, E. J. Olson, and C. Majestic, "Remote Excitation of Neuronal Circuits Using Low-Intensity, Low-Frequency Ultrasound," *PLoS ONE*, vol. 3, no. 10, p. e3511, Oct. 2008, doi: 10.1371/journal.pone.0003511.
[52] D. Seo *et al.*, "Wireless recording in the peripheral nervous system with ultrasonic neural dust," *Neuron*, vol. 91, no. 3, pp. 529–539, 2016.
[53] M. Imbault, D. Chauvet, J.-L. Gennisson, L. Capelle, and M. Tanter, "Intraoperative Functional Ultrasound Imaging of Human Brain Activity," *Scientific Reports*, vol. 7, no. 1, p. 7304, Aug. 2017, doi: 10.1038/s41598-017-06474-8.
[54] C. Errico, B.-F. Osmanski, S. Pezet, O. Couture, Z. Lenkei, and M. Tanter, "Transcranial functional ultrasound imaging of the brain using microbubble-enhanced ultrasensitive Doppler," *NeuroImage*, vol. 124, no. Part A, pp. 752–761, Jan. 2016, doi: 10.1016/j.neuroimage.2015.09.037.
[55] Y. Tamura, I. Hatta, T. Matsuda, H. Sugi, and T. Tsuchiya, "Changes in muscle stiffness during contraction recorded using ultrasonic waves," *Nature*, vol. 299, no. 5884, pp. 631–633, Oct. 1982, doi: 10.1038/299631a0.
[56] I. Hatta, H. Sugi, and Y. Tamura, "Stiffness changes in frog skeletal muscle during contraction recorded using ultrasonic waves.," *The Journal of Physiology*, vol. 403, no. 1, pp. 193–209, Sep. 1988, doi: 10.1113/jphysiol.1988.sp017245.
[57] P. Peetrons, "Ultrasound of muscles," *Eur Radiol*, vol. 12, no. 1, pp. 35–43, Jan. 2002, doi: 10.1007/s00330-001-1164-6.
[58] Q. Zhang, A. Iyer, K. Lambeth, K. Kim, and N. Sharma, "Ultrasound Echogenicity as an Indicator of Muscle Fatigue during Functional Electrical Stimulation," *Sensors*, vol. 22, no. 1, p. 335, Jan. 2022, doi: 10.3390/s22010335.
[59] T. Tanaka, S. Hori, R. Yamaguchi, M. Q. Feng, and S. Moromugi, "Ultrasonic sensor disk for detecting muscular force," in *The 12th IEEE International Workshop on Robot and Human Interactive Communication, 2003. Proceedings. ROMAN 2003.*, Nov. 2003, pp. 291–295. doi: 10.1109/ROMAN.2003.1251860.
[60] Y. Tsutsui, Y. Sakata, T. Tanaka, S. Kaneko, and M. Q. Feng, "Human Joint Movement Recognition by Using Ultrasound Echo Based on Test Feature Classifier," in *2007 IEEE Sensors*, Atlanta, GA, USA, 2007, pp. 1205–1208. doi: 10.1109/ICSENS.2007.4388625.
[61] T. Koyama, T. Tanaka, S. Kaneko, S. Moromugi, and M. Q. Feng, "Integral Ultrasonic Muscle Activity Sensor for Detecting Human Motion," in *2005 IEEE International Conference on Systems, Man and Cybernetics*, Waikoloa, HI, USA, 2005, vol. 2, pp. 1669–1674. doi: 10.1109/ICSMC.2005.1571388.
[62] Y. Tsutsui, T. Tanaka, S. Kaneko, and M. Q. Feng, "Duplex Ultrasonic Muscle Activity Sensor," in *IEEE Sensors, 2005.*, Irvine, CA, USA, 2005, p. 310. doi: 10.1109/ICSENS.2005.1597698.
[63] J. Majdi, A. Baker, M. Harris-Love, and S. Sikdar, "Closed-loop Hybrid Exoskeleton Utilizing Wearable Ultrasound Sensors for Measuring Fatigue," presented at the 2018 Cyber-Physical Systems Principle Investigators Meeting,

Hilton Alexandria Mark Center Hotel, 5000 Seminary Road, Alexandria, VA 22311, Nov. 15, 2018.
[64] R. J. Cunningham and I. D. Loram, “Estimation of Absolute States of Human Skeletal Muscle via Standard B-Mode Ultrasound Imaging and Deep Convolutional Neural Networks,” *arXiv preprint arXiv*, p. 12, Jul. 2019.
[65] J. A. Majdi, S. A. Acuña, P. V. Chitnis, and S. Sikdar, “Toward a wearable monitor of local muscle fatigue during electrical muscle stimulation using tissue Doppler imaging,” *Wearable Technol.*, vol. 3, pp. e16-1 to e16-20, 2022, doi: 10.1017/wtc.2022.10.
[66] N. Babault, C. Cometti, N. A. Maffiuletti, and G. Deley, “Does electrical stimulation enhance post-exercise performance recovery?,” *Eur J Appl Physiol*, vol. 111, no. 10, pp. 2501–2507, Oct. 2011, doi: 10.1007/s00421-011-2117-7.
[67] D. A. Lake, “Neuromuscular electrical stimulation. An overview and its application in the treatment of sports injuries.,” *Sports Med*, vol. 13, no. 5, pp. 320–336, May 1992, doi: 10.2165/00007256-199213050-00003.
[68] A. Cuesta-Gómez, F. Molina-Rueda, M. Carratala-Tejada, E. Imatz-Ojanguren, D. Torricelli, and J. C. Miangolarra-Page, “The Use of Functional Electrical Stimulation on the Upper Limb and Interscapular Muscles of Patients with Stroke for the Improvement of Reaching Movements: A Feasibility Study,” *Frontiers in Neurology*, vol. 8, May 2017, doi: 10.3389/fneur.2017.00186.
[69] M. Laubacher *et al.*, “Stimulation of paralysed quadriceps muscles with sequentially and spatially distributed electrodes during dynamic knee extension,” *J NeuroEngineering Rehabil*, vol. 16, no. 1, p. 5, Dec. 2019, doi: 10.1186/s12984-018-0471-y.
[70] B. M. Doucet, A. Lam, and L. Griffin, “neuromuscular Electrical Stimulation for Skeletal Muscle Function,” *Yale Journal of Biology and Medicine*, vol. 85, no. 2, pp. 201–215, Jun. 2012.
[71] N. A. Maffiuletti, M. A. Minetto, D. Farina, and R. Bottinelli, “Electrical stimulation for neuromuscular testing and training: state-of-the art and unresolved issues,” *Eur J Appl Physiol*, vol. 111, no. 10, pp. 2391–2397, Oct. 2011, doi: 10.1007/s00421-011-2133-7.
[72] J. Wan, Z. Qin, P. Wang, Y. Sun, and X. Liu, “Muscle fatigue: general understanding and treatment,” *Experimental & Molecular Medicine*, vol. 49, no. 10, p. e384, Oct. 2017, doi: 10.1038/emm.2017.194.
[73] A. J. Buckmire, T. J. Arakeri, J. P. Reinhard, and A. J. Fuglevand, “Mitigation of excessive fatigue associated with functional electrical stimulation,” *J. Neural Eng.*, vol. 15, no. 6, p. 066004, Dec. 2018, doi: 10.1088/1741-2552/aade1c.
[74] M. Schmoll, R. Le Guillou, D. Lobato Borges, C. Fattal, E. Fachin-Martins, and C. Azevedo Coste, “Standardizing fatigue-resistance testing during electrical stimulation of paralysed human quadriceps muscles, a practical approach,” *J NeuroEngineering Rehabil*, vol. 18, no. 1, p. 11, Dec. 2021, doi: 10.1186/s12984-021-00805-7.
[75] S. A. Binder-Macleod and L. Snyder-Mackler, “Muscle Fatigue: Clinical Implications for Fatigue Assessment and Neuromuscular Electrical Stimulation,”

Physical Therapy, vol. 73, no. 12, pp. 902–910, Dec. 1993, doi: 10.1093/ptj/73.12.902.
[76] J. Gondin, P. J. Cozzone, and D. Bendahan, "Is high-frequency neuromuscular electrical stimulation a suitable tool for muscle performance improvement in both healthy humans and athletes?," *Eur J Appl Physiol*, vol. 111, no. 10, pp. 2473–2487, Oct. 2011, doi: 10.1007/s00421-011-2101-2.
[77] S. A. Dugan and W. R. Frontera, "Muscle Fatigue and Muscle Injury," *Physical Medicine and Rehabilitation Clinics of North America*, vol. 11, no. 2, pp. 385–403, May 2000, doi: 10.1016/S1047-9651(18)30135-9.
[78] D. G. Sayenko, R. Nguyen, M. R. Popovic, and K. Masani, "Reducing muscle fatigue during transcutaneous neuromuscular electrical stimulation by spatially and sequentially distributing electrical stimulation sources," *Eur J Appl Physiol*, vol. 114, no. 4, pp. 793–804, Apr. 2014, doi: 10.1007/s00421-013-2807-4.
[79] G. Ye, S. S. Ali, A. J. Bergquist, M. R. Popovic, and K. Masani, "A Generic Sequential Stimulation Adapter for Reducing Muscle Fatigue during Functional Electrical Stimulation," *Sensors (Basel)*, vol. 21, no. 21, p. 7248, Oct. 2021, doi: 10.3390/s21217248.
[80] G. M. Graham, T. A. Thrasher, and M. R. Popovic, "The effect of random modulation of functional electrical stimulation parameters on muscle fatigue," *IEEE Transactions on Neural Systems and Rehabilitation Engineering*, vol. 14, no. 1, pp. 38–45, Mar. 2006, doi: 10.1109/TNSRE.2006.870490.
[81] Y. Shimada, H. Ito, T. Matsunaga, A. Misawa, M. Kawatani, and E. Itoi, "Reduction of muscle fatigue by catchlike-inducing intermittent electrical stimulation in rat skeletal muscle," *Biomed. Res.*, vol. 27, no. 4, pp. 183–189, 2006, doi: 10.2220/biomedres.27.183.
[82] M. Cifrek, V. Medved, S. Tonković, and S. Ostojić, "Surface EMG based muscle fatigue evaluation in biomechanics," *Clinical Biomechanics*, vol. 24, no. 4, pp. 327–340, May 2009, doi: 10.1016/j.clinbiomech.2009.01.010.
[83] H. A. Yousif *et al.*, "Assessment of Muscles Fatigue Based on Surface EMG Signals Using Machine Learning and Statistical Approaches: A Review," *IOP Conf. Ser.: Mater. Sci. Eng.*, vol. 705, no. 1, p. 012010, Nov. 2019, doi: 10.1088/1757-899X/705/1/012010.
[84] H. Tankisi *et al.*, "Standards of instrumentation of EMG," *Clinical Neurophysiology*, vol. 131, no. 1, pp. 243–258, Jan. 2020, doi: 10.1016/j.clinph.2019.07.025.
[85] F. Mandrile, D. Farina, M. Pozzo, and R. Merletti, "Stimulation artifact in surface EMG signal: effect of the stimulation waveform, detection system, and current amplitude using hybrid stimulation technique," *IEEE Transactions on Neural Systems and Rehabilitation Engineering*, vol. 11, no. 4, pp. 407–415, Dec. 2003, doi: 10.1109/TNSRE.2003.819791.
[86] J. Jung, D.-W. Lee, Y. K. Son, B. S. Kim, and H. C. Shin, "Volitional EMG Estimation Method during Functional Electrical Stimulation by Dual-Channel Surface EMGs," *Sensors*, vol. 21, no. 23, p. 8015, Nov. 2021, doi: 10.3390/s21238015.

[87] J. Liu, S. Li, X. Li, C. Klein, W. Z. Rymer, and P. Zhou, “Suppression of Stimulus Artifact Contaminating Electrically Evoked Electromyography,” *NeuroRehabilitation*, vol. 34, no. 2, pp. 381–389, Jan. 2014, doi: 10.3233/NRE-131045.
[88] Q. Zhang, M. Hayashibe, P. Fraisse, and D. Guiraud, “FES-Induced Torque Prediction With Evoked EMG Sensing for Muscle Fatigue Tracking,” *IEEE/ASME Transactions on Mechatronics*, vol. 16, no. 5, pp. 816–826, Oct. 2011, doi: 10.1109/TMECH.2011.2160809.
[89] R. Uwamahoro, K. Sundaraj, and I. D. Subramaniam, “Assessment of muscle activity using electrical stimulation and mechanomyography: a systematic review,” *BioMed Eng OnLine*, vol. 20, no. 1, p. 1, Dec. 2021, doi: 10.1186/s12938-020-00840-w.
[90] Y. Yoshitake, H. Ue, M. Miyazaki, and T. Moritani, “Assessment of lower-back muscle fatigue using electromyography, mechanomyography, and near-infrared spectroscopy,” *European Journal of Applied Physiology*, vol. 84, no. 3, pp. 174–179, Mar. 2001, doi: 10.1007/s004210170001.
[91] Md. A. Islam, K. Sundaraj, R. B. Ahmad, and N. U. Ahamed, “Mechanomyogram for Muscle Function Assessment: A Review,” *PLoS ONE*, vol. 8, no. 3, p. e58902, Mar. 2013, doi: 10.1371/journal.pone.0058902.
[92] R. B. Woodward, M. J. Stokes, S. J. Shefelbine, and R. Vaidyanathan, “Segmenting Mechanomyography Measures of Muscle Activity Phases Using Inertial Data,” *Sci Rep*, vol. 9, no. 1, p. 5569, Dec. 2019, doi: 10.1038/s41598-019-41860-4.
[93] A. Scano *et al.*, “Sustained fatigue assessment during isometric exercises with time-domain near infrared spectroscopy and surface electromyography signals,” *Biomed. Opt. Express*, vol. 11, no. 12, p. 7357, Dec. 2020, doi: 10.1364/BOE.403976.
[94] S. Sikdar *et al.*, “Novel applications of ultrasound technology to visualize and characterize myofascial trigger points and surrounding soft tissue,” *Archives of physical medicine and rehabilitation*, vol. 90, no. 11, pp. 1829–1838, 2009.
[95] S. Sikdar, Q. Wei, and N. Cortes, “Dynamic Ultrasound Imaging Applications to Quantify Musculoskeletal Function,” *Exerc Sport Sci Rev*, vol. 42, no. 3, pp. 126–135, Jul. 2014, doi: 10.1249/JES.0000000000000015.
[96] J. R. Franz, L. C. Slane, K. Rasske, and D. G. Thelen, “Non-uniform in vivo deformations of the human Achilles tendon during walking,” *Gait & Posture*, vol. 41, no. 1, pp. 192–197, Jan. 2015, doi: 10.1016/j.gaitpost.2014.10.001.
[97] Z. Sheng, N. Sharma, and K. Kim, “Quantitative Assessment of Changes in Muscle Contractility Due to Fatigue During NMES: An Ultrasound Imaging Approach,” *IEEE Transactions on Biomedical Engineering*, pp. 1–1, 2019, doi: 10.1109/TBME.2019.2921754.
[98] I. AlMohimeed and Y. Ono, “Ultrasound Measurement of Skeletal Muscle Contractile Parameters Using Flexible and Wearable Single-Element Ultrasonic Sensor,” *Sensors*, vol. 20, no. 13, p. 3616, Jun. 2020, doi: 10.3390/s20133616.
[99] F. Weidemann and J. M. Strotmann, “Use of tissue Doppler imaging to identify and manage systemic diseases,” *Clin Res Cardiol*, vol. 97, no. 2, pp. 65–73, Feb. 2008, doi: 10.1007/s00392-007-0566-0.

[100] S. E. Campbell, R. Adler, and C. M. Sofka, “Ultrasound of Muscle Abnormalities,” *Ultrasound Quarterly*, vol. 21, no. 2, p. 8, 2005.
[101] E. Koh and E. McNally, “Ultrasound of Skeletal Muscle Injury,” *Semin Musculoskelet Radiol*, vol. 11, no. 2, pp. 162–173, Jun. 2007, doi: 10.1055/s-2007-1001881.
[102] A. Nordez, T. Gallot, S. Catheline, A. Guével, C. Cornu, and F. Hug, “Electromechanical delay revisited using very high frame rate ultrasound,” *Journal of Applied Physiology*, vol. 106, no. 6, pp. 1970–1975, Jun. 2009, doi: 10.1152/japplphysiol.00221.2009.
[103] T. Shiina, M. M. Doyley, and J. C. Bamber, “Strain imaging using combined RF and envelope autocorrelation processing,” in *1996 IEEE Ultrasonics Symposium. Proceedings*, Nov. 1996, vol. 2, pp. 1331–1336 vol.2. doi: 10.1109/ULTSYM.1996.584292.
[104] H. Misra, S. Ikbal, H. Bourlard, and H. Hermansky, “Spectral entropy based feature for robust ASR,” in *2004 IEEE International Conference on Acoustics, Speech, and Signal Processing*, May 2004, vol. 1, p. I–193. doi: 10.1109/ICASSP.2004.1325955.
[105] L. A. Hallock, A. Kato, and R. Bajcsy, “Empirical Quantification and Modeling of Muscle Deformation: Toward Ultrasound-Driven Assistive Device Control * This work was supported by the NSF National Robotics Initiative (award no. 81774), Siemens Healthcare (85993), and the NSF Graduate Research Fellowship Program.,” in *2018 IEEE International Conference on Robotics and Automation (ICRA)*, May 2018, pp. 1825–1832. doi: 10.1109/ICRA.2018.8462887.
[106] L. A. Hallock, A. Velu, A. Schwartz, and R. Bajcsy, “Muscle deformation correlates with output force during isometric contraction,” in *2020 8th IEEE RAS/EMBS International Conference for Biomedical Robotics and Biomechatronics (BioRob)*, Nov. 2020, pp. 1188–1195. doi: 10.1109/BioRob49111.2020.9224391.
[107] E. Azizi and A. R. Deslauriers, “Regional heterogeneity in muscle fiber strain: the role of fiber architecture,” *Front. Physiol.*, vol. 5, Aug. 2014, doi: 10.3389/fphys.2014.00303.
[108] N. K. Vøllestad, “Measurement of human muscle fatigue,” *Journal of Neuroscience Methods*, vol. 74, no. 2, pp. 219–227, Jun. 1997, doi: 10.1016/S0165-0270(97)02251-6.
[109] D. T. Barry, T. Hill, and D. Im, “MUSCLE FATIGUE MEASURED WITH EVOKED MUSCLE VIBRATIONS,” *Muscle & Nerve*, vol. 15, pp. 303–309, 1992.
[110] D. G. Sale, “Postactivation Potentiation: Role in Human Performance:,” *Exercise and Sport Sciences Reviews*, vol. 30, no. 3, pp. 138–143, Jul. 2002, doi: 10.1097/00003677-200207000-00008.
[111] L. L. Rankin, R. M. Enoka, K. A. Volz, and D. G. Stuart, “Coexistence of twitch potentiation and tetanic force decline in rat hindlimb muscle,” *Journal of Applied Physiology*, vol. 65, no. 6, pp. 2687–2695, Dec. 1988, doi: 10.1152/jappl.1988.65.6.2687.

[112] D. E. Rassier and B. R. MacIntosh, “Coexistence of potentiation and fatigue in skeletal muscle,” *Brazilian Journal of Medical and Biological Research*, vol. 33, no. 5, pp. 499–508, May 2000, doi: 10.1590/S0100-879X2000000500003.
[113] P. Muanjai *et al.*, “Low frequency fatigue and changes in muscle fascicle length following eccentric exercise of the knee extensors,” *Exp Physiol*, p. EP088237, Jan. 2020, doi: 10.1113/EP088237.
[114] A. J. Baker, K. G. Kostov, R. G. Miller, and M. W. Weiner, “Slow force recovery after long-duration exercise: metabolic and activation factors in muscle fatigue,” *Journal of Applied Physiology*, vol. 74, no. 5, pp. 2294–2300, May 1993, doi: 10.1152/jappl.1993.74.5.2294.
[115] R. K. Shields, L. F. Law, B. Reiling, K. Sass, and J. Wilwert, “Effects of electrically induced fatigue on the twitch and tetanus of paralyzed soleus muscle in humans,” *Journal of Applied Physiology*, vol. 82, no. 5, pp. 1499–1507, May 1997, doi: 10.1152/jappl.1997.82.5.1499.
[116] Q. Zhang, A. Iyer, and N. Sharma, “Ultrasound-Based Sensing and Control of Functional Electrical Stimulation for Ankle Joint Dorsiflexion: Preliminary Study,” in *Wearable Robotics: Challenges and Trends*, vol. 27, J. C. Moreno, J. Masood, U. Schneider, C. Maufroy, and J. L. Pons, Eds. Cham: Springer International Publishing, 2022, pp. 307–311. doi: 10.1007/978-3-030-69547-7_50.
[117] C. T. Freeman, K. Yang, J. Tudor, and M. Kutlu, “Feedback control of electrical stimulation electrode arrays,” *Medical Engineering & Physics*, vol. 38, no. 11, pp. 1185–1194, Nov. 2016, doi: 10.1016/j.medengphy.2016.07.002.
[118] C. Phongamwong, P. Rowe, K. Chase, A. Kerr, and L. Millar, “Treadmill training augmented with real-time visualisation feedback and function electrical stimulation for gait rehabilitation after stroke: a feasibility study,” *BMC biomed eng*, vol. 1, no. 1, p. 20, Dec. 2019, doi: 10.1186/s42490-019-0020-1.
[119] R. K. Shields, S. Dudley-Javoroski, and K. R. Cole, “Feedback-controlled stimulation enhances human paralyzed muscle performance,” *J Appl Physiol*, vol. 101, no. 5, pp. 1312–1319, Nov. 2006, doi: 10.1152/japplphysiol.00385.2006.
[120] Y. Zhou, Y. Fang, K. Gui, K. Li, D. Zhang, and H. Liu, “sEMG Bias-Driven Functional Electrical Stimulation System for Upper-Limb Stroke Rehabilitation,” *IEEE Sensors J.*, vol. 18, no. 16, pp. 6812–6821, Aug. 2018, doi: 10.1109/JSEN.2018.2848726.
[121] C.-H. Chang, J. Casas, S. W. Brose, and V. H. Duenas, “Closed-Loop Torque and Kinematic Control of a Hybrid Lower-Limb Exoskeleton for Treadmill Walking,” *Front. Robot. AI*, vol. 8, p. 702860, Jan. 2022, doi: 10.3389/frobt.2021.702860.
[122] M. Gobbo, N. A. Maffiuletti, C. Orizio, and M. A. Minetto, “Muscle motor point identification is essential for optimizing neuromuscular electrical stimulation use,” *J NeuroEngineering Rehabil*, vol. 11, no. 1, p. 17, 2014, doi: 10.1186/1743-0003-11-17.
[123] J. A. Majdi, P. Chitnis, and S. Sikdar, “Estimation of joint torque and muscle fatigue for assistive technology applications using a wearable ultrasound system,” presented at the Rehabilitation Engineering and Assistive Technology Society of North America Annual Conference, Washington, DC, 2020. Accessed: Nov. 29,

2020. [Online]. Available: https://www.resna.org/sites/default/files/conference/2020/PDFs/StudentScientificPapers/NewAndEmergingTechnology/99Majdi.pdf

[124] M. Kunita, M. Sudo, S. Inoue, and M. Akahane, "A new method for blood velocity measurements using ultrasound FMCW signals," *IEEE transactions on ultrasonics, ferroelectrics, and frequency control*, vol. 57, no. 5, 2010, Accessed: Sep. 24, 2017. [Online]. Available: http://ieeexplore.ieee.org/abstract/document/5456255/

[125] E. Tarbox *et al.*, "Low-power ultrasound imaging systems using time delay spectrometry," in *2017 IEEE International Ultrasonics Symposium (IUS)*, 2017, pp. 1–4.

[126] M. E. Héroux, P. W. Stubbs, and R. D. Herbert, "Behavior of human gastrocnemius muscle fascicles during ramped submaximal isometric contractions," *Physiological Reports*, vol. 4, no. 17, p. e12947, 2016, doi: 10.14814/phy2.12947.

[127] V. Ravindra and C. Castellini, "A Comparative Analysis of Three Non-Invasive Human-Machine Interfaces for the Disabled," *Front. Neurorobot.*, vol. 8, 2014, doi: 10.3389/fnbot.2014.00024.

[128] C. Castellini, "Design Principles of a Light, Wearable Upper Limb Interface for Prosthetics and Teleoperation," in *Wearable Robotics*, Elsevier, 2020, pp. 377–391. doi: 10.1016/B978-0-12-814659-0.00020-5.

[129] N. Sharma, N. A. Kirsch, N. A. Alibeji, and W. E. Dixon, "A Non-Linear Control Method to Compensate for Muscle Fatigue during Neuromuscular Electrical Stimulation," *Frontiers in Robotics and AI*, vol. 4, Dec. 2017, doi: 10.3389/frobt.2017.00068.

[130] J.-L. Shen, J.-W. Hung, and L.-S. Lee, "Robust entropy-based endpoint detection for speech recognition in noisy environments," 1998.

[131] R. J. Downey, M. Merad, E. J. Gonzalez, and W. E. Dixon, "The Time-Varying Nature of Electromechanical Delay and Muscle Control Effectiveness in Response to Stimulation-Induced Fatigue," *IEEE Transactions on Neural Systems and Rehabilitation Engineering*, vol. 25, no. 9, pp. 1397–1408, Sep. 2017, doi: 10.1109/TNSRE.2016.2626471.

[132] V. Carriou, S. Boudaoud, J. Laforet, A. Mendes, F. Canon, and D. Guiraud, "Multiscale Hill-type modeling of the mechanical muscle behavior driven by the neural drive in isometric conditions," *Computers in Biology and Medicine*, vol. 115, p. 103480, Dec. 2019, doi: 10.1016/j.compbiomed.2019.103480.

[133] J. M. Wakeling, S. S. M. Lee, A. S. Arnold, M. de Boef Miara, and A. A. Biewener, "A Muscle's Force Depends on the Recruitment Patterns of Its Fibers," *Ann Biomed Eng*, vol. 40, no. 8, pp. 1708–1720, Aug. 2012, doi: 10.1007/s10439-012-0531-6.

[134] D. G. Allen, G. D. Lamb, and H. Westerblad, "Impaired calcium release during fatigue," *Journal of Applied Physiology*, vol. 104, no. 1, pp. 296–305, Jan. 2008, doi: 10.1152/japplphysiol.00908.2007.

[135] M. Benoussaad, P. Poignet, M. Hayashibe, C. Azevedo-Coste, C. Fattal, and D. Guiraud, "Experimental parameter identification of a multi-scale musculoskeletal

model controlled by electrical stimulation: application to patients with spinal cord injury," *Med Biol Eng Comput*, vol. 51, no. 6, pp. 617–631, Jun. 2013, doi: 10.1007/s11517-013-1032-y.

[136] S. H. Scott and D. A. Winter, "A comparison of three muscle pennation assumptions and their effect on isometric and isotonic force," *Journal of Biomechanics*, vol. 24, no. 2, pp. 163–167, Jan. 1991, doi: 10.1016/0021-9290(91)90361-P.

[137] R. Rockenfeller *et al.*, "Exhaustion of Skeletal Muscle Fibers Within Seconds: Incorporating Phosphate Kinetics Into a Hill-Type Model," *Front. Physiol.*, vol. 11, p. 25, May 2020, doi: 10.3389/fphys.2020.00306.

[138] A. A. Oglat, M. Z. Matjafri, N. Suardi, M. A. Oqlat, M. A. Abdelrahman, and A. A. Oqlat, "A Review of Medical Doppler Ultrasonography of Blood Flow in General and Especially in Common Carotid Artery," *J Med Ultrasound*, vol. 26, no. 1, pp. 3–13, 2018, doi: 10.4103/JMU.JMU_11_17.

BIOGRAPHY

Joseph Amir Majdi graduated from Clear Creek High School, League City, Texas, in 2006. He received biomedical engineering Bachelor of Science in Engineering and Master of Science degrees from Tulane University in 2012, and an electrical and computer engineering Master of Science degree from George Mason University in 2017. Between degrees, he worked at the US Food and Drug Administration in the Office of Science and Engineering Laboratories.